CHAPTER 11

ELECTRONIC STRUCTURE AND CHEMISTRY OF THE HEAVIEST ELEMENTS

V. PERSHINA

GSI Helmholtzzentrum für Schwerionenforschung GmbH, Planckstr. 1, D-64291 Darmstadt, Germany
e-mail: V.Pershina@gsi.de

Abstract: Investigations of chemical properties of the heaviest elements are among the most fundamental in all of chemistry. They seek to probe the uppermost reaches of the periodic table of the elements where the nuclei are unstable and relativistic effects on the electronic shells are very strong. Theoretical research in this area is extremely important. It is often the only source of useful chemical information. It also enables one to predict behaviour of the heaviest elements in the sophisticated and expensive experiments with single atoms. Spectacular developments in the relativistic quantum theory and computational algorithms allowed for accurate predictions of properties of the heaviest elements and their experimental behaviour. The works on the relativistic electronic structure calculations for the heaviest elements are overviewed. Preference is given to those related to the experimental research. Role of relativistic effects is discussed.

Keywords: Heaviest elements, Relativistic effects, Electronic structure, Chemical properties, Volatility, Complex formation

11.1. INTRODUCTION

Elements considered in this chapter are those with $Z = 104$ and heavier. They are called transactinides, since they are located after the actinide element series which ends with element 103, Lr. The heaviest among them, whose production was confirmed by the IUPAC and IUPAP, is element 112. Observation of even heavier elements, 113 through 118 with the exception of 117, has been claimed but not yet confirmed and approved by the commissions.

The heaviest elements are very special: Located at the bottom of the periodic table of the elements, their nuclei are extremely unstable and electronic shells are influenced by strong relativistic effects [1–10].

Due to the instability of isotopes of these elements and low production rates, experimental chemical research in this area is very complex: Special techniques had to be developed that allow for studying macrochemical properties on the basis

M. Barysz and Y. Ishikawa (eds.), *Relativistic Methods for Chemists*,
Challenges and Advances in Computational Chemistry and Physics 10,
DOI 10.1007/978-1-4020-9975-5_11,

of single atom events. Not less challenging is the theoretical chemical research in this area. It should be based on the most accurate relativistic atomic and molecular calculations in order to reliably predict properties and experimental behaviour of the new elements. It needs also development of special approaches which bridge calculations with quantities that cannot be predicted in a straightforward way via quantum-chemical calculations.

Due to recent developments in the relativistic quantum theory, calculational algorithms and computer techniques, very accurate calculations of heavy element properties became possible. In this chapter, we will overview advances in the theoretical studies of chemical properties of the heaviest elements and predictions of their experimental behaviour. We will pay particular attention to the influence of relativistic effects on chemical properties and trends in the periodic table.

11.2. PRODUCTION AND IDENTIFICATION OF THE HEAVIEST ELEMENTS

Elements heavier than U (Z = 92) are all produced by man-made nuclear reactions. The first members of the transactinides series, Z = 104 through 106 were discovered (in 1969 through 1974) in heavy-ion accelerators by bombardment of heavy actinide (Pu-Cf) targets with light ions (carbon, boron, neon, oxygen), so called "hot-fusion" reactions. The institutions involved in the production of these elements were the LBNL (USA) and the JINR (Russia) (see [11–13] for reviews).

In the 1970s, a different type of fusion reaction was discovered and later used in the discovery of elements with Z larger than 106. These so called "cold-fusion" reactions were based on targets in the vicinity of doubly-magic ^{208}Pb (mainly lead and bismuth) and beams of the complementary medium-mass projectiles with Z $\geq$ 24. Elements with Z = 107 through 112 were produced and identified in this way between 1981 and 1996 at the GSI in Darmstadt (see [14,15] for reviews). Recently, the RIKEN laboratory (Japan) has announced the production of element 113 in the reaction of the ^{70}Zn beams with a ^{209}Bi target [16].

The lifetime of the heaviest elements was found to be very short, for example, the half-life of ^{277}112 is only 0.7 ms (Figure 11-1). The cross-section was also found to decrease rapidly with increasing Z. It is, for example, only ~0.5 pb for ^{277}112. It was, therefore, concluded that it would be very difficult to reach even heavier elements in this way.

More recently, production of the superheavy elements 112 through 118 (except for 117) using "hot" fusion reactions between ^{48}Ca ions and ^{238}U, ^{242,244}Pu, ^{243}Am, ^{245,248}Cm, and ^{249}Cf targets was reported by a Dubna/Livermore collaboration working at the JINR (see [17] for a review). These results are of considerable interest for chemical studies because the reported half-lives are much longer (many orders of magnitude) than those of the isotopes produced by "cold" fusion reactions which lead to more neutron-deficient isotopes. Thus, e.g., $t_{1/2}(^{283}112) = 3.8$ s, and $t_{1/2}(^{287}114) = 0.48$ s. The first chemistry experiments have already been performed with this isotope of element 112 (see below) and experiments for the heavier

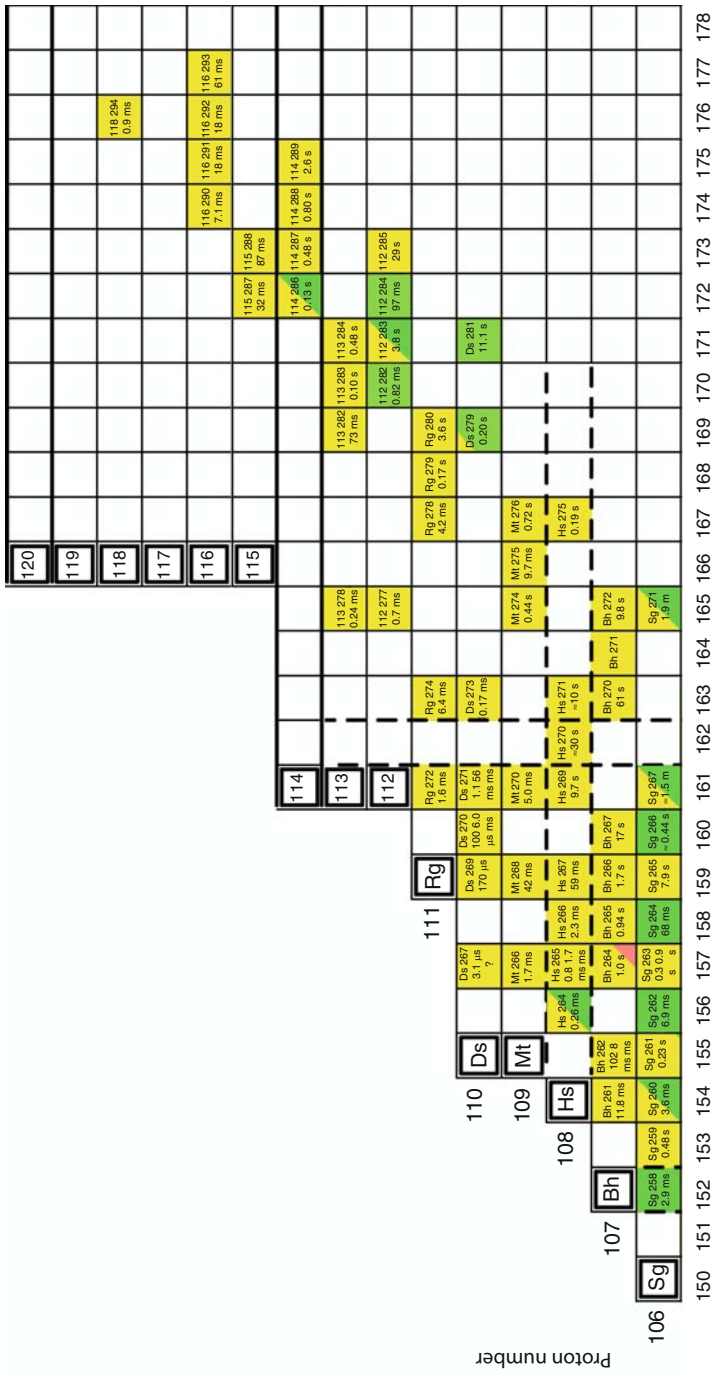

Figure 11-1. The upper part of the chart of nuclides (Light grey – α decay, dark grey – spontaneous fission)

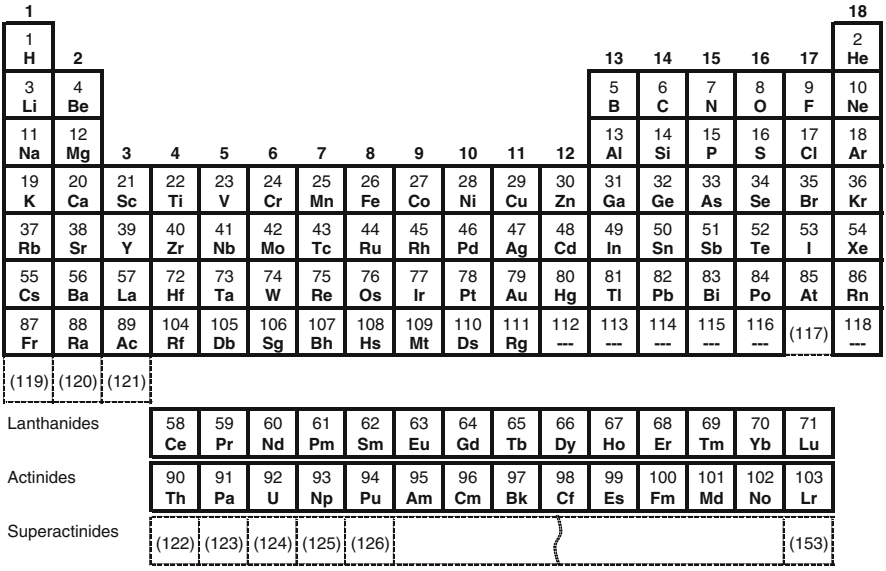

Figure 11-2. The periodic table of the elements 2008

elements 113 and 114 are scheduled. The modern chart of nuclides at its upper end is shown in Figure 11-1. The periodic table as of 2008 is shown in Figure 11-2.

The names and symbols for the transactinide elements approved by the IUPAC are: rutherfordium (Rf) for $Z = 104$, dubnium (Db) for $Z = 105$, seaborgium (Sg) for $Z = 106$, bohrium (Bh) for $Z = 107$, hassium (Hs) for $Z = 108$, meitnerium (Mt) for $Z = 109$, darmstadtium (Ds) for $Z = 110$, and röntgenium (Rg) for $Z = 111$ [18]. As discovery claims on elements with $Z \geq 112$ are under review, these elements are still awaiting naming.

In order to positively identify a new element and place it in its proper position in the periodic table, its atomic number, Z, must be determined or deduced in some way. The elements beyond 101 have been identified first by "physical" techniques because of their very small production rates and short half-lives. One widely used technique is that of $\alpha - \alpha$ correlation of the element's α-decay to a known daughter and/or granddaughter nucleus that also decays by α-emission. For example, elements 111 and 112 produced in "cold-fusion" reactions were identified in this way. Positive identification becomes even more difficult for species that decay predominantly by spontaneous fission (SF). Although detection of SF is a very sensitive technique, it is to date impossible to determine what the nuclear charge Z of the fissioning species might have been since only the fission fragments are detected. The nuclear charge Z of *both primary fragments* would have to be identified in coincidence in order to obtain the total Z of the new element. For example, the claimed α-decay chain associated with $^{292}116$ produced in the $^{248}\mathrm{Cm}(^{48}\mathrm{Ca}, 4n)$ reaction and its daughters goes through $^{288}114$ and $^{284}112$, which undergoes SF. In this case the α chain ends up at an unknown isotope, so that a firm assignment is not possible.

Thus, chemical experiments designed so that the behavior of the unknown isotope will be compared to that of a lighter homolog in a chemical group will help to identify Z (see [11–15] for reviews on experimental techniques for the transactinide elements synthesis and characterization).

The possibility of discovery of even heavier elements is presently a matter of theoretical discussions, and predictions of centers of stabilities in the superheavy element region depend on the model used and are often in disagreement with each other. About 50 years ago it was assumed that the periodic table would end at about $Z = 100$, since the attractive strong interactions can no longer counter-balance the Coulomb repulsion between the many protons. It was then realized that shell-closing effects would increase the nuclear stability substantially. It was, indeed, shown that the stability of nuclei with $Z > 102$ is due to quantum shell effects. Consequently, calculations based on shell correction method (macroscopic-microscopic models, which depend on a large number of parameters, since the form of the potential for strong attractive interactions is not known) predicted the peak of an island of stability at $Z = 114$, $N = 184$ ($^{298}114$) due to both, proton- as well as neutron-shell closures at these numbers [19, 20]. Only in the 1990s, this point of view was challenged by calculations based on more refined models such as self-consistent-field theory and realistic effective nucleon-nucleon interactions. Most of the self-consistent calculations suggest that the center of the proton shell stability should be around higher proton numbers, $Z = 120$, 124, or 126. For the neutrons, relativistic mean-field theory predicts $N = 172$, in contrast to the nonrelativistic prediction for $Z = 184$, which neglects spin-orbit interaction. For reviews on those theoretical works, see [21, 22]. It will be a matter of future investigations to confirm or contradict these theoretical predictions by experiment.

11.3. EXPERIMENTAL CHEMICAL STUDIES

Even though the atomic number can be positively assigned by α-decay chains, no knowledge is obtained about electronic configurations or chemical properties of a new element from these physical methods. The elements are just placed in the periodic table in corresponding chemical groups or periods according to its atomic number and the calculated electronic structures. Thus, it is a matter of experimental chemistry to attempt to validate or contradict these predictions: By assessing similarity in the chemical behaviour with that of lighter homologs a unique position of the new element in a chemical group can be confirmed. It is also essential to establish whether trends in the chemical groups observed for the lighter elements is continued with the transactinides, or whether deviations occur due to the strong relativistic effects. Fundamental properties which enable one to decide about such similarity are oxidation states, ionic radii and complex formation.

Experimental studies of the heaviest elements require use of isotope with a half-life long enough to permit chemical separation and a reasonable production and detection rate. This may range for the heaviest elements from a few atoms per minute for Rf to only an atom per week in the case of element 112. The chemical

procedures used in atom-at-a-time studies must be fast enough to be accomplished in times comparable to the half-lives of the isotopes used in those studies and must give the same results as for macro amounts.

Chemical methods in which a single atom rapidly participates in many identical chemical interactions to two-phase systems with fast kinetics that reach equilibrium quickly have proven to be valid. Thus, it is sufficient to combine the results of many separate one-atom-at-a-time experiments, or identical experiments with only one atom, in order to get statistically significant results [23]. The two main types — gas phase and liquid chemistry — of separations are based on this principle.

11.3.1. Gas-Phase Chemistry

Gas-phase chromatography experiments allow for studying volatility of single chemical species. The measure of this property of macroamounts is the sublimation enthalpy, ΔH_{sub}. A pioneer experiment that allowed an approximation to the sublimation process by adsorption of single species on metallic columns was designed in Dubna [24]. Many assumptions are involved in this approach allowing for a loose correlation between the heat of adsorption and the heat of sublimation. In this method, a longitudinal, negative temperature gradient is established along the chromatography column through which a gas stream is conducted. It contains the volatile species of interest (atoms or molecules) that deposit on the surface of the chromatography column according to their volatilities. The deposition zones are registered by detectors along the column, which are associated with specific deposition (adsorption) temperatures, T_{ads}. The obtained T_{ads} are then used to deduce the adsorption enthalpy ΔH_{ads} using adsorption models and a Monte Carlo simulation.

The first investigations of volatility of the heaviest element compounds were performed in Dubna for Rf (kurchatovium, Ku, in the Russian works at that time), in the form of a chloride, $RfCl_4$ (since it is impossible to stabilize the heaviest 6d elements in the atomic state) using this chromatography technique [25]. Later, volatility of HsO_4 [26] and of element 112 [27], which is stable in the elemental state, was studied in this way. Volatile elements 113 and 114 are to be studied next.

In another technique, isothermal chromatography, the entire column is kept at a constant temperature. Volatile species pass through the column undergoing numerous adsorption-desorption steps. Their retention time is indicative of the volatility at a given temperature. A series of temperatures is run and the chemical yield of the species is studied as a function of the temperature. The temperature, $T_{50\%}$, at which 50% of the species pass through the column, i.e. 50% of the chemical yield, is taken as a measure of volatility in a comparative study. A Monte Carlo program is used to deduce ΔH_{ads} from the measured $T_{50\%}$ using a thermodynamic model of adsorption. The volatility of the Rf, Db, Sg and Bh compounds was successfully studied using this technique [28–31]. Reviews of the gas-phase experimental techniques and applications can be found in [8, 32, 33].

11.3.2. Liquid-Phase Chemistry

Liquid-liquid or ion (cation, CIX, or anion, AIX) exchange chromatography experiments are used to study the complex formation of the heaviest elements and their homologs in aqueous solutions.

An anionic complex $ML_i{}^{z-i}$ is formed according to the reaction

$$M^{z+} + iL^- = ML_i{}^{z-i}, \tag{11-1}$$

with the complex formation constant $\beta_i = [ML_i][M]^{-1}[L]^{-i}$. It is extracted from aqueous solutions by an anion-exchanger according to the following reaction

$$pRB^+L^-(org) + ML_i{}^{-p} = (RB^+)_p(ML_i)^{p-}(org) + pL^-, \tag{11-2}$$

with the equilibrium constant K_{DM}. The distribution coefficient is then

$$K_d = \frac{K_{DM}[RB^+L^-]^p_{org}\beta_i[L^-]^{i-p}}{\sum\limits_0^N \beta_n[L^-]^n}, \tag{11-3}$$

where $p = i - z$, z is the metal formal charge and N is the maximum coordination number. Obtained distribution coefficients K_d (usually plots of K_d values (vs.) acid concentration) are used to judge stabilities of the formed complexes. Also, knowing the K_d values, the complex formation β_i can be obtained.

In experiments with radioactive species, K_d is measured as a ratio of the activity of a studied species in the organic phase to that in the aqueous phase [34–36]. It is closely related to the key observable, the retention time, t_r, in the chromatography column

$$K_d = (t_r - t_0)\frac{V}{M}, \tag{11-4}$$

where t_0 – column hold-up time due to the free column volume, V – flow rate of the mobile phase, and M is the mass of the ion exchanger. In this way, complex formation of Rf, Db and Sg in various acidic solutions has been studied using the AIX and CIX separations [34, 35].

A promising method of separation of the heaviest elements is the electrochemical deposition from aqueous solutions. Electrochemical deposition produces an almost ideal sample for α-spectrometry and at the same time, as least a partial separation from interfering nuclides is achieved. It is presently tested for the homologs of elements 108 and 112 and heavier, e.g., Os, Hg, Pb, Bi and Po. The measured quantities in this method are E_{cri} and $E_{50\%}$ which are the critical potential and the electrode potential when 50% of the atoms are deposited. They both are a measure of the stability of a specific oxidation state and the strength of the metal-metal interaction of the studied metal atom with the electrode material [34, 35]. Reviews of the aqueous chemistry experimental studies can be found in [8, 9, 33–36].

11.4. THEORETICAL STUDIES

11.4.1. Role of Theoretical Studies

Except for the few properties, like volatility or complex formation, many others cannot be directly measured for the heaviest element. They can only be evaluated. For example, chemical composition of compounds can only be assumed on the basis of analogy in the experimental behaviour with that of the lighter congeners in the chemical groups. Ionisation potentials (IP), electron affinities (EA), dissociation energies (D_e) or geometrical structures (e.g., bond lengths, R_e) can not presently be measured at all. They can only be calculated. Thus, in the area of the heaviest elements, theory becomes extremely important and is often the only source of useful chemical information. Finally, it is only the theory that can reveal relativistic effects influence on chemical properties and experimental behaviour: only by comparing the observed behaviour with that predicted on the basis of relativistic (vs.) nonrelativistic calculations, can the importance and magnitude of relativistic effects be established.

Earlier predictions of chemical properties of the heaviest elements were based on results of the relativistic Dirac-Slater (DS) and Dirac-Fock (DF) atomic calculations and extrapolations of periodic trends (see reviews [5,37–40]). These and later works have revealed that use of the relativistic quantum theory and most advanced relativistic methods is mandatory for calculations of properties of the heaviest elements where relativistic effects become most important. Early molecular calculations have shown that trends in properties in the chemical groups can be predicted in an erroneous way for the heaviest elements by using nonrelativistic codes. Some simple extrapolations of the periodic trends, though sometimes useful, must also be made cautiously. Previous reviews of the theoretical works on molecular calculations for the heaviest elements are those of [6–10,41–43].

11.4.2. Relativistic and QED Effects on Atomic Electronic Shells of the Heaviest Elements

Relativistic effects on atomic orbitals (AOs) are well known: this is the contraction and stabilization of the s and $p_{1/2}$ AOs, the destabilisation and expansion of the $p_{3/2}$, d and f AOs, and the spin-orbit (SO) splitting of the AOs with $l > 0$. All the three effects change approximately as Z^2 for valence shells down a column of the periodic table. For the heaviest elements with large Z, these effects are of paramount importance. Figure 11-3 shows, e.g., the relativistic stabilization of the ns and $np_{1/2}$ AO and the SO splitting of the np AOs of the group 14 elements, with the latter amounting to 50 eV for element 164 [5].

Figure 11-4 shows the relativistic contraction $\Delta_R\langle r\rangle_{7s} = (\langle r\rangle_{nr} - \langle r\rangle_{rel})/\langle r\rangle_{nr} = 25\%$ of the 7s AO in Db. (See also Figure 7-3 in the Chapter of E. Eliav and U. Kaldor for the relativistic contraction of the 7s(Rg) AO.)

The relativistic contraction and stabilization of the ns AO reach the maximum in the seventh row at element 112 [6] (Figure 11-5). The shift of the maximum to

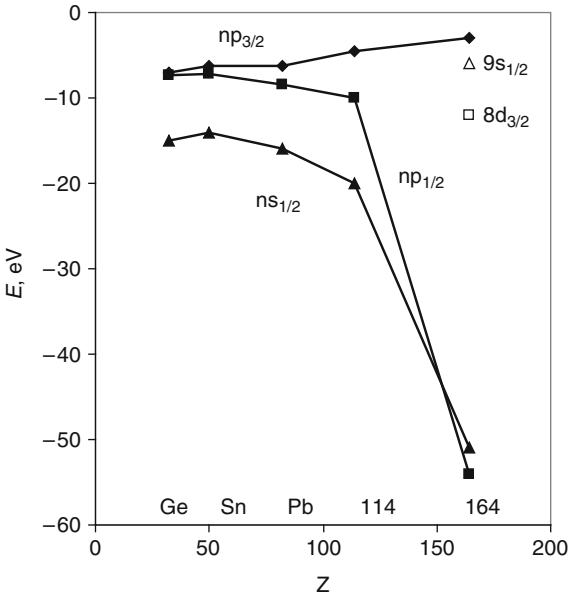

Figure 11-3. DS eigenvalues of the valence electrons of group 14 elements in the sp^2p configuration (Re-drawn from [5])

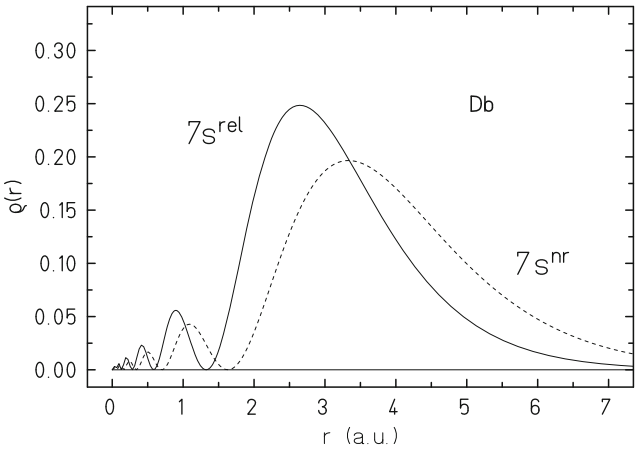

Figure 11-4. Relativistic (solid line) and nonrelativistic (dashed line) radial distribution of the 7s valence electrons in element 105, Db (From [43])

element 112 in the seventh row in contrast to gold in the sixth row [44] is due to the fact that in both elements 111 and 112 the ground state electronic configuration is d^qs^2, while the electronic configuration changes from Au($d^{10}s^1$) to Hg($d^{10}s^2$).

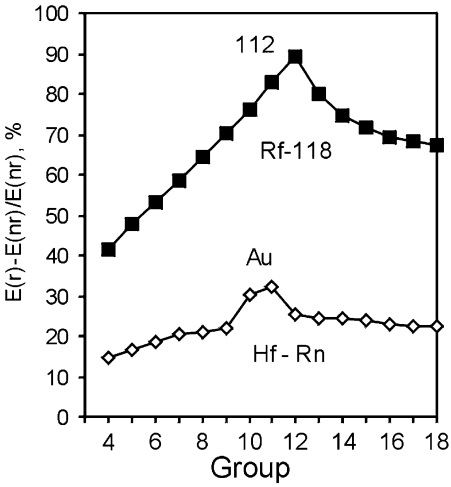

Figure 11-5. The relativistic stabilization of the 6s and 7s orbitals in the sixth and seventh row of the periodic table (Re-drawn from [6]). The DF data are from [45]

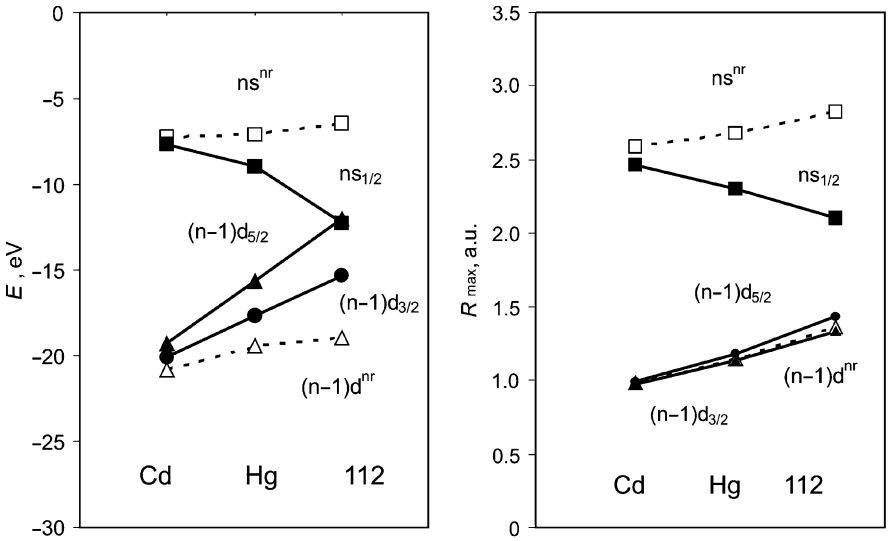

Figure 11-6. Relativistic DF (full lines) and non-relativistic HF (dashed lines) AO energies, E, and radii of the maximum electronic charge density, R_{max}, of the valence AO of group 12 elements [6, 45] (From [46])

The 7s(112) AO stabilization is ∼10 eV, according to the DF calculations [6, 45] (Figure 11-6).

The relativistic destabilization of the 6d AOs increases along the 6d series and reaches its maximum at element 112 with the SO splitting of 3.3 eV (Figure 11-6).

Together with the stabilization of the 7s AOs, this results in the inversion of the 7s and 6d energy levels, so that the first ionized electron of element 112 is $6d_{5/2}$ and not 7s as in Hg. (An inversion of the 7s and 6d levels in the seventh row starts already at Hs.) Figure 11-6 also shows that trends in the relativistic and non-relativistic energies of the ns AOs (the same is valid for the $np_{1/2}$ AOs) become opposite as one proceeds from the sixth to the seventh row of the periodic table, which will result in opposite trends in relativistic and nonrelativistic properties defined by those AOs.

In the 7p series of the elements, the stabilization of the $7s^2$ is so large that it becomes practically an inert pair. The stabilization of the $7p_{1/2}$ AO and the SO splitting of the 7p AOs is also very large for these elements reaching 11.8 eV for element 118. For the heavier elements, relativistic effects on their valence orbitals are even more pronounced and could lead to properties which are very different to those of the lighter homologs. The periodic table up to element 172 and relativistic effects on properties of these elements are discussed in [5].

Breit effects (accounting for magnetostatic interaction) on valence orbital energies and IP of the heaviest elements are small, for example, only 0.02 eV for element 121 [47]. They can, however, reach few % for the fine structure level splitting in the 7p elements and are of the order of correlation effects there. In element 121, they can be as large as 0.1 eV for transition energies between states including f orbitals [47].

Quantum electrodynamic (QED) effects are known to be very important for inner-shells, for example, in accurate calculations of X-ray spectra [48]. For highly charged few electron atoms they were found to be of similar size as the Breit correction to the electron-electron interaction [49]. Importance of the QED effects was also shown for valence ns electrons of neutral alkali-metal and coinage metal atoms: They are of the order of 1–2% of the kinetic relativistic effects there [50]. The result for the valence ns electron is a destabilization, while for $(n - 1)$d electron is an indirect stabilization. In the middle range ($Z = 30$–80) both the valence-shell Breit and the Lamb-shift terms behave similarly to the kinetic relativistic effects scaling as Z^2. For the highest Z values the increase is faster. Nuclear volume effects grow even faster with Z. Consequently, for the superheavy elements its contribution to the orbital energy will be the second important one after the relativistic contribution.

For element 118, QED effects (self-energy and vacuum polarization corrections to the binding energy of the 8s electron) were found to amount to 9% reduction (0.0059 eV) of the EA [51].

11.5. RELATIVISTIC QUANTUM CHEMICAL METHODS

The most appropriate quantum chemistry methods for the heaviest elements are those which treat both relativity and correlation at the highest level of theory. Most of them are described in this volume, as well as they were overviewed recently [52]. Thus, only those which were applied to the heaviest elements and their compounds will be mentioned here.

11.5.1. Atomic Codes

The best theoretical level for the many-body methods if the Dirac-Coulomb-Breit (DCB) Hamiltonian

$$h_{DCB} = h_{DC} + \sum_{i<j} B_{ij}. \tag{11-5}$$

It contains the one-electron Dirac Hamiltonian h_D plus the nuclear potential, V^n, and the operator $V_{ij} = 1/r_{ij}$ for the instantaneous Coulomb interaction between electrons

$$h_{DC} = \sum_i (c\boldsymbol{\alpha}_i \boldsymbol{\rho}_i + (\beta_i - 1)) + V^n + \sum_{i<j} 1/r_{ij}. \tag{11-6}$$

B_{ij} is the Breit term

$$B_{ij} = -1/2[(\boldsymbol{\alpha}_i \boldsymbol{\alpha}_j) r_{ij}^{-1} + (\boldsymbol{\alpha}_i \boldsymbol{r}_{ij})(\boldsymbol{\alpha}_j \boldsymbol{r}_{ij}) r_{ij}^{-3}]. \tag{11-7}$$

The V^n includes the effect of the finite nuclear size, while some finer effects, like QED, can be added to h_{DCB} perturbatively. The DCB Hamiltonian in this form contains all effects through the second order in α, the fine-structure constant. Correlation effects are taken into account by the configuration interaction (CI), many-body perturbation theory (MBPT) and, presently at the highest level of theory, the coupled cluster single double excitations (CCSD) technique.

The Fock-space (FS) DCB CC method [53] is presently the most powerful method which was applied to heavy and the heaviest elements (see the Chapter of E. Eliav and U. Kaldor in this issue). The method has an accuracy of few hundredths of an eV for excitation energies in heavy elements, since it takes into account most of the dynamic correlation (states with high l). Calculations using this method have shown, for example, a principally different ground state electronic configuration of Rf ($7s^2 6d^2$) [54] in contrast to the multiconfiguration (MC) DF calculations ($6d^2 7s 7p_{1/2}$) [55, 56]. The heaviest element treated by this method is 122 [57]. Due to the present limitation of the FS CCSD method in treating electronic configurations with no more than two electrons (holes) beyond the closed shell, the calculations for the middle of the 6d-series (elements 105 through 110) have not yet been performed.

Further developments are under way to remove this limitation. Thus, high-sectors FSCC code is under development which will allow for treating systems with up to six valence electrons/holes in an open shell. Relativistic Hilbert space CC (HSCC) method is also worked on, which could be used for systems with more than a couple of electrons/holes in the active valence shell. The mixed sector CC (MSCC) method will be a generalization of the previous two (FSCC and HSCC) and will combine their advantages.

The DC FS CCSD and CCSD(T) methods incorporated in the DIRAC package [58] have a slightly lower accuracy than the DCB FSCC one. They were used for calculations of properties of the heaviest elements 112 through 118 (see below). The used basis sets are the universal ones [59], those of Visscher [60], and Faegri [61].

The latter proved to be the most suitable for the heaviest elements. The prolapse-free relativistic Gaussian basis sets for the superheavy elements up to Z = 119 suitable for four-component ($4c$) molecular calculations were also published recently [62].

A practical instrument for many-electron open-shell system is the MCDF method [63, 64]. Based on the CI technique, it accounts for most of the correlation effects while retaining a relatively small number of configurations. It omits, however, dynamic correlation which makes it less accurate than the DC(B) CCSD one. Calculations of multiple IPs for Lr through Hs, and of elements 112 and 114 and their homologs were performed with its use [55, 56, 65–69]. Results are discussed below.

Atomic calculations for the heaviest elements were also performed using other approaches. Thus, e.g., the electronic states of element 114 were calculated using the relativistic complete active space MCSCF (CASMCSCF) CI method [70]. Also, many atomic calculations were performed while calculating molecular properties with the use of molecular codes (see below).

Overall, results of the modern accurate atomic calculations agree rather well with predictions made with the use of the earlier DF and DS methods, where the calculated energy terms were corrected by the difference with experiment for the lighter homologs [5]. Elements up to Z = 172 were treated with the use of the latter methods [71]. Element 184 was also considered in [5], as an example of an even heavier element.

11.5.2. Molecular Methods

The most accurate way to solve the Dirac many-electron Eq. (11-5) is that without approximation. Nevertheless, the problems of electron correlation and proper basis sets make the use of *ab initio* DF methods very limited with respect to the heavy-element systems. Most of the molecular *ab initio* DF calculations account for correlation via the CI, Møller-Plesset, MP2, or CCSD(T) techniques [72]. The DC method suitable for molecular calculations is also implemented in the DIRAC package [58]. The basis sets are described in [61].

The *ab initio* DF methods are still too computer time intensive and not sufficiently economic to be applied to the heaviest element systems in a routine manner, especially to the complex systems studied experimentally. Mostly small molecules, like hydrides or fluorides, were studied at this level of theory [73–78]. The main aim of those calculations was to study relativistic and correlation effects on model systems. The DF calculations without correlation were performed for some heaviest element molecules, like $RfCl_4$, $SgBr_6$ or HsO_4 [79, 80], though binding energies are up to 50% inaccurate. Pioneer calculations of Pyykkö and Desclaux for RfH_4 and SgH_6 using the DF one center expansion method should also be mentioned [81].

Effective core potentials (ECP) were successfully applied to the heaviest element systems (see the Chapter of M. Dolg in this issue): the energy-adjusted pseudo potentials (PP) [82] known as Stuttgart ones and the relativistic ECP (RECP) [83].

The PPs were used for calculations of the electronic structures and properties of compounds of elements 111 through 114 [75, 84–87]. Performed at different levels of theory for relativity (HF, spin-average relativistic effective core potentials, AREP, AREP + SO) and correlation (MP2, CCSD(T)), they enabled one to establish the influence of relativistic and correlation effects on properties of chemically interesting molecules and complexes.

The RECP at different levels of theory for correlation (MP2, complete active space MSCF (CAS-MCSCF), CCSD(T)), were also used for a number of chemically interesting gas-phase chlorides and oxychlorides of elements Rf through Sg, as well as for some hydrides and fluorides of the 7p elements including element 118 [88–97]. The RECPs are published by Nash [98]. Generalized RECPs accounting for Breit effects were developed for elements 112, 113 and 114 [99].

The density functional theory (DFT) was applied at most for the heaviest element compounds, complexes in solutions and solid state. Due to its overall simplicity and efficiency of the calculational algorithms, the DFT methods are well suited for treating chemically interesting large systems, adsorption processes, solid state and solutions. (Thus, e.g., the computing time in the DFT for a system of many atoms grows as $N_{at}{}^2$ or $N_{at}{}^3$, while in traditional methods as $\exp(N_{at})$.) The modern DFT theory is exact [100] and the accuracy depends on the adequate choice of the exchange-correlation potential [101].

The Dirac-Slater Discrete Variational (DS-DV) method [102] was extensively used in the past for calculations of ground state properties of the heaviest element compounds — gas-phases molecules and complexes in solutions (see [10] for a review). Even though it was inaccurate with respect to binding energies, it allowed for reliable predictions of ionization energies and character of chemical bonding.

Introduction of the RGGA approximation for the exchange-correlation potential, improvement in the integration scheme and basis set technique [103] allowed for accurate calculations of binding energies and geometry optimization. The most recent version used nowadays for the heaviest element compounds is the 4*c*-DFT one combined with the noncollinear spin-polarized formalism [104] (see examples below). According to this method, the total energy of a molecular system is given by the following expression

$$E = \sum_{i=1}^{M} n_i \langle \phi_i | \hat{t} | \phi_i \rangle + \int V^N \rho d^3\vec{r} + \frac{1}{2} \int V^H \rho d^3\vec{r} + E^{xc}[\rho, \vec{m}] + \sum_{p>q} \frac{Z_p Z_q}{|\vec{R}_p - \vec{R}_q|} \tag{11-8}$$

with the electronic density, ρ

$$\rho(\vec{r}) = \sum_{i=1}^{M} n_i {\phi_i}^+(\vec{r}) \phi_i(\vec{r}) \tag{11-9}$$

and the magnetization density, m

$$\vec{m}(\vec{r}) = -\mu_B \sum_{i=1}^{M} n_i \phi_i^+(\vec{r}) \beta \vec{\Sigma} \phi_i(\vec{r}). \tag{11-10}$$

Here, n_i are the occupation numbers, $\vec{r}$ is the electronic coordinates, respectively, and μ_B is the Bohr-magneton. The index i runs over all occupied molecular orbitals M, which are four-component Dirac spinors. The four-component spin operator $\vec{\sum} = (\sum_x, \sum_y, \sum_z)$ is built from two-component Pauli matrix σ. The Dirac kinetic energy operator has the form

$$\hat{t} = c\vec{\alpha} \cdot \vec{p} + c^2(\beta - I), \tag{11-11}$$

where $\vec{\alpha} = (\alpha_x \alpha_y \alpha_z)$ and β are the four-component Dirac matrices in the standard representation, and I is the four-component unit matrix. V^N is the nuclear potential, E^{xc} is the exchange correlation energy functional and V^H is the electronic Hartree potential

$$V^H(\vec{r}) = \int \frac{\rho(\vec{r'})}{|\vec{r} - \vec{r'}|} d_3\vec{r'}. \tag{11-12}$$

Application of the variational principle with the constraint that the number of electrons in the system should be conserved leads to the single particle Kohn-Sham equations in their non-collinear form

$$\left\{ \vec{t} + V^N + \tilde{V}^H + \frac{\delta E^{xc}[\rho, \vec{m}]}{\delta \rho} - \mu_B \beta \vec{\Sigma} \frac{\delta E^{xc} \lfloor \rho, \vec{m} \rfloor}{\delta \vec{m}} \right\} \phi_i = \varepsilon_i \phi_i \, {}^{i=1\ldots M'} \tag{11-13}$$

Here $\tilde{V}^H$ is the Hartree potentials from the model-density and $M' \geq M$ is the number of molecular orbitals.

Self-consistent, all-electron calculations are performed within the relativistic local density approximation (LDA). The nonlocal corrections (i.e., the generalized gradient approximation, GGA) are then included perturbatively using the Becke 1988 [105] functional for exchange and the Perdew 1986 [106] functional for correlation. Many other functionals are also included in the method, though the B88/P86 one was found to be the most appropriate. (In the following, results of the 4c-DFT calculations will be given for this potential.)

The non-collinear approximation allows the magnetization density to point at any direction at any point of the system under consideration. Accordingly, nearly each electron is treated by its own wavefunction with a quantum number j and magnetic number m_j. This permits treatment of open shell system. (The collinear approximation is also implemented in the method.)

The method uses numerical wave-functions. The basis set optimization procedure is described in [104]. It is developed for very large systems, e.g., clusters with up to more than 100 atoms and is, therefore, suitable for treatment of adsorption process and complex formation.

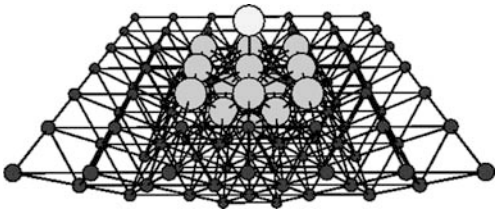

Figure 11-7. Embedded M-M_{14} system

A possibility to treat even a larger number of atoms economically is achieved via the embedded cluster procedure [107] (Figure 11-7).

According to the embedding technique, the total density of a system can be divided into two parts

$$\tilde{\rho}(\vec{r}) = \tilde{\rho}^{cl} + \tilde{\rho}^{env}(\vec{r}). \tag{11-14}$$

The action of the environment on the cluster can be treated as an external potential due to the external charge density $\tilde{\rho}^{env}(\vec{r})$. The external potential V^{ext} is

$$V^{ext} = V^{n}_{ext} + V^{C}_{ext} + V^{ex}_{ext}, \tag{11-15}$$

where V^{n}_{ext} is the Coulomb potential of the nuclei, V^{C}_{ext} is the Coulomb potential of the electronic charge density of the environment, and V^{xc}_{ext} is the exchange-correlation potential. The original KS-equation then reads

$$\left(\hat{t} + V^{n}_{cl}(\rho^{cl}) + V^{C}_{cl}(\rho^{cl}) + V^{xc}_{cl}(\rho^{cl}) + V^{ext}\right)\phi_i(\vec{r}) = \varepsilon_i \phi_i(\vec{r}). \tag{11-16}$$

This equation is solved self-consistently with respect to ρ^{cl} given by Eq. (11-9) where i runs over all cluster electrons. The embedded cluster method was used, e.g., for studying adsorption of Hg and element 112 on gold (see Section 11.7.3.3).

Another 4*c*-DFT method used for some heaviest element compounds is the Beijing one (BDF) [108–111]. It differs from the 4*c*-DFT method [104] by the basis set technique: 4*c*-numerical atomic spinors obtained by finite-difference atomic calculations are used for cores, while basis sets for valence spinors are a combination of numerical atomic spinors and kinetically balanced Slater-type functions. The non-relativistic GGA for the exchange-correlation potentials is used. Results for the same systems, like e.g. $(114)_2$, obtained with the use of the 4*c*-DFT [104] and BDF [111] methods are very similar.

Several quasi-relativistic approximations, e.g., 2*c*-DFT using Douglas-Kroll (DK) approach [112], or zero-order regular approximation (ZORA) [108], also implemented in the Amsterdam density functional (ADF) method [113], were used for the heaviest element compounds as well. The SO ZORA demonstrated very good agreement with the 4*c*-DFT results, as is shown in [108].

Some other methods like, e.g., Douglas-Kroll-Hess [114], were also applied to small heaviest element species. Examples of the calculations with the use of the various methods are considered in the following sections.

11.6. ATOMIC PROPERTIES OF THE HEAVIEST ELEMENTS AND RELATIVISTIC EFFECTS

11.6.1. Electronic Configurations

Results of the atomic relativistic calculations have shown that the relativistic stabilization of the 7s-AO in the seventh row results in the availability of the $7s^2$ electron pair in the ground state of the 6d and 7p elements, $7s^26d^q$ and the $7s^27p^q$, respectively. This is in contrast to the sixth row, where Pt and Au have different, $5d^96s$ and $5d^{10}6s$, ground states, respectively (Table 11-1). The first excited states also differ for the two series: those for the 6d-elements contain the $7s^2$ pair all. Relativistic stabilization of the $7p_{1/2}$ AO results in the ground state of Lr different to that of the lighter homolog Lu (Table 11-1).

It is remarkable that the controversy about ground states of Lr and Rf was finally solved with the use of the DCB FS CCSD method. The DCB CCSD calculations for Lr [115] confirmed the MCDF $7s^27p_{1/2}$ state [116], but corrected the MCDF $7s^27p6d$ one for Rf [55, 56] giving the $7s^26d^2$ state as ground [54]. A very high level of correlation with the $l = 6$ was needed to reach this accuracy. The DF calculations [45] have revealed that element 120 has the $7p^68s^2$ relativistic ground state in difference to the non-relativistic $7p^67d8s$ state [6]. According to the DCB CCSD result [47], element 121 should have a $8s^28p_{1/2}$ ground state (in agreement with earlier DF results [5]) which is 0.4 eV lower in energy than the $8s^27d$ state, which is the ground state for the lighter group-3 homologs. Element 122 should have the $8s^27d8p$ state in contrast to the $7s^26d^2$ state of Th [57]. Thus, the relativistic stabilization of the $8p_{1/2}$ is responsible for this unusual configuration.

For the heavier elements, the older DS and DF [5] data are available. The DFT + QED calculations were recently performed for elements 121–131 [117]. The proximity of the 7d, 6f and 5g levels, and their partial filling makes the usual classification on the basis of a simple electronic configuration difficult, so that the placement of these elements in the periodic table becomes problematic. It will be a challenge for theoreticians to accurately predict electronic states of those superheavy elements.

Table 11-1 Ground state electronic configurations of the 5d and 6d elements. Lu and Lr are also included

Lu	Hf	Ta	W	Re	Os	Ir	Pt	Au	Hg
$5d6s^2$	$5d^26s^2$	$5d^36s^2$	$5d^46s^2$	$5d^56s^2$	$5d^66s^2$	$5d^76s^2$	$5d^96s$	$5d^{10}6s$	$5d^{10}6s^2$
Lr	Rf	Db	Sg	Bh	Hs	Mt	Ds	Rg	112
$7s^27p_{1/2}$	$6d^27s^2$	$6d^37s^2$	$6d^47s^2$	$6d^57s^2$	$6d^67s^2$	$6d^77s^2$	$6d^87s^2$	$6d^97s^2$	$6d^{10}7s^2$

11.6.2. Ionization Potentials, Electron Affinities and Stable Oxidation States

The first IPs of elements 104 through 166 were calculated using the DF and DS methods (see [5] for a review). The multiple IPs of Rf through Hs, and of elements 112 and 114, as well as the first IPs for elements 113–119 were calculated using the MCDF method [56, 65–69, 118]. The DCB CCSD results were reported for IPs of elements 104, 111–115, 121 and 122 [47, 54, 57, 119–123].

The IPs for the seventh row of the elements in comparison with those for the sixth row are shown in Figure 11-8. The values can be found in [8].

Relativistic effects on IPs reflect those on the valence AOs responsible for the ionisation. Thus, the relativistic destabilization of the 6d-AOs is a reason for the first IPs of Rf through Mt being lower compared to the 5d homologs. In elements 110 through 112, the first ionized electron is also 6d in contrast to the lighter homologs Pt through Hg, though the ionisation energies are higher. In elements 113 through 118, the first ionized electron is 7p as expected. A large 7p AO SO splitting explains a drastic decrease in the IP from element 114 to 115 due to the filling of the $7p_{3/2}$ shell for element 115, which is more destabilized than the $6p_{3/2}$ shell of Bi. A large 7p AO SO splitting also explains the smaller IPs of elements 115 through 118 in comparison with their homologs Bi through Rn.

Element 118 is expected to be the most electronegative in the group of the noble gases: Its outer 8s orbital is relativistically stabilized to give the atom a positive EA of 0.058 eV according to DCB CCSD + QED calculations [51, 125]. The inclusion of both relativistic and correlation effects was required to obtain this result. Similar calculations did not give a ^2S bound state for Rn^-. The DC CCSD(T) IP(118) is 8.92 eV [126], the smallest in group 18.

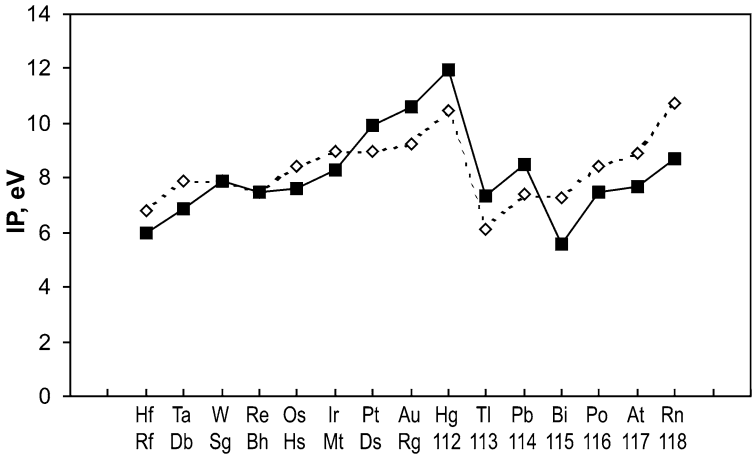

Figure 11-8. Ionization potentials of the sixth row elements (dashed line, experimental values [124]) and the seventh row (solid line, calculated values)

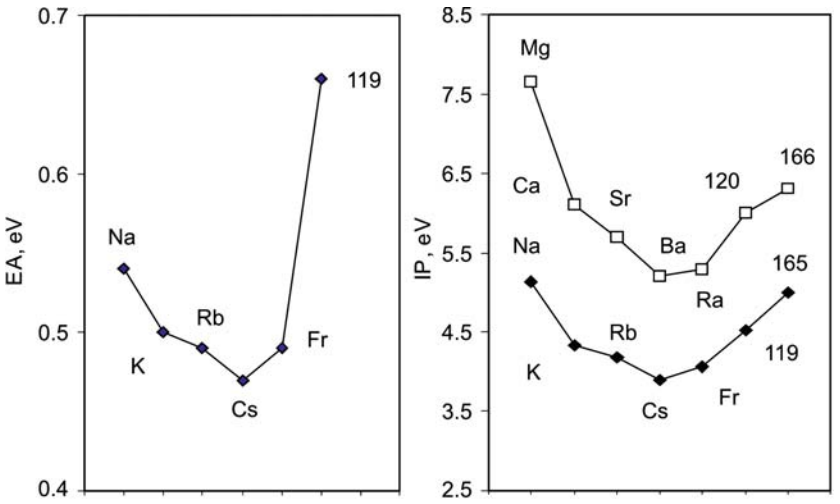

Figure 11-9. Electron affinities, EA, and ionisation potentials, IP, for alkali and alkaline-earth elements. The data for Na through Fr and Mg through Ra are experimental [124]

The relativistic stabilization of the $np_{1/2}$ AOs in group 13 and 14 is also responsible for a trend reversal in the decreasing IPs beyond In and Sn, respectively. Similarly, an upturn in the IPs is observed from Sc to element 119 and Ba to element 120 in group 1 and 2 due to the relativistic stabilization of the outer $ns_{1/2}$ electrons. The IP of element 119 is relativistically increased from 3.31 to 4.53 eV, as DK CCSD calculations show [127].

The decreasing trend in EA in the group of alkali elements from Na to Cs (Figure 11-9) is reversed beyond Cs due to the relativistic stabilization of the 7s(Fr) and 8s(119) AOs.

Due to the relativistic stabilization of the 8s AO, EA(119) is 662 meV, being also the highest in group 1, according to DCB CCSD calculations [128]. The CCSD IP(121) = 4.45 eV and EA(121) = 0.57 eV, the highest in group 3 [47]. The DCB CCSD IP(122) = 5.59 eV [57] as compared to the IP(Th) = 6.52 eV: this relative decrease is due to the relativistically stabilized $8p_{1/2}$ electron of element 122. The DF and DS IPs of even heavier elements can be found in [5].

IPs of internal conversion electrons (1s and 2s) for the element 112, 114, 116 and 118 are predicted to an accuracy of a few 10 eV using DHF theory and taking into account QED and nuclear-size effects [48]. The $K_{\alpha 1}$ transition energies for different ionization states of Mt were accurately predicted using the same approach and compared with recent experiments in the α-decay of ^{272}Rg [129].

The relativistic stabilization of the 7s AO and destabilization of the 6d AOs over the 6d series of the elements results in the increased stability of higher oxidation states, in agreement with the observed trends in the chemical groups. The MCDF calculations of the multiple IPs for elements Rf through Hs [56,65–67] have, indeed, shown a decrease in IP($0 \rightarrow Z^{+}{}_{max}$), as illustrated in Figure 11-10. Due to the same

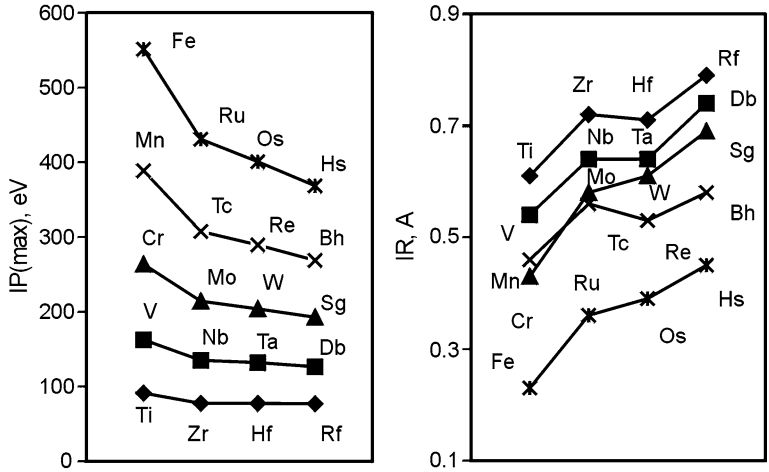

Figure 11-10. Multiple ionization potentials: IP(0 → 4+) for group-4, IP(0 → 5+) for group-5, IP(0 → 6+) for group-6, IP(0 → 7+) for group-7, and IP(0 → 8+) for group-8 elements, as well as ionic radii, IR, for these elements in their maximum oxidation states obtained from the MCDF calculations [56, 65–67] (From [43])

reason, lower oxidation states at the beginning of the 6d series will be unstable: the step-wise ionization process results, for example, in the $6d^2$ and not in the $7s^2$ configurations for Db^{3+} or Sg^{4+}. Since the 6d orbitals of the 6d elements are more destabilized than the (n − 1)d orbitals of the 4d and 5d elements, Db^{3+} and Sg^{4+} will even be less stable than Ta^{3+} and W^{4+}, respectively.

A trend to an increase in the stability of the 3+ and 5+ oxidation states of Rg was also attributed to relativistic effects. Due to a relatively high EA of Rg, the 1− oxidation state may be accessible with appropriate ligands. The 4+ state of element 112 should also be more stable than those of Au and Hg, respectively. The 0 oxidation state will dominate for element 112 due to its closed shell (the EA is 0 [120]).

The large relativistic stabilization of the $7s^2$ electrons and, hence, a large 7s-7p gap hindering hybridization, is the reason for enhanced stability of lower oxidation states at the beginning of the 7p-series. Thus, the 1+ oxidation state will be more important than the 3+ state for element 113. Due to the relativistic stabilization of the $7p_{1/2}$ electrons of element 114, the 2+ state should predominate over the 4+ state to a greater extent than in the case of Pb. The 6d AOs should be still accessible for hybridization for elements 113 and 114 and should take part in bonding leading to the formation of compounds of these elements in higher oxidation states like, e.g., $113F_6^-$ [78] or $114F_6^{2-}$ [77]. For elements 115 through 118, on the contrary, lower oxidation states should be more stable than those of the lighter homologs due to the inaccessibility of the relativistically stabilized $7p_{1/2}$ AO for bonding. For element 115, the 1+ state should be more important due to the SO destabilized $7p_{3/2}$ electron. The 3+ state should also be possible, while 5+ not. For element 116,

a decrease in the stability of the 4+ oxidation state is expected due to a large SO splitting of the 7p AOs, and the 2+ state should be important due to the two destabilized $7p_{3/2}$ electrons. For element 117, the 1+ and 3+ oxidation states should be the most important, while 5+ and 7+ are less. The 1- state of element 117 having one electron hole on the $7p_{3/2}$ AO should therefore be less important (its EA is the smallest in the group). For element 118, 2+ and 4+ states are possible, while the 6+ one will be less important, because of the strong binding of the $7p_{1/2}$ electrons. Oxidation states of heavier elements are discussed in [5].

11.6.3. Atomic/Ionic/Covalent Radii and Polarizability

Atomic (AR) and ionic radii (IR) are defined by the maximum of the radial charge density, $R_{\max}$, of the outer valence AO. The DF $R_{\max}$ values for elements up to Z = 120 were tabulated by Desclaux [45]. The MCDF $R_{\max}$ for Rf through Hs and their lighter homologs in the chemical groups in various oxidation states were calculated by Johnson, Fricke et al. [56, 65–67]. In those works, IR of the transactinides were obtained via a linear correlation between $R_{\max}$ and known IR [130] in the chemical groups. The IR of elements Rf through Hs in the highest oxidation states are shown in Figure 11-10.

Figure 11-10 shows that the IR of the 4d and 5d elements are almost equal due to the lanthanide contraction (of 0.020 Å) which is roughly 86% a nonrelativistic effect: The diminished shielding of the nucleus charge by the 4f electrons causes the contraction of the valence shells. The IR of the transactinides are about 0.05 Å larger than the IR of the 5d elements. This is due to an orbital expansion of the outer $6p_{3/2}$ orbitals responsible for the size of the ions. The IR of the transactinides are, however, still smaller than the IR of the actinides due to the actinide contraction (0.030 Å), being larger than the lanthanide contraction, which is mostly a relativistic effect: The 5f shells are more diffuse than the 4f shells, so that the contraction of the outermore valence shells is increased by relativity to a larger extent in the case of the 6d elements as compared to the 5d elements. The DF and HF calculations [85] for the 5d and 6d elements with and without the 4f and 5f shells, respectively, have shown that the shell-structure contraction is, indeed, enhanced by relativistic effects and that the orbital and relativistic effects are not additive.

A set of atomic single and triple bond covalent radii (CR) for most of the elements of the periodic table including the heaviest ones till Z = 118 and 112, respectively, are given in [131, 132]. They were deduced from the calculated molecular bond lengths of various covalent compounds. The obtained single bond CR for the group 4 through 8 6d-elements are consistent with their IR: they are about 0.06 Å on the average larger than the CR of the 5d elements (Figure 11-11). (The triple bond CR are slightly larger, i.e., 0.08 Å on the average.) An important finding of those works is a decrease in the CR_{6d}-CR_{5d} difference starting from group 9, reaching negative values in groups 11 and 12, as a result of the relativistic bond contraction. This was called a “transactinide break” [132].

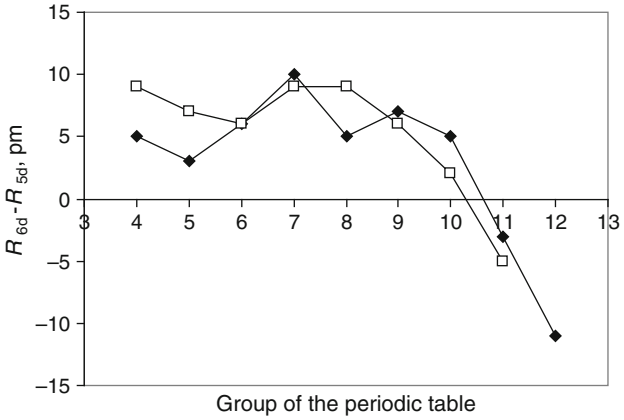

Figure 11-11. The difference in the lengths of the single (filled rhomboids) and triple (open squares) bonds between the 6d and 5d metals [131, 132]

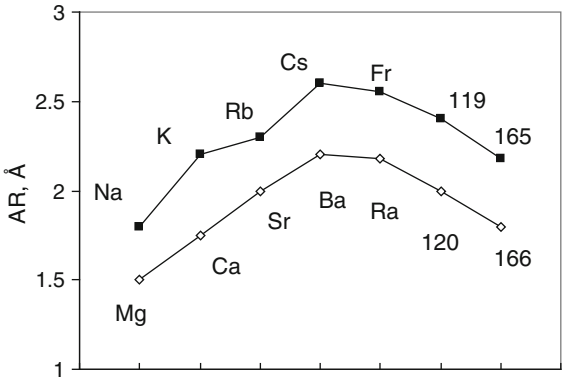

Figure 11-12. Atomic radii, AR, of alkali and alkaline earth elements. The data for Na through Cs and Mg through Ra are experimental. The other data are from DS calculations (Re-drawn from [133])

Thus, the calculations for elements 111 and 112 have shown that they should have the smallest AR and CR in the respective chemical groups due to the relativistic contraction of the 7s AO.

The DS/DF calculations [5] have also shown that within the alkaline and alkaline earth series of elements a reversal of increasing AR occurs beyond Cs and Ba, respectively (Figure 11-12). The shell-contraction effects are, however, much smaller in the group-1 series of elements compared to the group-11 ones.

The static dipole polarizabilities α were calculated most accurately at the DC CCSD(T) level for elements 112 through 118 [126, 134–136]. As a comparison of results of several calculations for Hg and element 112 shows (Table 11-2), relativistic effects significantly decrease α of both species, with the effect being much more

Table 11-2 Polarizabilities, α (in a.u.), of Hg and element 112 calculated within different approximations

Atom	Method	α				Ref.
		HF	MP2	CCSD	CCSD(T)	
Hg	NR	82.25	–	–	37.83	[86]
	PP					
	AR	44.78	28.33	35.26	34.42	[86]
	PP					
	ECP	32.46	27.13	28.82	28.48	[95]
	DC	44.90	27.47	35.31	34.15	[134]
	Exp.	–	–	–	33.91	[137]
112	NR	107.85	–	–	74.66	[86]
	PP					
	AR	29.19	23.57	25.84	25.82	[86]
	PP					
	ECP	30.30	27.67	28.61	28.68	[95]
	DC	29.46	25.11	27.66	27.64	[134]

pronounced for the heavier element (a relativistic decreased from 74.7 to 25.8 a.u., as was shown by the PP CCSD(T) calculations [86]). Correlation also decreases α in both cases much more at the nonrelativistic level.

According to the calculations, α of element 112 should be the smallest in group 12 due to the relativistic contraction of the outer 7s AO. Polarizabilities of elements 113 and 114 are also smaller than those of In and Tl, and Sn and Pb, respectively, which is due to the relativistic stabilization of the outer $7p_{1/2}$ AO (see below). A reversal of the trends in α is observed in group 13 and 14 beyond In and Sn, respectively, similarly to those in AR, or $R_{\max}(np_{1/2})$-AO. Correlation effects on α of group 13 and 14 elements are similar to those of group 12 elements. For elements 115 through 118, α are the largest in the respective chemical groups [136] due to the largest $R_{\max}(np_{3/2})$-AO [45]. The polarizability of element 118 is the largest among all the rare gases [126]. For element 119, α is also relativistically decreased from 693.9 to 184.8 a.u., as calculated at the DK CCSD(T) level. An improved basis set has given l65.98 a.u. for the latter [127].

11.7. GAS-PHASE CHEMISTRY

11.7.1. Rf Through Hs

11.7.1.1. Electronic Structures and Properties of Group 4 Through 8 Compounds

The 4*c*-DFT electronic structure calculations were performed for MF_4, MCl_4, MBr_4(M = Zr, Hf and Rf), MCl_5, MBr_5, $MOCl_3$ (M = Nb, Ta and Db), MCl_6, MO_3, $MOCl_4$, MO_2Cl_2 and $M(CO)_6$ (M = Mo, W and Sg), MO_3Cl (M = Tc, Re and Bh), and MO_4 (M = Ru, Os and Hs) (see [7,43] for reviews) and the RECP ones

for some group 4 through 6 halides and oxyhalides [83, 88]. Covalent compounds of the type MX (X = H, N, B and C) and some others were also considered in various studies (see [131, 132] for a summary). One of the aims of these works was clarifying role of relativistic and correlation effects.

The calculations have shown that the compounds of the heaviest elements are, indeed, homologs of the lighter elements in the chemical groups and that bonding is defined by the valence (n − 1)d AOs. An important finding was an increase in the stability of the maximum oxidation state in the chemical groups. A comparison of the relativistic with non-relativistic results for MCl_5 (M = Nb, Ta and Db) [138, 139], for example, has shown that this is a pure relativistic effect. Relativistic effects increase the energy gap ΔE between the bonding MO of the ligand character and antibonding MO of the (n − 1)d character due to the relativistic destabilization of the (n − 1)d AOs. This results in an increase in the energies of the electron charge-transitions which are associated with the reduction of the metal [139].

The calculations have also shown that relativistic effects are responsible for an increase in covalence of the group 4 through 8 compounds. Figure 11-13 shows relativistic and non-relativistic values of the effective metal charges, Q_M, and overlap populations (OP) obtained from a Mulliken analysis of the electronic density distribution in MCl_5 (M = V, Nb, Ta and Db), as an example [138]. One can see that the relativistic and non-relativistic values are opposite from Ta to Db.

A partial OP analysis shows that this behaviour is due to the opposite relativistic and orbital effects on the ns and $np_{1/2}$ AOs, while in the case of the (n − 1)d AO, relativistic effects enhances the orbital one (Figure 11-14).

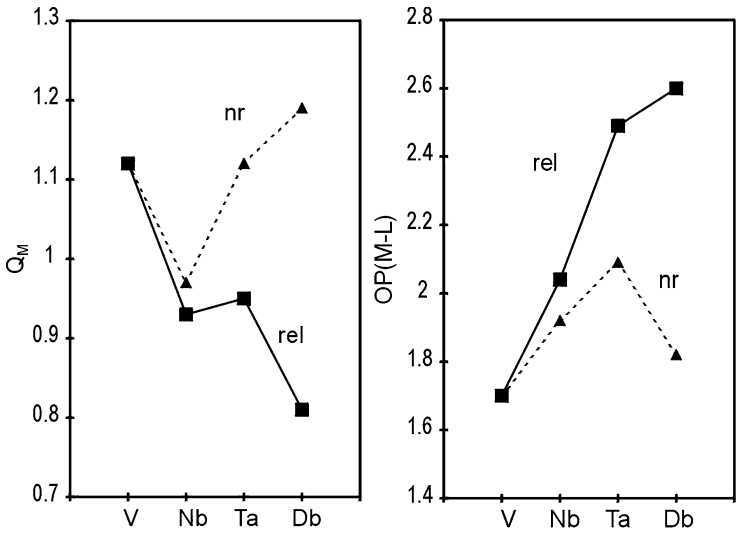

Figure 11-13. Relativistic (solid lines) and nonrelativistic (dashed lines) effective charges, Q_M, and overlap populations, OP, for MCl_5 (M = V, Nb, Ta and Db) [138]. L denotes the ligand (From [43])

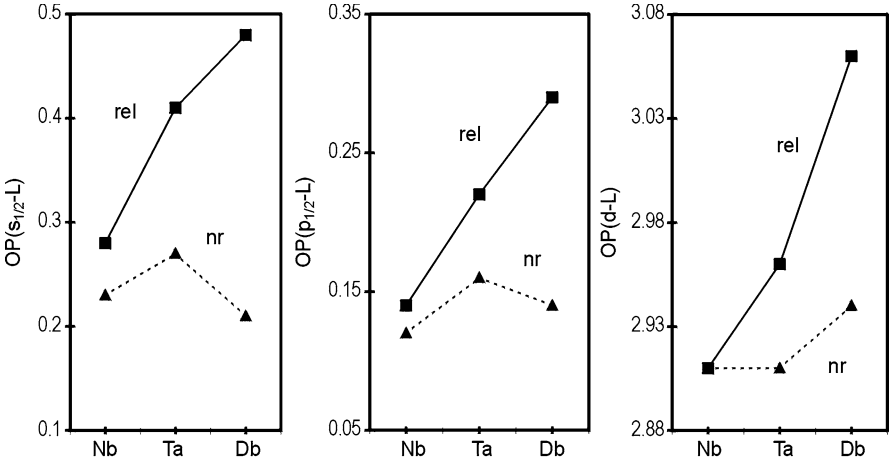

Figure 11-14. Relativistic (solid lines) and nonrelativistic (dashed lines) partial overlap populations in MCl_5 (M = Nb, Ta and Db). L denotes valence orbitals of the ligand. The data are from [138] (From [43])

Table 11-3 Atomization energies of WO_2Cl_2 and SgO_2Cl_2 calculated at various levels of approximation using the RECP method [88]. The additional SO effect is shown in the parentheses

Molecule	HF (AREP)	MP2	CCSD	CCSD(T)	Exp.[a]
WO_2Cl_2	11.7	24.4	20.9	22.1	23.5
SgO_2Cl_2	14.6 (−0.4)	24.8 (−1.3)	21.6 (−1.4)	22.5 (−1.6)	–

[a]Calculated via a Born-Haber cycle

The RECP CCSD(T) calculations for the group 6 oxyhalides [88] without and with SO coupling have shown that a slight decrease in D_e of the 6d compounds with respect to the 5d ones occurs due to the SO splitting of the 6d-AOs. A comparison of the average relativistic HF (AREP) and CCSD values has also demonstrated importance of electron correlation, accounting for about 65% in the D_e of SgO_2Cl_2 (Table 11-3).

Both the 4*c*-DFT [140] and RECP [88] calculations agreed on the most stable type of compound among the group 6 oxychlorides, MO_2Cl_2 (M = Mo, W and Sg). Gas-phase chromatography experiments were then conducted with these species [30]. The DS-DV calculations were performed for $M(CO)_6$ (M = Mo, W, Sg and U) [141]. $Sg(CO)_6$ was found to be very similar to $W(CO)_6$ and different from $U(CO)_6$.

Geometry optimization calculations for various group 4–8 halides, oxyhalides, oxides and other compounds [88, 131, 132, 142–146] have shown that R_e of the 4d and 5d compounds are almost equal as a result of the lanthanide contraction, while those of the 6d compounds are about 0.05–0.06 Å larger (Figures 11-11 and 11-15). The latter is due to the both orbital and relativistic effects on the (n-1)d AOs.

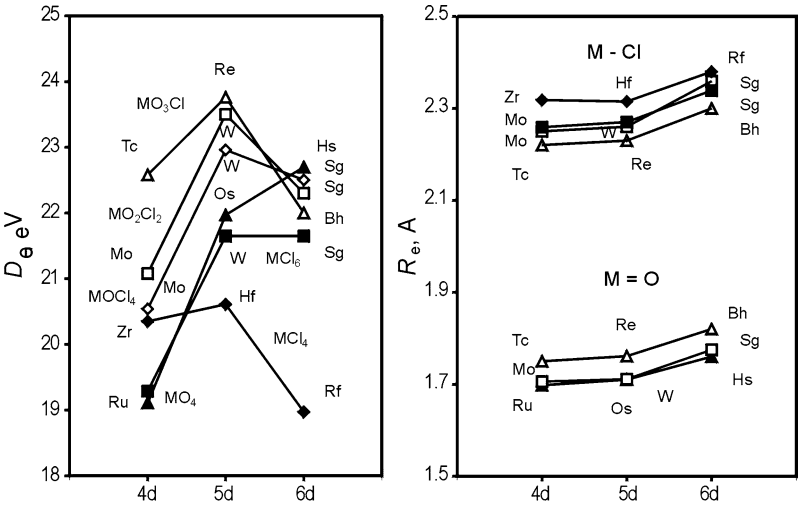

Figure 11-15. The 4*c*-DFT [142–146] and RECP [88] atomization energies, D_e, and optimized bond lengths, R_e, for various gas-phase compounds of group-4 through 8 elements (From [43])

11.7.1.2. Predictions of Experimental Behaviour

Prediction of ΔH_{ads} of a heavy-element molecule on a surface is presently still a formidable task for first principle calculations. A way was, therefore, suggested in [143–146] to obtain it with the use of physisorption models and accurately calculated molecular properties. The models are based on a principle of the molecule-slab interaction, where the interaction is subdivided into usual types for the long-range forces: dipole-dipole, dipole-induced dipole and van der Waals (dispersion) one. Thus, e.g., for a molecule with a dipole moment interacting with a (metal) surface charge Q, the interaction energy is [143]

$$E(x) = -\frac{2Qe\mu_{mol}{}^2}{x^2} - \frac{Q^2e^2\alpha_{mol}}{2x^4} - \frac{3}{2}\frac{\alpha_{mol}\alpha_{slab}}{\left(\frac{1}{IP_{mol}} + \frac{1}{IP_{slab}}\right)x^6}, \qquad (11\text{-}17)$$

where the electric dipole moment, μ_{mol}, IP_{mol} and α_{mol} belong to the molecule, while those with the index "slab" to the surface atom, and x is the molecule-surface separation distance. The latter is well approximated by the van der Waals radius, R_{vdW}.

For a molecule without dipole moment interacting with a dielectric surface, the energy is [144]

$$E(x) = -\frac{3}{16}\left(\frac{\varepsilon - 1}{\varepsilon + 2}\right)\frac{\alpha_{mol}}{\left(\frac{1}{IP_{slab}} + \frac{1}{IP_{mol}}\right)x^3}, \qquad (11\text{-}18)$$

where ε is the dielectric constant of the adsorbent material. All the molecular properties except of x can be accurately calculated using relativistic codes. The x can be deduced from the measured ΔH_{ads} for the lighter compounds using equations of the types (11-17) and (11-18) and the calculated molecular properties. The unknown x values for the heaviest element compounds are then evaluated with respect to the x for the lighter homologs using molecular R_{vdW}. The latter is obtained from the calculated R_e values and radii of the ligand spheres. As an example, the 4*c*-DFT calculated energy contributions to ΔH_{ads} for the group 7 MO_3Cl (M = Tc, Re and Bh) [143] are given in Table 11-4.

On their basis, $-\Delta H_{ads}$ of 78.5 kJ/mol and of 48.2 kJ/mol were calculated for BhO_3Cl and TcO_3Cl, respectively, relative to the measured 61 kJ/mol for ReO_3Cl. This gives a trend in volatility as $TcO_3Cl > ReO_3Cl > BhO_3Cl$. The calculations have shown that this trend is defined by the trend in the dipole moments of these molecules.

Experimental investigations of volatility of the group 7 oxychlorides performed using the isothermal gas-phase chromatography [31] has, indeed, confirmed the theoretically predicted trend (Figure 11-16). Also, the deduced by a Monte Carlo simulation $-\Delta H_{ads}$ of 75 and 51 kJ/mol for BhO_3Cl and TcO_3Cl, respectively, are in perfect agreement with the theoretical values.

Table 11-4 Contributions to the interaction energy, $E(x)$, between the MO_3Cl molecules (M = Tc, Re, and Bh) and Cl^Q (surface) for $Q = -0.4$ (From [143])

	μ-*Q*e	α-*Q*e	α-α(Cl)
Molecule	$E10^{16}x^2$, eV cm^2	$E10^{32}x^4$, eV cm^3	$E10^{48}x^6$, eV cm^6
TcO_3Cl	2.23	5.69	379.1
ReO_3Cl	3.10	6.81	460.6
BhO_3Cl	4.67	8.64	591.2

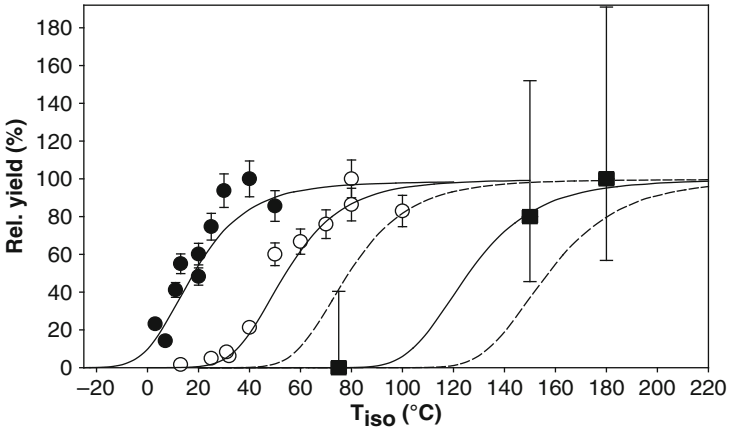

Figure 11-16. The relative yields of TcO_3Cl (filled black circles), ReO_3Cl (open circles) and BhO_3Cl (filled black squares) as a function of the isothermal temperatures, T_{iso} (From [31])

Prediction of the energy of weak interactions of the very similar MO_4 (M = Ru, Os, and Hs) species with an inert surface required, however, a much higher level of accuracy of the calculated properties than in the case of relatively strong dipole-dipole interactions of MO_3Cl (M = Tc, Re and Bh). Thus, the 4*c*-DFT calculations with extremely extended basis sets (e.g., a minimal set plus the 7p7d6f8s8p5g one for Hs) had to be performed to achieve the required accuracy [146] (see Table 11-5 for the calculated and experimental values).

The obtained IP and α for MO_4 (M = Ru, Os and Hs), in perfect agreement with experimental data for the Ru and Os oxides, show a reversal of the trend in group 8, while R_e increases steadily in the group (Figure 11-17).

Table 11-5 Ionization potentials, *I* (in eV), polarizabilities, α (in a.u.), bond lengths, R_e (in Å), vibrational frequencies, *ν*, of the M-O bond (in cm^{-1}), molecule-surface separation distances, *x* (in Å), and adsorption enthalpies, $-\Delta H_{ads}$ (in kJ/mol) on quartz for MO_4 (M = Ru, Os, and Hs)

Property	Method	RuO_4	OsO_4	HsO_4	Ref.
I	Calc.	12.21	12.35	12.29	[146]
	Exp.	12.19	12.35	–	[147]
α	Calc.	58.07	55.28	65.99	[146]
	Exp.	58.64	55.13	–	[137]
R_e	Calc.	1.712	1.719	1.779	[146]
	Exp.	1.706	1.711	–	[148]
ν	Calc.	851	900	989	[146]
	Exp.	880	965	–	[148]
x	Calc.	2.23	2.23	2.25	[146]
$-\Delta H_{ads}$	Calc.	41.0 ± 1	39.0 ± 1	45.4 ± 1	[146]
	Exp.	–	39 ± 1	46 ± 2	[26]

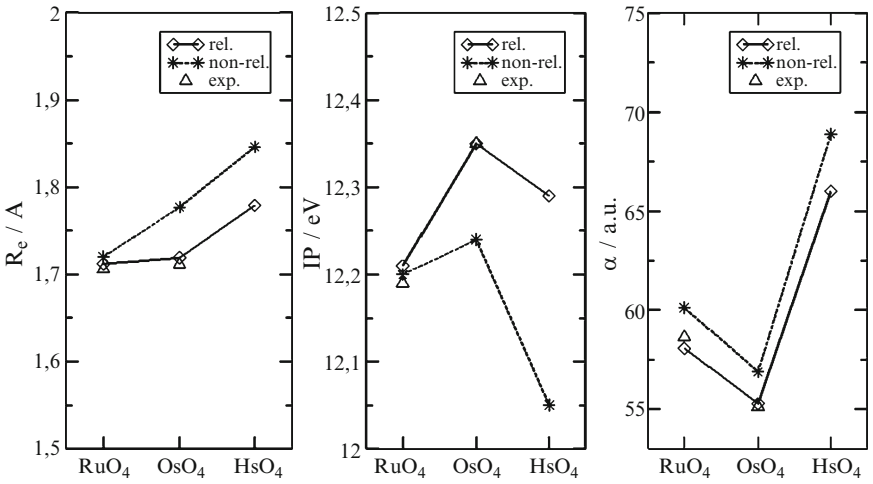

Figure 11-17. Relativistic (rel.) and nonrelativistic (non-rel.) bond lengths, R_e, ionization potentials, IP, and polarizabilities, α, in MO_4 (M = Ru, Os, and Hs) (From [146])

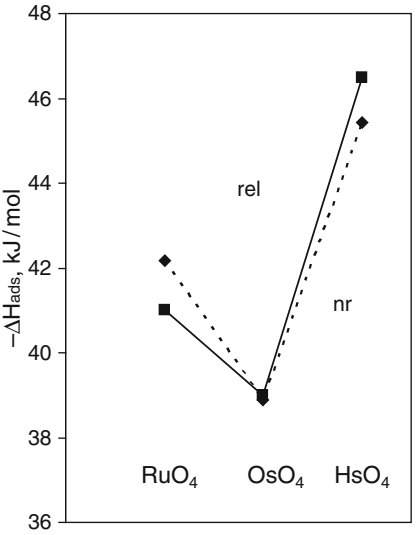

Figure 11-18. Relativistic (solid line) and nonrelativistic (dashed line) adsorption enthalpies of MO_4 (M = Ru, Os, and Hs) on quartz [146]

The trends in these properties proved to be in agreement with the trends in the energies and R_{max} of the (n − 1)d AO in group 8, respectively.

Using the calculated molecular properties and the physisorption model (Eq. 11-18), ΔH_{ads} on quartz (silicon nitride) were calculated for RuO_4 and HsO_4 with respect to OsO_4 (see Table 11-5 and Figure 11-18). They have indicated the same reversal of the trend in group 8 as that in α (Figure 11-17).

Thermochromatography experiments on volatility of OsO_4 and HsO_4 revealed that HsO_4 is, indeed, about 6 kJ/mol stronger adsorbed on the silicon nitride surface of detectors than OsO_4 [26]. (RuO_4 was not experimentally studied due to its decomposition). Also, the measured ΔH_{ads} of HsO_4 is very close to the calculated one (Table 11-5). The experimentally observed adsorption positions of the tetroxides is shown in Figure 11-19.

Thus, both theoretical and experimental studies have established a reversal of the trend in volatility of the group 8 tetroxides in line with the trend in the polarizabilities of these molecules. This remarkable case demonstrates importance of both accurate calculations and statistically meaningful experiments. It also shows that straightforward extrapolations of properties in the chemical groups can be unreliable.

In the same work [146], influence of relativistic effects on spectroscopic properties and volatility of the MO_4 species was studied with the help of additional non-relativistic calculations (Figure 11-17). The non-relativistic values revealed the same trends in group 8 as relativistic, since the orbital and relativistic effects on the (n-1)d-AO act in the same direction. Relativistic effects on ΔH_{ads} were shown to

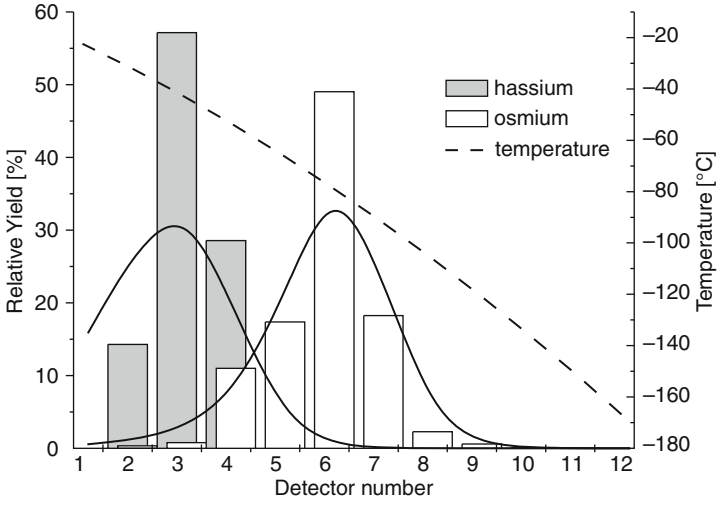

Figure 11-19. Observed adsorption behaviour of OsO_4 and HsO_4 in the gas-phase thermochromatography experiments [26]

be negligible (Figure 11-18). There were some other attempts to interpret volatility of HsO_4 [80,149]. These works reveal, however, some deficiency of the calculations, as discussed in [145].

11.7.2. Rg

In group 11, relativistic stabilization of the ns AO results in the change of the ground state electronic configuration from $d^{10}s^1$ for Cu, Ag and Au to d^9s^2 for Rg [119], which should influence dissociation energies of compounds of these elements. The maximum of relativistic effects on the 7s-shell of Rg in group 11 is also a reason to observe anomalous properties of its low coordination compounds. The large relativistic destabilization and expansion of the 6d AOs is expected to enhance the stability of higher coordination compounds of this element.

A number of molecular relativistic calculations were performed for simple compounds of Rg at various levels of theory. The electronic structure of the simplest molecule RgH, used as a test system for benchmark calculations as AuH, was studied in detail with the use of various methods, DF, DK, PP, and DFT (see Table 11-6). A comparison of the relativistic (ARPP) with the nonrelativistic (NRPP) calculations shows that scalar relativistic effects double D_e, though the SO splitting for the Rg atom ($7s^26d^9$) diminishes it by 0.7 eV (the ARPP CCSD – SOPP CCSD difference) [75]. Thus, the trend to an increase in D_e from AgH to AuH turned out to be inversed from AuH to RgH (Figure 11-20).

The PP CCSD calculations [75] have also shown that the bond in RgH is substantially shortened by relativity ($\Delta R_e = -0.4$ Å) and it is the shortest in the series AgH, AuH and RgH, so that the trend to a decrease in R_e is continued with RgH.

Table 11-6 Bond lengths (in Å) in AuH and RgH

Molecule	R_e	Method	Ref.
AuH	1.5236	Experiment	[150]
RgH	1.499	SO PP CCSD(T)	[75]
	1.523	DHF CCST(T)	[75]
	1.503	SO PP-CCSD(T)	[75]
	1.529	PP CCSD(T)	[151]
	1.506	SC-PP CCSD(T)[a]	[152]
	1.543	ADF ZORA	[131]
	1.546	BDF	[110]
	1.520	4*c*-DFT	[153]

[a]Shape-consistent (SC)

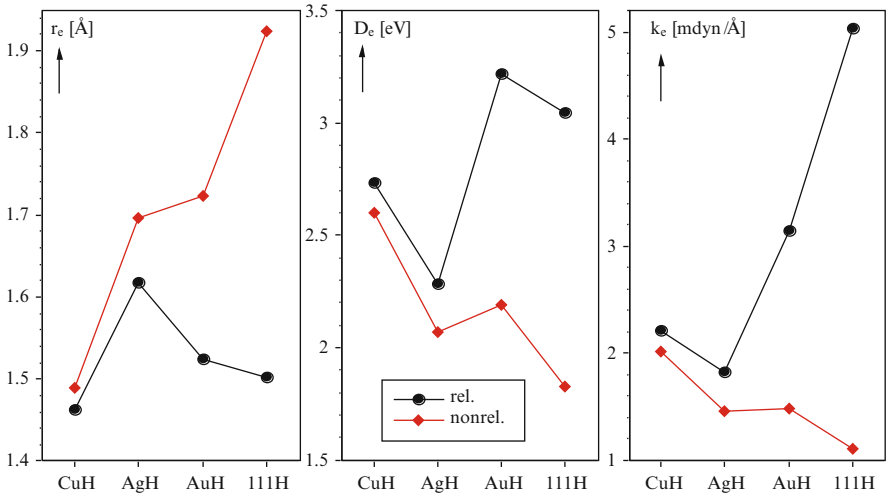

Figure 11-20. Nonrelativistic and relativistic bond lengths, r_e (see also Table 11-6 for various values for RgH), dissociation energies, D_e, and force constants, k_e, of the group-11 hydrides (From [75])

The BDF calculations [110] have, however, revealed that R_e(RgH) is slightly larger than R_e(AuH). The different trends in R_e obtained in these two types of the calculations are obviously connected to a different contribution of the contracted 7s and expanded 6d AOs to bonding (though the 6d contribution was found to be predominant in both cases). Results of various calculations for R_e(RgH) are summarized in Table 11-6 (see also [75, 131]). They indicate that R_e(RgH) should be similar to R_e(AuH).

Both the PP and DFT calculations established that the trend to an increase in k_e is continued with RgH having the largest value of all known diatomic molecules (Figure 11-20).

The μ_e was shown to decrease relativistically from AgH to AuH and to RgH, indicating that RgH is more covalent and element Rg(I) is more electronegative than Au(I). Large SO effects were found on R_e (SO increased) and k_e (SO decreased) [110].

Results of the 4*c*-BDF [110] and 4*c*-DFT calculations [153] for other dimers, AuX and RgX (X = F, Cl, Br, O, Au, Rg), indicate that relativistic effects follow a similar pattern to that for RgH except for RgF and RgO, where the SO splitting increases D_e. The PP calculations for RgH, RgLi and RgF [75] have, however, shown that the SO effects on R_e are very small, but they are large for D_e, decreasing it in all the cases, in difference to the BDF calculations for RgF [110]. The scalar relativistic effects increase D_e(RgLi), but decrease D_e(RgF). They decrease R_e by about 0.4 Å in all the cases. The singlet state was found to be the ground for Rg_2 in comparison to the triplet [153]. The dissociation energy was found to change in the following order: $Au_2 > RgAu > Rg_2$.

To study the stability of higher oxidation states, energies of the $MF_6^- \rightarrow MF_4^- + F_2$ and $MF_4^- \rightarrow MF_2^- + F_2$ (M = Cu, Ag, Au and Rg) decomposition reactions were calculated at the PP MP2 and CCSD levels of the theory [84, 87]. Relativistic effects were shown to stabilize higher oxidation states in the high-coordination compounds of Rg due to a destabilization of the 6d AOs and their larger involvement in bonding. RgF_6^- was shown to be the most stable in this group. SO coupling stabilizes the molecules in the following order: $RgF_6^- > RgF_4^- > RgF_2^-$. This order is consistent with the relative involvement of the 6d electrons in bonding for each type of molecule.

11.7.3. Element 112

It is known that with increasing relativistic stabilization and contraction of the ns AO in group 12, elements become more inert. Thus, bulk Hg is known to be a liquid, however, very different from the condensed noble gases. In the case of element 112, relativistic effects are expected to be further amplified.

Earlier, Pitzer [154] suggested that the very high excitation energy $6d^{10}7s^2 \rightarrow 6d^{10}7s7p_{1/2}$ of about 8.6 eV of element 112 into the configuration of the metallic state will not be compensated by the energy gain of the metal-metal bond formation. An extrapolation of ΔH_{sub} of metals in group 12 has given 22.2 kJ/mol for element 112, which is the lowest in group 12 [155]. The questions to the electronic structure theory, therefore, were: Is element 112 metallic in the solid state, or is it more like a solid noble gas? How volatile and reactive is the element 112 atom in comparison with Hg and Rn?

11.7.3.1. Relativistic Effects on Atomic Properties

Atomic properties of Hg and element 112 were calculated at various levels of theory: 4*c*-BDF with the Perdew-Burke-Ernzerhof (PBE) functionals, and the PB self-interaction correction (PBESIC) [156], QR-PP CCSD(T), ARPP CCSD(T) [86], ECP CCSD(T) [95] and DC(B) CCSD(T) [120,134]. The results are summarized in Tables 11-7 and 11-8.

Table 11-7 Polarizabilities, α (in a.u.), and ionization potentials, IP (in eV), of Hg and element 112

	Hg		112		
Method	α	IP	α	IP	Ref.
4*c*-BDF PBE	35.1	10.61	29.0	11.78	[156]
4*c*-BDF PBESIC	36.4	10.40	29.8	11.40	[156]
QR-PP CCSD(T)	34.2	10.37	28.0	13.17	[156]
AR-PP CCSD(T)	34.42	–	25.82	–	[86]
ECP CCSD(T)	28.48	10.39	28.68	11.675	[95]
DC CCSD(T)	34.15	–	27.64	–	[134]
DCB CCSD	–	10.445	–	11.97	[120]
Exp.	33.919	10.4375	–	–	[137]

Table 11-8 Spectroscopic properties: bond lengths, R_e (in Å), and dissociation energies, D_e (in eV), of Hg_2 and $(112)_2$

	Hg_2		$(112)_2$		
Method	R_e	D_e	R_e	D_e	Ref.
4*c*-BDF PBE	3.439	0.053	3.089	0.156	[156]
4*c*-BDF PBESIC	3.904	0.025	3.363	0.075	[156]
QR-PP CCSD(T)	3.769	0.044	3.386	0.097	[156]
4*c*-DFT(B88/P86)	3.63	0.01	3.45	0.05	[153]
Exp.	3.63	0.043	–	–	[158, 159]

AR was obtained as a half of $R_e[(112)_2]$ (see below) [46, 153]. $R_{vdW}(112) = 3.76 \pm 0.03$ a.u. was estimated with respect to $R_{vdW}(Hg) = 3.95 \pm 0.02$ a.u. [157] using a ratio of their R_{max}(ns)-AOs [45].

Additional non-relativistic calculations [46, 84, 86] have shown that relativistic IP(112) is 4 eV larger than the non-relativistic one, because relativistically, the first ionized electron is $6d_{5/2}$, while nonrelativistically, it is the destabilized 7s one. The α is 45 a.u. decreased due to the relativistic contraction of the 7s AOs. Thus, IP(112) is the largest in group 12, while α is the smallest [46] reflecting the AO energies and R_{max}, respectively (Figure 11-6). Due to the same reason, AR(112) is 0.5 a.u. relativistically contracted and it is the smallest in group 12. The CR show the same trend in the group [131, 132]. The non-relativistic values have opposite trends beyond Cd (Figure 11-21).

11.7.3.2. Volatility as Sublimation: Van der Waals Systems

Homonuclear dimers. The first step to treat the sublimation process of the element 112 "macroamount" is to find out how strong element 112 is bound to itself. Accordingly, calculations of the spectroscopic properties of Hg_2 and $(112)_2$ were performed with the use of various methods: 4*c*-BDF PBE, ECP CCSD(T), QP-PP CCSD(T) [156] and 4*c*-DFT [46, 153]. The results are summarized in Table 11-8.

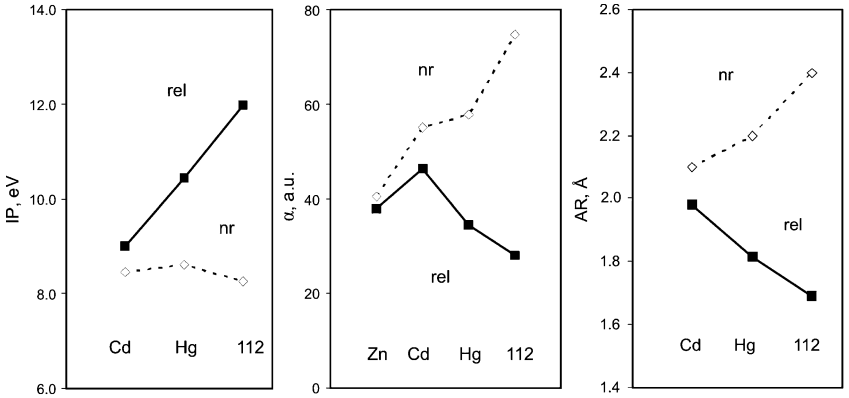

Figure 11-21. Relativistic (solid lines) and non-relativistic (dashed lines) ionization potentials, IP, atomic radii, AR, and polarizabilities, α, of group 12 element [46]

The 4*c*-DFT calculations for $(112)_2$ [153] have shown that the 6d(112)-AOs are active and mixing up with the 7s-AOs in the highest occupied MOs. The 4*c*-DFT $R_e(Hg_2)$ perfectly agrees with the experimental value [158], though $R_e[(112)_2]$ is larger than that of the PP calculations [156]. $D_e(Hg_2)$ is better reproduced by the PP calculations [156], as is expected for the preferentially van der Waals type of bonding. Both the DFT and PP calculations agree on an increase in D_e of about 0.04 eV from the Hg to element 112 dimer with shortening of the bond, in line with the smaller R_{max}[7s(112)] AO with respect to R_{max}[6s(Hg)] AO (Figures 11-22 and 11-6). Thus, due to the relativistic 7s AO contraction $(112)_2$ should be more bound than Hg_2. The PP calculations for Hg_2 [160] have shown that bonding in this molecule is not of pure van der Waals type, and a partial overlap occurs. The same was found for $(112)_2$ [153]. Thus, a half of the $R_e(M)_2$ (M = Hg and element 112) gives, therefore, rather AR than R_{vdW}.

Solid state. The LDA DFT (non-relativistic, scalar relativistic, SR, and 4*c*-relativistic) band structure calculations were performed on the element 112 solid state [161]. It was found that element 112 prefers the *hcp* structure (as that of Zn and Cd) in difference to Hg (*fcc*). Thus, it should differ from its lighter homolog Hg on a structural level and resemble the solid state noble gases. A cohesive energy of 1.13 eV was obtained for element 112 at the SR-level of theory, which is larger than that of Hg (0.64 eV) and is an order of magnitude larger than those of the solid noble gases. This result is consistent with the larger $D_e[(112)_2]$ with respect to $D_e(Hg_2)$ (see Table 11-8). It was concluded that element 112 is not a metal, but rather a semiconductor with a band gap of at least 0.2 eV. (The results of the LDA calculations were considered as a lower bound.) In this sense, element 112 resembles the group 12 metals more closely than it does the noble gases.

Adsorption on inert surfaces. Knowledge of ΔH_{ads} of element 112 on inert surfaces such as quartz and ice was desired for designing gas-phase chromatography

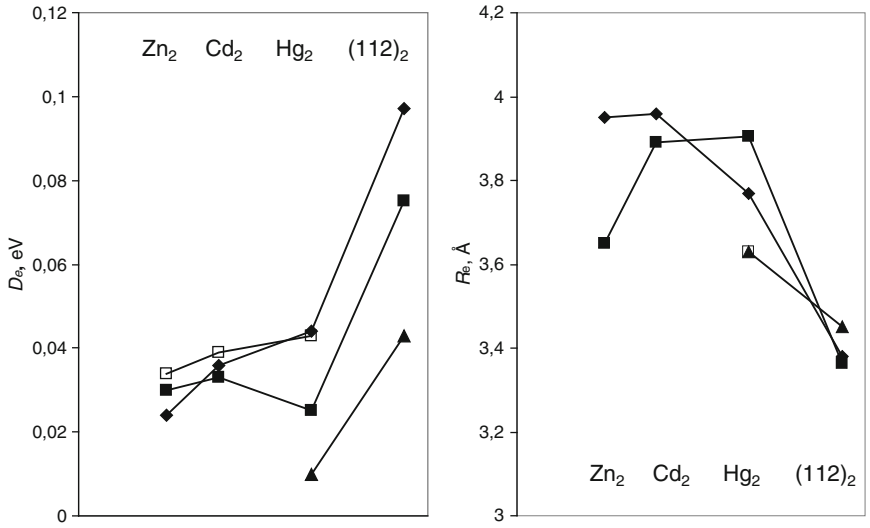

Figure 11-22. The QR PP CCSD(T) (filled rhomboids), 4*c*-BDF PBESIC (filled squares) [156], 4*c*-DFT (filled triangles) [153] and experimental (open squares) dissociation energies, D_e, and bond lengths, R_e, respectively, in the group 12 dimers (see Table 11-8)

experiments. With this aim in view, ΔH_{ads} of Hg and element 112, as well as Rn for comparison purposes, on quartz and ice were calculated using the adsorption model (Eq. (11-18)) and calculated atomic properties [46, 134] (Table 11-7). Since bonding of Hg and element 112 with inert surfaces was assumed to be similar to that in M_2(M = Hg and element 112), x was taken as half of the bond length in M_2, and not as R_{vdW}. The obtained $-\Delta H_{ads} = 40.5$ kJ/mol for Hg on quartz and 25.20 kJ/mol on ice are in very good agreement with the experimental values of 42 ± 2 and 25.5 ± 2 kJ/mol, respectively [162]. For element 112, $-\Delta H_{ads} = 43.2 \pm 0.2$ kJ/mol (for AR) on quartz and $-\Delta H_{ads} = 26.3 \pm 0.1$ kJ/mol on ice were predicted. Thus, element 112 was expected to be somewhat stronger adsorbed on inert surfaces than Hg, i.e., it was expected to be deposited on ice in the thermochromatography column at slightly higher temperatures than Hg.

By using relativistic (vs.) non-relativistic values of the atomic properties (Figure 11-21), influence of relativistic effects on ΔH_{ads} and its trend in group 12 was elucidated [46]. Since α is proportional to 1/IP, the different trends in the relativistic (vs.) nonrelativistic values in the group (Figure 11-21) cancel in the product αIP, so that the trends in the relativistic (vs.) non-relativistic $E(x)$ are finally determined by trends in the relativistic (vs.) non-relativistic x, or AR values. Consequently, the relativistic contraction of the AR (due to the contraction of the 7s(112) AO) results in an increase in $-\Delta H_{ads}$ from Hg to element 112, while non-relativistically, it is the other way around.

An important conclusion for the chemistry is that element 112 is stronger bound by van der Waals forces than Hg both in the homonuclear dimer, solid state and adsorbed state on an inert surface, and this is a relativistic effect caused by the contraction of the 7s AO (see Figure 11-26 below).

11.7.3.3. Volatility as Measured in the Gas-Phase Experiments: Interaction with Metals

In the gas-phase thermochromatography experiments, volatility of element 112, as well as of Hg and Rn, for comparison purposes, was studied as adsorption on gold plated silicon detectors of the chromatography column [27]. Prediction of ΔH_{ads} of these elements on a gold surface was, therefore, desirable.

Heteronuclear dimers. As a first step to study adsorption of Hg and element 112 on noble metal surfaces, electronic structure calculations were performed for HgM and 112M, where M = Ag, Au, Pt, Pd and Cu using the 4*c*-DFT [163]. It was demonstrated that element 112 forms chemical bond with Au primarily due to the interaction between the double occupied 7s(112) AO and the single occupied 6s(Au) AO (see Figure 11-23).

The ground state of 112Au is $^2\Sigma^+$ $d_{Au}{}^{10}\sigma_{Au}{}^2\sigma^*{}_{112}{}^1$. A Mulliken analysis indicates that the σ^* HOMO is a mixture of the 7s(112) and 6s(Au) AOs. Below are two non-bonding π MOs of the $5d_{5/2}$(Au) AOs. The composition of the bonding σ MO lying at −6.76 eV is (in %): (1.2)7s(112) + (4)$6d_{5/2}$(112) + (87)$5d_{5/2}$(Au) + (4)6s(Au). Thus, one can see that the 6d(112)AOs are also active in 112Au. A comparison of D_e(112M) with D_e(HgM) shows that element 112 is about 0.1–0.2 eV weaker bound with a transition metal atom M, depending on the metal, than Hg and the bonds are longer.

Relativistic effects influence on the properties of HgAu and 112Au was investigated via additional nonrelativistic calculations [46]. The results are presented in Table 11-9. Relativistic effects were shown to increase D_e in HgAu by 0.13 eV,

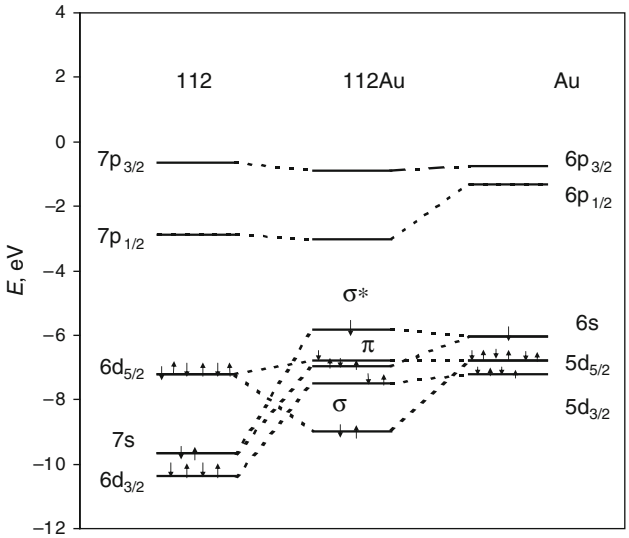

Figure 11-23. Bond formation (principal MOs) of the 112Au molecule

Table 11-9 Nonrelativistic and relativistic spectroscopic properties of AuHg and 112Au: dissociation energies, D_e (in eV), bond lengths, R_e (in a.u.), vibrational frequencies, w_e (in cm^{-1}), effective charges, Q_M, and overlap populations, OP [46]

Molecule	Case	R_e	D_e	w_e	Q_M	OP
HgAu	Nr	5.44	0.36	75.89	0.05	0.44
	Rel	5.04	0.49	102.96	0.10	0.34
112Au	Nr	5.65	0.47	77.19	0.08	0.48
	Rel	5.15	0.36	81.74	0.01	0.24

but decrease it by about the same value (0.12 eV) in 112Au. This makes trends in the nonrelativistic (vs.) relativistic D_e values opposite from HgAu to 112Au, so that $D_e{}^{nr}(112Au) > D_e{}^{nr}(HgAu)$, while $D_e{}^{rel}(112Au) < D_e{}^{rel}(HgAu)$. R_e is decreased by relativistic effects in both systems. The trends are, however, the same both for the non-relativistic and relativistic R_e. Relativistic effects increase vibrational frequencies w_e in each compound, but to a much lesser extent in 112Au than in HgAu, which makes trends in the relativistic and non-relativistic values opposite from HgAu to 112Au. Trends in the relativistic and non-relativistic values of Q_M and OP are also different from HgAu to 112Au: $Q_{Hg}{}^{rel}(HgAu) > Q_{112}{}^{rel}(112Au)$ and $OP^{rel}(HgAu) > OP^{rel}(112Au)$, while $Q_{Hg}{}^{nr}(HgAu) < Q_{112}{}^{nr}(112Au)$ and $OP^{nr}(HgAu) < OP^{nr}(112Au)$.

A partial OP analysis shows that such a decrease in both the ionic and covalent contributions of element 112 to bonding is a result of a decreasing involvement of the relativistically stabilized 7s AO.

Interaction with gold clusters. To proceed further to the description of the adsorption of Hg and element 112 on a gold surface, calculations for metal atom — gold cluster systems were performed using the 4*c*-DFT method [46, 164, 165, 168]. Since the structure of the gold layers covering the silicon detectors is not known, two types of the ideal surface were considered: Au(100) and Au(111). Accordingly, clusters of various size, from very small ones of nine and 14 atoms to very large once of more than 100 atoms (in order to reach the convergence for binding energies with the cluster size), were constructed to simulate these types of surfaces.

For the Au(100) surface, results of the calculations for the M-Au_n and embedded M-Au_nAu_m (M = Hg and element 112, $n_{max} = 36$ and m = 156) systems [165] have shown that element 112 is 0.1–0.3 eV weaker bound with gold than Hg depending on the adsorption position, and that the bridge position should be preferential (Table 11-10). Potential energy curves are shown in Figure 11-24. Using the difference between the calculated $E_b = 1.52$ eV and experimental $-\Delta H_{ads} = 1.03$ eV for Hg on gold [166], $-\Delta H_{ads}(112) = 0.65$ eV of element 112 was given as an early prediction (Table 11-10).

The absolute value of E_b(Hg) in the bridge position on the Au_nAu_m cluster obtained in this way is, however, about 0.5 eV larger than the experimentally observed $-\Delta H_{ads}$(Hg) on gold evidencing that the Au(100) surface is obviously not the one used in the experiments. The LDA DFT calculations [167] demonstrated that

Table 11-10 Calculated binding energies, E_b (in eV), for the M-Au_n and M-Au_nAu_m systems (m = 156), where M = Hg and element 112 [165]

M	E_b(M-Au_n)			E_b(M-Au_nAu_{156})			$-\Delta H_{ads}$
	Top n = 14	Bridge n = 14	Hollow n = 9	Top n = 34	Bridge n = 36	Hollow n = 29	Exp.
Hg	0.86	1.00	0.85	1.02	1.52	0.84	1.03[a]
112	0.71	0.82	0.79	0.65	1.14(0.65)[b]	0.74	0.54[c]

[a]Ref. [166]
[b]Predicted value of $-\Delta H_{ads}$
[c]Ref. [27]

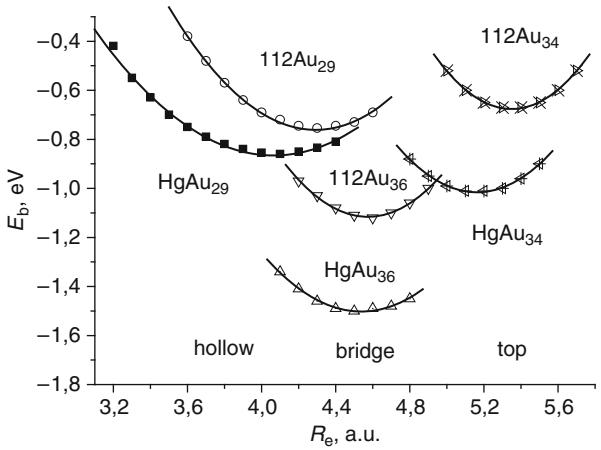

Figure 11-24. The 4*c*-DFT calculated potential energy curves for M-Au_nAu_{156} clusters (M = Hg and element 112) in the three adsorption positions: top, hollow and bridge [165]

Au(111) surface should be about 0.4 eV more stabilized than the Au(100) one. Consequently, $-\Delta H_{ads}$(M) on the Au(111) surface should be about this value smaller, which fits better to the experimental $-\Delta H_{ads}$(Hg) [166].

The 4*c*-DFT calculations for Hg and element 112 interacting with large gold clusters (n = 95 for the top, n = 94 for the bridge, n = 120 for the hollow1 and n = 107 for the hollow2 positions) simulating the Au(111) surface have also been completed [168]. Results show the same relation between E_b of Hg and element 112 as for the Au(100) surface: element 112 is about 0.1–0.2 eV weaker bound to gold than Hg. Overall, E_b with the clusters simulating the Au(111) surface are smaller than those with clusters simulating the Au(100) surface. $E_b(112) = 0.46$ eV.

In the first thermochromatography experiment with element 112 [27], two decay chains attributed to the 112 isotope were observed in two separate experiments with difference temperature gradients. (Earlier, experiments using a slightly different technique were performed, showing that element 112 is very volatile [169].) Later, four more events were observed attributed to element 112 [170]. From the observed

T_{ads}, $-\Delta H_{ads} = 52^{+4}_{-3}$ kJ/mol was deduced using a Monte Carlo simulation. Rn was deposited at the last detectors in the column giving $-\Delta H_{ads} = 20$ kJ/mol. Thus, the experiments demonstrated that element 112 does not behave like Rn. It obviously forms chemical bonding with gold similarly, though weaker than, to Hg. (The deposition of Hg took place right on the first detectors in the column, at the highest temperatures.) This finding was in agreement with the theoretical predictions [163–165, 168] indicating that element 112 is not a rare gas-like, but a 6d-metal-like. Also, the observed and calculated [168] ΔH_{ads} are very close to each other.

In [46], influence of relativistic effects on the adsorption process of Hg and element 112 on metal surfaces was investigated on the example of small metal-gold cluster systems. Two extreme cases were considered: the ad-atom in the top position and in the hollow one: In the first case, the ns and $np_{1/2}$ AOs of the adsorbed atom should be active, while in the second case, the (n-1)d ones. Accordingly, additional non-relativistic calculations were performed for the M-Au_{14} and M-Au_9 systems (Figure 11-25). Results are presented in Table 11-11. They indicate that upon adsorption in the top position, relativistic effects increase E_b by 0.22 eV in $HgAu_{14}$, while they do not increase E_b in $112Au_{14}$ due to the relativistic stabilization of the 7s(112) AO. This is similar to the case of the dimers HgAu and 112Au (Table 11-9). Relations between $E_b(HgAu_{14})$ and $E_b(112Au_{14})$

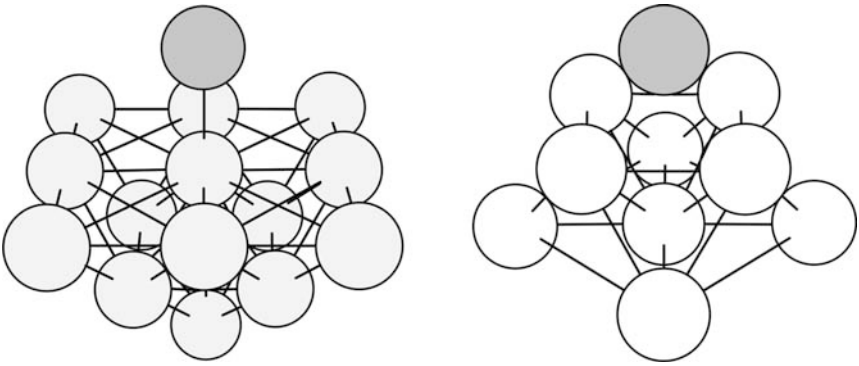

Figure 11-25. The M-Au_{14} and M-Au_9 systems simulating adsorption of M in the top and hollow positions on the Au(100) surface, respectively

Table 11-11 Relativistic and non-relativistic binding energies, E_b (in eV), and the M-Au_n separation distance, R_e (in a.u.), in the M-Au_{14} and M-Au_9 systems [46]

System	Case	M-Au_{14}(top)		M-Au_9 (hollow)	
		R_e	D_e	R_e	D_e
$HgAu_n$	Nr	5.5	0.64	4.6	0.41
	Rel	5.0	0.86	3.8	0.85
$112Au_n$	Nr	5.8	0.70	4.9	0.52
	Rel	5.2	0.71	4.2	0.79

for non-relativistic and relativistic cases are also similar to those for the dimers: $E_b^{rel}(HgAu_{14}) > E_b^{rel}(112Au_{14})$, while $E_b^{nr}(HgAu_{14}) < E_b^{nr}(112Au_{14})$.

For adsorption in the hollow position, even though the trends in E_b are the same as for the top position, e.g. $E_b^{rel}(HgAu_9) > E_b^{rel}(112Au_9)$ and $E_b^{nr}(HgAu_9) < E_b^{nr}(112Au_9)$, relativistic effects increase E_b in both $HgAu_9$ and $112Au_9$. This makes the difference in E_b between $HgAu_9$ and $112Au_9$ (0.06 eV) smaller than for the top position case (0.15 eV). Such a relative small decrease in bonding from Hg to element 112 is connected with the larger involvement of the relativistically destabilized 6d(112) AOs in the hollow position. Relativistic effects were shown to decrease the distance of the ad-atom to the surface, R_e, in all the systems.

To conclude, the relativistic calculations for various M–Au_n (M = Hg and element 112) systems demonstrated that bonding of element 112 with gold is about 20–40 kJ/mol weaker than that of Hg. This is a relativistic effect caused by the contraction and stabilization of the 7s AOs, which is less accessible for bonding than the 6s(Hg) AO. This case is different to the case where element 112 is bound by van der Waals forces, e.g., in the homonuclear dimer, solid state and adsorbed state on an inert surface. There, element 112 is stronger bound than Hg due to the relativistically contracted AR.

Plots summarising all the cases are shown in Figure 11-26. One can see that a linear correlation between ΔH_{sub} and $-\Delta H_{ads}$ (as that used in [170]) is not

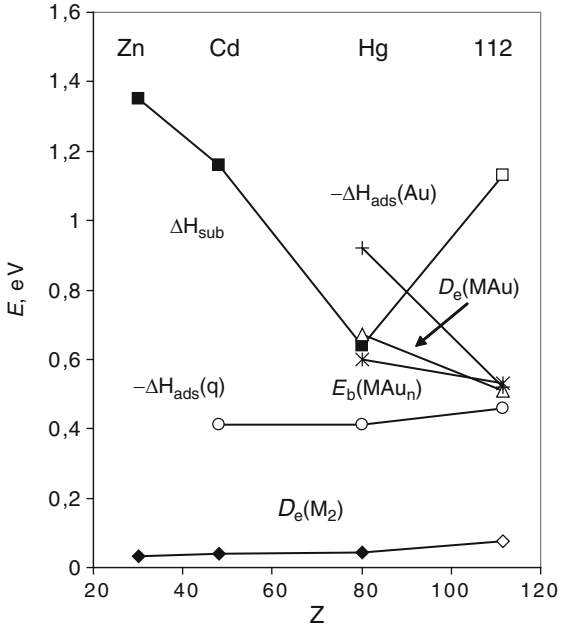

Figure 11-26. Binding energies of group 12 elements in various systems: $D_e(M_2)$ in the dimers M_2 (rhomboids), $-\Delta H_{ads}(q)$ on quartz (circles), $\Delta H_{sub}(M)$ of metals (squares), $D_e(MAu)$ of the dimers MAu (triangles); E_b of M-Au_n (stars); experimental $-\Delta H_{ads}(Au)$ on gold (crosses), where M = Zn, Cd, Hg and element 112. Filled symbols are experiment, open ones are calculations

generally valid, since bonding between atoms of the same type and atoms of various types may be different. Also, ΔH_{sub} of element 112 obtained via a straightforward extrapolation in group 12 is obviously underestimated [155].

The RECP + DFT (SO corrected) calculations for the Hg and element 112 interacting with small gold clusters (n = 1 till 4, and 10) were also reported [171]. Performed at a lower level of theory, they have overall confirmed the earlier 4*c*-DFT results [46, 163, 164]: element 112 should be less bound than Hg with the gold clusters.

11.7.3.4. Other Compounds

The relativistic contraction of the 7s AO is expected to manifest itself also in properties of other element 112 compounds. The PP calculations [86] have shown that the relativistic bond length contraction in $112H^+$ is similar to that in RgH, and that $R_e(112H^+)$ is the smallest among all others, CdH^+, HgH^+ and $112H^+$, and is similar to $R_e(ZnH^+)$, in agreement with the GRECP calculations [172]. (The RECP CCSD(T) calculations [95] for HgH^+ and $112H^+$ have, however, given a larger R_e for the latter compound.) Another interesting point is that, in contrast to the group-11 hydrides, the trend in the dissociation energies from Cd to Hg is continued with element 112, i.e. $D_e(CdH^+) < D_e(HgH^+) < D_e(112H^+)$, but $D_e(AgH) < D_e(AuH) > D_e(RgH)$ [85, 95, 172]. The reason for this difference is greater relativistic effects in $112H^+$ than in RgH.

The second (DK2) and third-order DK (DK3) method was also applied to 112H, $112H^+$ and $112H^-$ [173]. It was shown that scalar relativistic effects on the properties of $112H^-$ are similar to those on 113H and are smaller than those on $112H^+$ and 112H. The DK results for 112H differ, however, from the GRECP ones [172]: according to the former, $R_e(HgH) < R_e(112H)$, and $D_e(HgH) > D_e(112H)$, while the latter give $R_e(HgH) > R_e(112H)$, and $D_e(HgM) \approx D_e(112H)$ (see discussions in [172]).

The destabilization of the 6d AOs should result in their larger involvement in bonding in high-coordination compounds of element 112. Thus, higher oxidation states of element 112 should also be observed. The PP CCSD(T) calculations of the energies of the $MF_4 \rightarrow MF_2 + F_2$ and $MF_2 \rightarrow M + F_2$ (M = Zn, Cd, Hg and element 112) decomposition reactions supported this assumption [86]. The results are presented in Table 11-12 and depicted in Figure 11-27.

Thus, the 2+ state is important for all three molecules, ZnF_2, CdF_2 and HgF_2, though the first two are more stable than HgF_2. The latter decomposes at 645°C. The small energy of the decomposition reaction of MF_2 into M and F_2 confirms the prediction that element 112 will be more inert than Hg, though the difference to Hg is not that large. Comparison with non-relativistic results shows that this is a pure relativistic effect: non-relativistically, $112F_2$ would be by far more stable (comparable to CdF_2) with decomposition energy of 509.8 kJ/mol.

The 4+ oxidation state is not known for Zn, Cd and Hg. Results of the PP calculations suggested that HgF_4 should be thermodynamically stable [174]. The energy

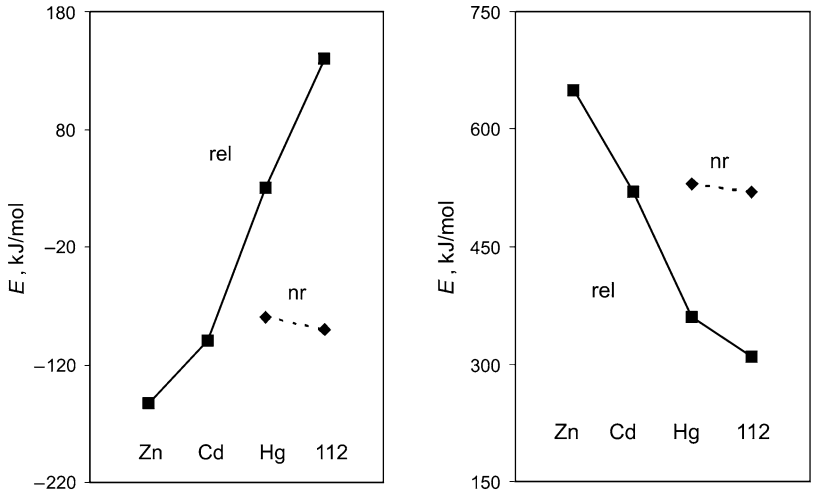

Figure 11-27. Relativistic (solid lines) and nonrelativistic (dashed lines) energies of the decomposition reactions $MF_4 \rightarrow MF_2 + F_2$ and $MF_2 \rightarrow M + F_2$ (M = Zn, Cd, Hg and element 112) (Re-drawn from the data of [86])

Table 11-12 Decomposition reaction energies for the element 112 fluorides (in kJ/mol) obtained in the PP calculations [84, 86]

	$MF_4 \rightarrow MF_2 + F_2$		$MF_2 \rightarrow M + F_2$	
Method	ARPP	NRPP	ARPP	NRPP
CCSD(T) + SO	129.5	–	315.2	–
CCSD(T)	95.0	−93.9	250.1	509.8
HF	66.4	−334.7	248.8	556.5

of the decomposition reaction of $112F_4$ of 129.5 kJ/mol indicates that the molecule should be thermodynamically more stable than HgF_4 (Figure 11-27). However, no definite conclusion about the existence of $112F_4$ can be drawn, since its decomposition energy is between 100 and 200 kJ/mol: experimentally, few compounds with the energy below 100 kJ/mol are known in the solid state. Nonrelativistically, $112F_4$ would be definitely unstable with the energy of the decomposition reaction of −93.9 kJ/mol. SO coupling increases energies of both reactions significantly (Table 11-12).

A Mulliken population analysis for MF_2 and MF_4 (M = Hg and 112) suggests that the 6d AOs of element 112 are involved in bonding to a larger extent than the 5d AOs of Hg [84, 86]. It was also found that the addition of F^- ions to HgF_2 and to HgF_4 is energetically favorable [174]. By analogy, it is assumed that in combination with appropriate polar solvent, $112F_5^-$ and/or $112F_3^-$ may be formed [86].

11.7.4. Element 113

11.7.4.1. Atomic Properties and Volatility

The ground electronic state of element 113 is $7s^2 7p_{1/2}$. The 7s AO is relativistically stabilized to such an extent that it becomes inaccessible for bonding. Properties of element 113 will, therefore, be defined by the $7p_{1/2}$ AO, which is also relativistically stabilized and contracted, not therefore favoring strong covalent bonds.

The best DCB FSCC calculated IP and EA of element 113 are 7.306 and 0.68 eV, respectively [121]. Both quantities are relativistically stabilized and larger than those of Tl of 6.11 and 0.4 eV, respectively (Figure 11-28). The best calculated α of Tl and element 113 are those via the DC FS CCSD method [135] (Table 11-13). The atomic properties were shown to exhibit a reversal of the trend in group 13 beyond In (Figure 11-28). This is caused by the strong contraction and stabilization of the outer $np_{1/2}$ AOs of Tl and element 113. The effect is strongest for element 113,

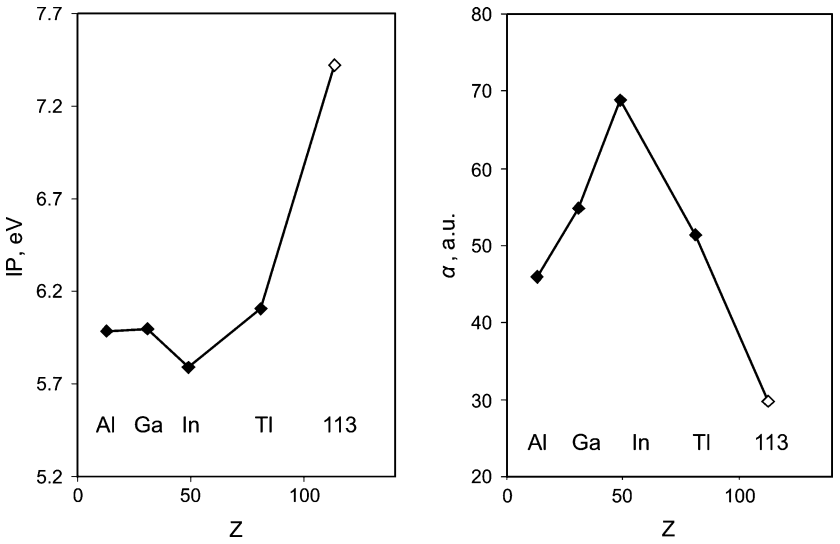

Figure 11-28. Ionization potentials, IP, and polarizabilities, α, of group 13 elements. The data for element 113 are from the DC(B) FSCC calculations [121, 135]

Table 11-13 Selected values of the Tl and element 113 properties: ionization potentials, IP (in eV), electron affinities, EA (in eV), polarizabilities, α (in a.u.), atomic radii, AR, and van der Waals radii, R_{vdW} (in Å)

Element	Method	IP	EA	α	AR	R_{vdW}	Ref.
Tl	Calc.	6.108[a]	0.40(5)[a]	51.29	1.38	1.90	[135]
	Exp.	6.110	0.377(13)	51(7)	–		[137]
113	Calc.	7.306[a]	0.68(5)[a]	29.85	1.22	1.84 ± 0.01	[135]

[a]DCB RCC [121]

resulting in the smallest α, AR and R_{vdW} in group 13 (except for B), while the IP and EA are the largest. R_{vdW} of Tl and element 113 were also obtained in [135] via a correlation of the known R_{vdW} in group 13 with $R_{max}(np_{1/2})$-AO [45].

Results of the best calculations for the properties of Tl and element 113 are summarized in Table 11-13. A comparison with other calculations is given in [135].

As the other 7p-elements, element 113 is expected to be volatile. Its adsorption on quartz and gold is, therefore, to be studied using the same gas-phase thermochromatography technique as that used for element 112 [27]. Test experiments have already been conducted on its nearest homolog, Tl [175]. Knowledge of ΔH_{ads} of element 113 and Tl on gold and ice was, therefore, required. Besides, ΔH_{ads} on Teflon or polyethylene (PE), of which the transport capillaries are made, should be known to guarantee its delivery from the target chamber to the chemistry set up.

In [135], ΔH_{ads} of group 13 elements Al through element 113 on Teflon and PE were predicted with the use of the adsorption model (Eq. (11-18)) and calculated atomic properties (Table 11-13). The obtained ΔH_{ads} are shown in Figure 11-29 where $-\Delta H_{ads}(113) = 14$ kJ/mol on Teflon and 16 kJ/mol on PE. These $-\Delta H_{ads}$ are about 6 kJ/mol smaller than the corresponding Tl values, making possible the separation and identification of the heavier element by the use of these surfaces.

The obtained ΔH_{ads} (Figure 11-29) exhibit a trend reversal beyond In in group 13, as that in the atomic properties (Figure 11-28). The extremely small α of element 113 is the main reason for its very low ΔH_{ads} on inert surfaces. This will allow for easy transport of element 113 through the Teflon capillaries.

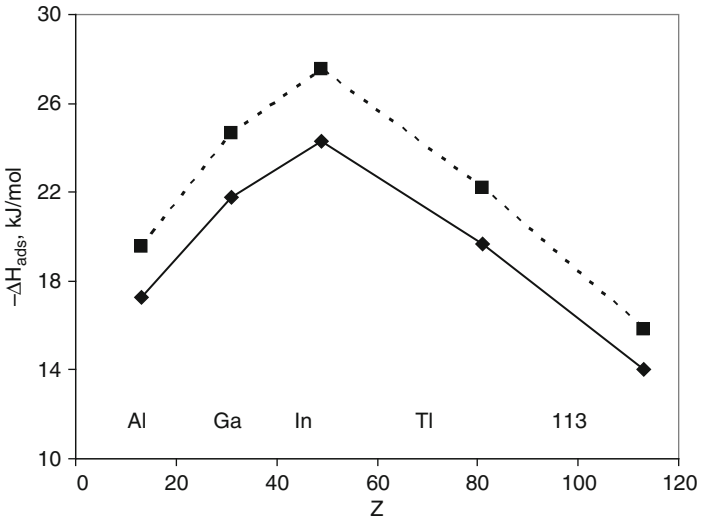

Figure 11-29. Calculated adsorption enthalpies of group 13 elements on Teflon (solid line) and polyethylene (dashed line) (From [135])

11.7.4.2. Properties of Compounds

A very large SO splitting of the 7p AOs is expected to influence properties of compounds of all the 7p elements, 113 through 118. The DFC, PP, RECP and 2*c*- and 4*c*-DFT calculations [78, 89, 91–93, 97, 111, 153, 176] were performed for MH (M = 113–118) and their lighter homologs in the chemical group. One of the aims of the studies was investigation of the influence of relativistic effects on molecular spectroscopic properties.

The 2*c*- and 4*c*-DFT results for 113H [176] are almost identical, and both are similar to the ECP CCSD(T) SO ones [97], as a comparison in [89, 108] shows. According to them, the 6d and 7s AOs participate little in bonding and all the effects are defined by the $7p_{1/2}$ shell. A large relativistic contraction of the $7p_{1/2}$ AO results in a large contraction of the 113-H bond: $\Delta R_e(\mathrm{SO}) = -0.206$ Å according to RECP CCSD(T) calculations [91] and $\Delta R_e(\mathrm{SO}) = -0.16$ Å according to DFC CCSD(T) and PP SO CCSD(T) calculations [78] (Figure 11-30). The RECP CI calculations [93, 97] show similar values. Such a bond contraction is not found in the other MH (M = elements 113–118): For 114H through 118H, both the relativistically contracted $7p_{1/2}$ and expanded $7p_{3/2}$ AOs take part in bonding, with the contribution of the $7p_{1/2}$ AO gradually decreasing along the 7p series, as expected.

In the series of the group-13 hydrides, a reversal of the trend in increasing R_e and μ_e was predicted from TlH to 113H [78, 91]. Element 113 was found to be more electronegative than Ga, In, Tl and even Al. D_e(113H) was shown to be destabilized by the large atomic SO splitting: RECP $\Delta D_e(\mathrm{SO}) = -0.93$ eV [91] and PP $\Delta D_e(\mathrm{SO}) = -0.97$ eV [78], in good agreement with each other. A decreasing trend in D_e and k_e from BH to 113H was predicted.

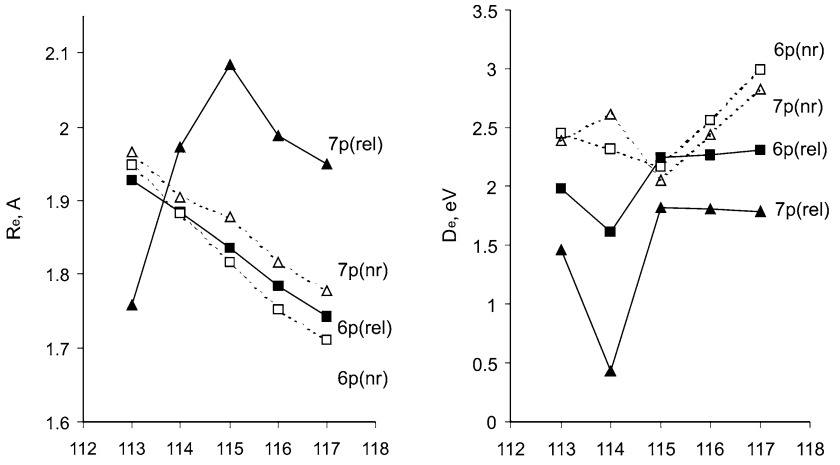

Figure 11-30. Bond lengths, R_e, and dissociation energies, D_e, for the 6p (Tl through At) and 7p (elements 113 through 117) element hydrides, MH [91–93, 111]

The dimer $(113)_2$ should also be weakly bound, as the DF calculations indicated [177]: the $7p_{1/2}$ electron yields a weak bond having $2/3\pi$ bonding and $1/3\sigma$ antibonding character. More recent, the $2c$- and $4c$-DFT calculations [176] have also shown that the binding energy is very small ($D_e = 0.08$ eV and $R_e = 3.51$ a.u. for the ground 1_u state for the BP potential, though the PBESCC result gives the 0_g^+ state as a ground with $D_e = 0.11$ eV and $R_e = 3.744$ a.u.).

The PP, DCB, RECP and $4c$-DFT calculations [78,84,89,153] for MF (M stands for all group 13 metals) have given increasing R_e and μ_e from TlF to 113F, in contrast to the decreasing values from TlH to 113H. These different trends in R_e and μ_e for the MF compounds as compared to MH are explained by a more ionic nature of the MF molecules.

An interesting case of the (113)(117) molecule was studied at the DF level [76]. There, both the low lying $7p_{1/2,1/2}(113)$ AO and the destabilized $7p_{3/2,1/2}(117)$ AO contribute to electron transfer to the group 13 atom. Thus, rather than the single electron of the group 13 atom completing the valence p shell of the group 17 atom, the electron flow is more the other way around: the high-lying $7p_{3/2,1/2}$ shell donates into the low-lying $7p_{1/2,1/2}$ shell of the group 13 atom. This results in a reversal of the dipole direction and a change of the sign of the dipole moment.

As was mentioned earlier, the relativistic destabilization of the 6d AOs is expected to influence properties of high-coordination compounds of element 113. This was confirmed by the PP and RECP calculations [78, 89, 92] for $113X_3$ (X = H, F, Cl, Br and I). As a consequence of the involvement of the 6d AOs, a T-shaped rather than trigonal planar geometric configuration was predicted for these molecules showing that the valence shell electron pair repulsion (VSERP) theory is not applicable to the heaviest elements. Relativistic effects on bond angles were assumed to be small. However, if Jahn-Teller distortions are involved, relativistic effects may significantly change bond angles, as was shown for AtF_3 [178].

The stable high-coordination compound $113F_6^-$ with the metal in the 5+ oxidation state is also foreseen. $113F_5$ will probably be unstable since the energy of the reaction $113F_5 \rightarrow 113F_3 + F_2$ is less than -100 kJ/mol [78]. The calculated energies of the decomposition reaction $MX_3 \rightarrow MX + X_2$ (from M = B, Al, Ga, In, Tl to element 113) suggest a decrease in the stability of the 3+ oxidation state in this group.

11.7.5. Element 114

11.7.5.1. Atomic Properties and Volatility

The electronic ground state of element 114 is a quasi-closed shell $7s^2 7p_{1/2}{}^2$ being a result of the strong relativistic stabilization of the $7p_{1/2}$ AO and a large SO splitting of the 7p AOs (Figure 11-3). Properties of element 114 and its compounds should, therefore, be determined by the relativistically stabilized and contracted, doubly occupied $7p_{1/2}$ AO. It is, therefore, expected to be rather inert and volatile.

Unusual properties of element 114 were predicted as early as in 1970 via an extrapolation in the periodic table [179]: A correlation of ΔH_f of gaseous atoms,

equal to ΔH_{sub} of metals, in group 14 (vs.) a raw of the periodic table has given 41.8 kJ/mol for element 114. A more grounded correlation of ΔH_f (vs.) Z has given a larger value of 71.5 ± 15 kJ/mol [155]. Both values are, however, the smallest among the group 14 elements.

Properties of element 114 predicted on the basis of atomic relativistic calculations also indicate its relative inertness. The DCB CCSD IP(114) = 8.539 eV [122] is in very good agreement with the predicted earlier DF value of 8.5 eV [5]. Polarizabilities of Pb and element 114 were calculated at various levels of theory [95, 134, 180]. The best results [134, 180], in agreement with each other, are shown in Table 11-14 (a more detailed comparison in given in [180]). The DC CCSD(T) value [134] (obtained with an additional 2h function in the basis set) for Pb is in very good agreement with experiment [180] and that for element 114 is recommended.

The SO coupling was shown to lead to a significant reduction of the polarizability of element 114 from 47.9 a.u. at the scalar-relativistic DK level to 31.5 a.u. at the DC level [180].

The data of Table 11-14 demonstrate that the influence of correlation on α of the group 14 elements with the outer $np_{1/2}$ AOs is much smaller than on α of the group 12 elements Hg and element 112 with the outer ns AO (Table 11-2), i.e., −3 a.u. for Pb and +1 a.u for element 114; again, the change is less negative for the heavier atom similarly to Hg and element 112. The polarizability of element 114 proved to be the smallest in group 14 due to the relativistic stabilization and contraction of the outer $7p_{1/2}$ AO (Figures 11-3 and 11-31).

R_{vdW} of element 114 was obtained via a correlation of known R_{vdW} in group 14 with $R_{max}(np_{1/2})$-AO [134]. The best calculated atomic properties for Pb and element 114 are given in Table 11-15.

Using the data of Table 11-15 and the adsorption model (Eq. (11-18)), ΔH_{ads} of group 14 elements on Teflon and PE were predicted [134]. The calculated $-\Delta H_{ads}$ for Pb and element 114 are 27.34 and 20.97 kJ/mol on PE, and 13.65 and 10.41 kJ/mol on Teflon, respectively. The enthalpies show the same reversal of the

Table 11-14 Electronic configurations, basis sets and polarizabilities, α (in a.u.), for Pb and element 114

Atom	Method	Basis set	α				Ref.
			HF	MP2	CCSD	CCSD(T)	
Pb	DC CCSD(T)[a]	26s24p18d13f5g2h	49.91	46.75	46.98	46.96[c]	[134]
	KR CCSD(T)[b]	37s33p25d19f2g	49.71	47.63	47.36	47.34[d]	[180]
	Calc.		–	–	–	45.89	[137]
	Exp.		–	–	–	47.1 ± 7	[180]
114	DC CCSD(T)[a]	26s24p18d13f5g2h	29.78	30.72	30.28	30.59[e]	[134]
	KR CCSD(T)[b]	32s31p24d18f3g	30.13	32.02	31.05	31.49[f]	[180]

[a] DIRAC04 code

[b] DC with Kramers symmetry in the CC procedure

[c,d,e,f] The values with Gaunt contribution are: 47.7; 47.3; 31.87; 31.0, respectively

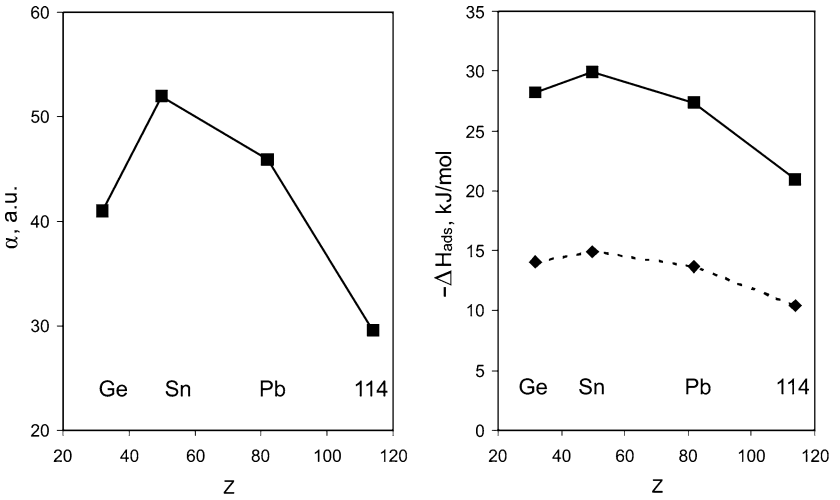

Figure 11-31. The DC CCSD(T) calculated polarizabilities, α, and adsorption enthalpies, $-\Delta H_{ads}$, of the group 14 elements on polyethylene (solid line) and Teflon (dashed line) [134]

Table 11-15 Selected values of the Pb and element 114 properties: ionization potentials, IP (in eV), electron affinities, EA (in eV), polarizabilities, α (in a.u.), atomic radii, AR, and van der Waals radii, R_{vdW} (in a.u.)

Element	Method	IP	α	AR	R_{vdW}	Ref.
Pb	Calc.	7.349[a]	46.96[b]	3.40[c]	4.06[c]	[134]
	Exp.	7.417	47.1 ± 7	3.40	4.16	[137, 180]
114	Calc.	8.539[a]	30.59[b]	3.30[c]	3.94[c]	[134]

[a]DCB CCSD [122]
[b]DC CCSD(T)
[c]Via correlation with $R_{max}(np_{1/2})$

trend as that for the $R_{max}(np_{1/2})$-AO and α of group 14 elements (Figure 11-31). According to these values, element 114 should be well transported from the target chamber to the chemistry set up through the Teflon capillary.

11.7.5.2. Homonuclear Dimers

Keeping in mind that bonding in the homonuclear dimers is a first indication about bonding in the solid state, the calculations of the electronic structures of M_2 (M = Ge, Sn, Pb and element 114) were performed with the use of various methods: 4*c*-BDF [111], 4*c*-DFT [181] and RECP CCSD(T) [95, 111]. The results for Pb and element 114 are summarized in Table 11-16. R_e and D_e for M_2 (M = Ge, Sn, Pb and element 114) are also depicted in Figure 11-32. Except for the calculations [95], performed with insufficiently large basis sets, where $(114)_2$ was obtained too bound, the other calculations agree with each other (see discussion in [181]). All the calculations agree on the fact that $(114)_2$ is stronger bound than a typical van der

Table 11-16 Bond lengths, R_e (in Å), dissociation energies, D_e (in eV), and vibrational frequencies, w_e (in cm^{-1}) of M_2 (M = Pb and element 114)

Molecule	Method	R_e	D_e	w_e	Ref.
Pb_2	ECP CCSD(T)	3.06	0.64	111	[111]
	RECP CCSD(T)	2.98	0.68	–	[95]
	4*c*-BDF	2.98	1.14	108	[111]
	2*c*-DFT SO ZORA	2.97	1.16	106	[108]
	4*c*-DFT	2.97	1.18	107	[181]
	Exp.	2.93	0.86	110	[182]
	Exp.	–	1.17	–	[183]
$(114)_2$	ECP CCSD(T)	3.73	0.07	26	[111]
	RECP CCSD(T)	3.07	0.38	–	[95]
	4*c*-BDF	3.49	0.12	50	[111]
	2*c*-DFT SO ZORA	3.46	0.12	40	[108]
	4*c*-DFT	3.49	0.13	26	[181]

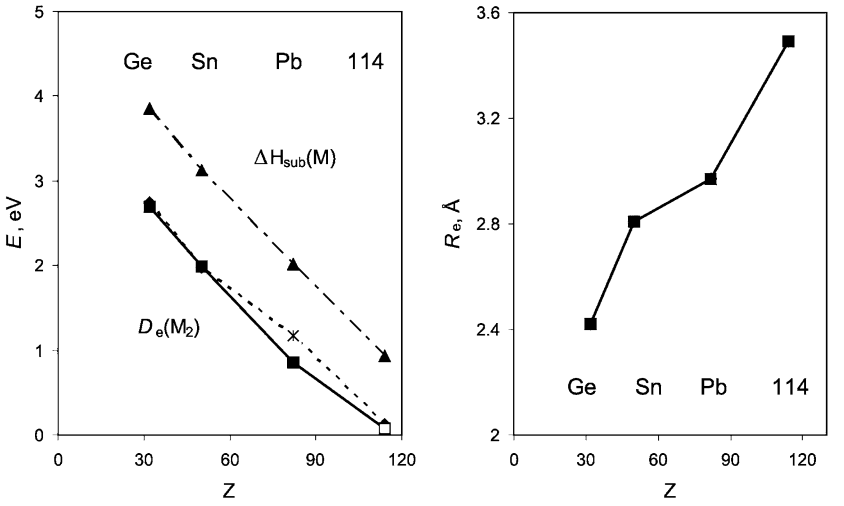

Figure 11-32. Dissociation energies, $D_e(M_2)$ (experimental for Ge_2 through Pb_2: two points for Pb_2 are two different experimental values [182, 183]; and calculated for $(114)_2$: two points are two different types of the calculations, 4*c*-DFT [181] and REC CCSD(T) [111]); sublimation enthalpies, $\Delta H_{sub}(M)$, and calculated bond lengths, $R_e(M_2)$ [181], where M = Ge, Sn, Pb and element 114

Waals system. It is stronger bound than $(112)_2$, but weaker than Pb_2. A Mulliken population analysis indicates that both the $7p_{1/2}$ and $7p_{3/2}$ AO take part in the bond formation: the HOMO of σ character is composed of 98% ($7p_{1/2}$) and 2%($7p_{3/2}$).

D_e and R_e for the group 14 dimers and ΔH_{sub} of the corresponding metals are shown in Figure 11-32.

One can see that the $D_e(M_2)$ and $\Delta H_{sub}(M)$ (M = Ge, Sn, Pb and element 114) plots are parallel (slightly better for the experimental D_e = 0.86 eV of Pb_2 [182])

and follow that of the energy of the $np_{1/2}$(M)-AO (Figure 11-3). This in another evidence that bonding in these species is, indeed, defined by the $np_{1/2}$ AO and its relativistic stabilization with increasing Z in group 14.

Using the correlation between $D_e(M_2)$ and $\Delta H_{sub}(M)$, and the calculated $D_e[(114)_2]$, $\Delta H_{sub}(114) = 1.22$ eV (118 kJ/mol) is predicted. (Using another experimental $D_e(Pb_2)$ value of 1.17 eV [183] for the correlation, $\Delta H_{sub}(114) = 0.80$ eV is obtained.)

11.7.5.3. Intermetallic Systems

Volatility of element 114 as adsorption on a metal surface is supposed to be studied using the same gas-phase thermochromatography column with gold covered detectors, as that used for element 112. (The feasibility experiments with Pb have already been conducted [184].) Accordingly, the 4*c*-DFT electronic structure calculations were performed for the MM′ dimers, where M = Ge, Sn, Pb and element 114, and M′ = Ni, Pb, Pt, Cu, Ag and Au [181]. (All these noble metals were considered, because some of them will be used as electrode materials in the experiments on the electrochemical deposition of element 114 from aqueous solution [34,35].) The obtained spectroscopic properties of PbM′ and 114M′ (M′ = Ni, Pd and Pt; Cu, Ag and Au) are summarized in Table 11-17.

Element 114 was shown to form a rather strong chemical bond with the group 10 and 11 metal atoms. In 114Au, the doubly occupied $7p_{1/2}(114)$ and the single occupied 6s(Au) AO form one double-occupied σ bonding MO and one single-occupied σ* untibonding MO, so that the ground state is $^2\Sigma^+ \; d_{Au}{}^{10}\sigma_{Au}{}^2\sigma \; *_{114}{}^1$. A Mulliken

Table 11-17 Calculated bond lengths, R_e (in Å), dissociation energies, D_e (in eV), and harmonic vibrational frequencies, w_e (in cm^{-1}), for PbM′ and 114M′, where M′ are group 10 and 11 elements [181]

Molecule	R_e	D_e	w_e
PbNi	2.37	1.84	238.9
PbPd	2.50	1.95	201.8
PbPt	2.45	3.53	213.5
PbCu	2.53	1.60	180.5
PbAg	2.67	1.22	231.8
PbAu	2.64	2.15	152.7
		1.29[a]	158.6[a]
114Ni	2.47	0.30	245.7
114Pd	2.69	0.79	137.82
114Pt	2.56	1.11	157.37
114Cu	2.74	0.47	283.6
114Ag	2.95	0.30	151.5
114Au	2.88	0.73	96.70

[a]Spectroscopic measurements (a low limit) [185]

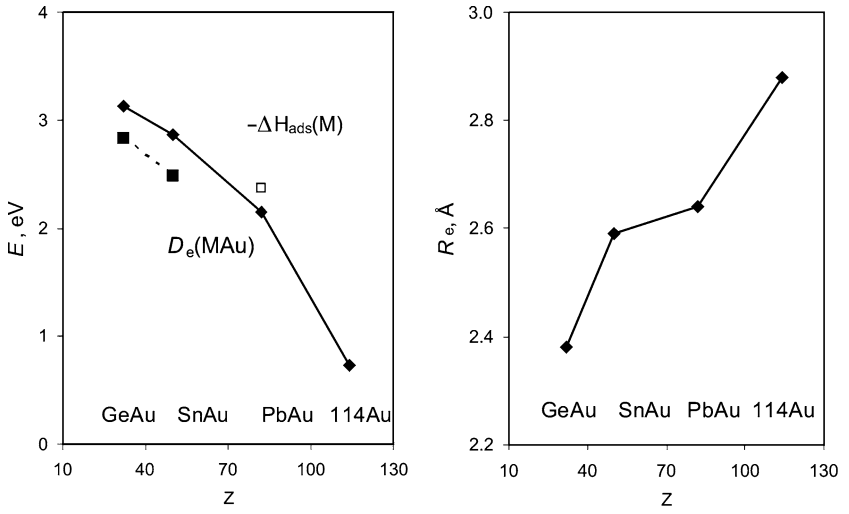

Figure 11-33. Dissociation energies, D_e (solid line – calculations [181], dashed line – experiment), and calculated bond lengths, R_e, in the MAu dimers (M = Ge, Sn, Pb and element 114). The measured $-\Delta H_{ads}$ of Pb on gold [184] is shown with an open square

population analysis shows that both the $7p_{1/2}(114)$ and $7p_{3/2}(114)$ AOs overlap with the 6d(Au) AOs. The type of bonding is similar to that of 112Au, though D_e(114Au) is about 0.2 eV larger than D_e(112Au). Among all the considered metals, bonding with Pt should be the strongest, while with Ag and Ni the weakest. The trends in the D_e and R_e values of PbM′ and 114M′ as a function of M′ were shown to be determined by the trends in the energies and R_{max} of the valence (n-1)d AO of the M′ atoms, respectively, and are similar for PbM′ and 114M′ (except for the Ni dimers) [181].

Figure 11-33 shows D_e and R_e for MAu as a function of Z(M), where M = Ge, Sn, Pb and element 114. The D_e plot has a pattern – a decrease with Z(M) – similar to that for $D_e(M_2)$ (Figure 11-32). This means that in group 14 the type of the M-M bonding is similar to the M-Au one (in difference to group 12): it is defined preferentially by the $np_{1/2}$(M) AO becoming less accessible for bonding with increasing Z (Figure 11-3). The R_e, however, increases with Z(M) due to the involvement of also the $np_{3/2}$(M) AO.

There is one measured value of $-\Delta H_{ads}$(Pb) = 2.37 eV on gold [184]. Assuming, that $-\Delta H_{ads}$(M) correlates with D_e(MAu), as ΔH_{sub}(M) does with $D_e(M_2)$, $\Delta H_{ads}(114) = -0.95$ eV on gold is predicted using the measured $-\Delta H_{ads}$(Pb) and the calculated D_e(114Au). This value is in very good agreement with $-\Delta H_{ads}(114) = 0.97$ eV obtained using semi-empirical models of adsorption on metals [186].

The 4*c*-DFT calculations for Pb and element 114 interacting with large gold clusters simulating the Au(111) surface have also been performed [168]. Results for M-Au_n (M = Pb and element 114, and n = 95 for the top, n = 94 for the bridge,

n = 120 for the hollow1 and n = 107 for the hollow2 positions) indicate that element 114 is about 1.3 eV weaker bound with gold than Pb, similarly to the dimers. A comparison with group 12 elements shows that bonding with gold should change in the following order: 112 < Hg < 114 ≪ Pb, as it was obtained for the gold dimers of these elements. Thus, in the thermochromatography gas-phase experiments, element 114 should be adsorbed at the very beginning of the chromatography column with an entrance temperature of 35°C, similarly to Hg.

At the end of this section, it is worth giving a summary of the predicted adsorption behaviour of elements 112 and 114 on different types of surfaces, since chemical experiments are to be performed using the same chemistry set up and nuclear production mode. Thus, on inert surfaces, element 112 should be 6 kJ/mol stronger adsorbed by van der Waals forces than element 114, since $R_{vdW}(112) < R_{vdW}(114)$. On the contrary, on transition metal surfaces, element 112 should be about 20 kJ/mol weaker adsorbed than element 114 by chemical forces, since the 7s(112) AO is more stabilized than the $7p_{1/2}(114)$ AO.

11.7.5.4. Other Compounds

A decreased involvement of the $7p_{1/2}$ electrons of element 114 in bonding in comparison with lighter homologs in the group was also demonstrated by calculations for other molecular systems. $D_e(114H)$ of about 0.4 eV (0.40 eV for BDF [111] and 0.43 eV for RECP CI [93]) is the smallest in the considered MH series and the smallest in group 14 (Figure 11-30). $D_e(114H)$ was shown to be drastically decreased by the SO interaction ($\Delta_{SO}(D_e) = -2.18$ eV for RECP CCSD(T) [91, 92], −2.07 for RECP CI [93] and −2.02 for BDF [111]). Thus, the small $D_e(114H)$ is a result of both the 7p SO splitting and the double occupancy of the $7p_{1/2}$ spinor. The influence of the SO interaction on R_e is relatively small (Figure 11-30) due to the contribution of both the contracted $7p_{1/2}$ and expanded $7p_{3/2}$ AOs. This is also, obviously, the reason why $R_e(114H) = 1.96$ Å is larger than $R_e(PbH) = 1.88$ Å [91, 92]. The RECP CCSD(T) calculations [95] for PbH^+ and $114H^+$ have also given a 0.48 eV stronger bond in the latter molecule, though 0.18 Å shorter. The CAS-SCF/SOCI RECP calculations for $114H_2$ demonstrated breakdown of the conventional singlet (X^1A_1) and triplet ($^3B_1$) states due to large relativistic effects including SO ones [187]. The SO effects are shown to destabilize $114H_2$ by almost 2.6 eV.

Results of an earlier work [188] (based on atomic calculations) on the stability of some 114^{2+} and 114^{4+} compounds also lead to the conclusion of a lower reactivity of element 114. All tetravalent compounds were considered to be unstable towards decomposition. Some divalent inorganic salts were predicted to be, however, stable.

The electronic structures of 114X (X = F, Cl, Br, I, O) and $114O_2$ were calculated using the 2*c*-RECP CCSD(T), 2*c*-DFT SO ZORA and 4*c*-BDF methods [108, 111]. Better agreement with experiment for the known compounds of Pb was shown by the RECP CCSD(T) values. Trends in R_e and D_e for the halides and oxides from Pb to element 114 were found to be similar to those for the hydrides. In contrast to PbO_2 ($D_e = 5.60$ eV), $114O_2$ ($D_e = 1.64$ eV) was predicted to be

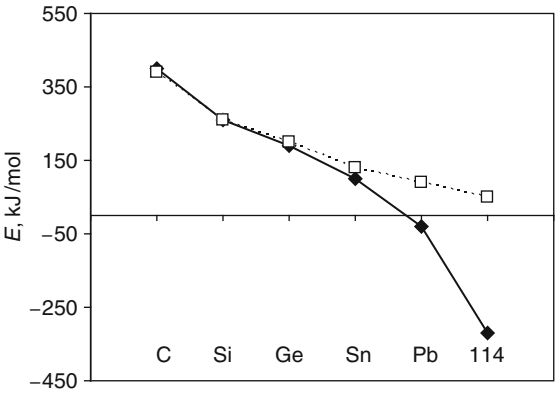

Figure 11-34. Relativistic DFC (solid line) and nonrelativistic HF (dashed line) calculated energies of the reaction $MH_4 \rightarrow MH_2 + H_2$ (M = C, Si, Ge, Sn, Pb and element 114) (From [77])

thermodynamically unstable with respect to the decomposition into the metal atom and O_2. Using results of these calculations, it was shown that element 114 should not react with O_2 at the experimental conditions [134].

The *ab initio* DF and PP calculations [76,77,84] for the decomposition reactions $MX_4 \rightarrow MX_2 + X_2$ and $MX_2 \rightarrow M + X_2$ (M = Si, Ge, Sn, Pb and element 114; X = H, F and Cl) also predicted a decrease in the stability of the 4+ oxidation state in agreement with earlier works [5]. The instability was shown to be a relativistic effect (see Figure 11-34 for MH_4, as an example). The neutral state was found to be more stable for element 114 than that for Pb. As a consequence, element 114 is expected to be less reactive than Pb, but about as reactive as Hg. This is similar to the predicted adsorption behaviour of the elements on gold: element 114 should be much weaker adsorbed than Pb, but slightly stronger than Hg. The possibility of the existence of $114F_6^{2-}$ was suggested [77].

11.7.6. Elements 115–118

11.7.6.1. Chemical Properties of Elements 115–117

Element 115 and 116. The chemistry of elements 115 and 116 has received little attention so far, though it is expected to be very interesting due to strong SO effects in the 7p AOs. Early studies based on extrapolations of properties and atomic DF calculations are summarized in [5,189].

The 4*c*-BDF and SO ZORA calculations were performed for 115H and $(115)_2$ in good agreement with each other [108,176]. The same 0_g^+ ground state was found for Bi_2 and $(115)_2$. The 115 dimer was found to be weaker bound than the Bi one: $D_e(115_2) = 0.83\,\text{eV}$ and $R_e = 3.08$ Å, while $D_e(Bi_2) = 2.45\,\text{eV}$ and $R_e = 2.69$ Å. Bonding in $(115)_2$ should be stronger than in $(113)_2$ and $(114)_2$.

Results of the RECP and BDF calculations [91,93,111] for R_e and D_e of 116H and PoH and influence of relativistic effects are shown in Figure 11-30. It was found that $D_e(\text{PoH}) > D_e(116\text{H})$, and $R_e(\text{PoH}) < R_e(116\text{H})$. Relativistic effects increase

R_e(116H) and decrease D_e(116H), as discussed in Section 11.7.4.2. The RECP were also applied to $116H_2$ [96]. The SO interaction was found to lengthen the 116-H bond and lead to a significant H-116-H bond angle increase in comparison with PoH_2. It was suggested that the result is a rehybridization of the valence 7p AO with a "supervalent" 8s AO of element 116.

A hypothesis of the decreasing stability of the 4+ oxidation state of element 116 was supported by estimates of formation enthalpies of MX_2 and MX_4 (M = Po and element 116; X = F, Cl, Br, I, SO_4^{2-}, CO_3^{2-}, NO_3^- and PO_4^{3-}) using results of the atomic MCDF calculations [188]. The chemistry of element 116 is expected to be mainly cationic: an ease of formation of the divalent compounds should approach that of Be or Mn, and tetravalent compounds should be formed with the most electronegative atoms, e.g., $116F_4$.

Element 117. The DF and RECP molecular calculations have shown that element 117 forms H117 by analogy with the other group-17 halogens [74, 92]. The bond in H117 should be weaker than in the other HM compounds (M = group 17 elements) in line with a decreasing trend in group 17. The bond length should be larger in H117 than in HAt, also in line with the trend (Figure 11-30). The reason for that is a decreasing contribution of the $np_{1/2}$ AO with increasing Z(M) in the group: bonding in H117 is formed predominantly by the $7p_{3/2}$ AO and is, therefore, 2/3 of the bonding of the 7p AOs without SO splitting. The DHF [74] and RECP [92] calculations for H117 have given the SO effects on R_e as 0.13 and 0.17 Å, respectively.

Analogously to the lighter homologs, element 117 should also form the dimer $(117)_2$. The DCB CCSD(T) calculations for X_2 (X = F through At) [190] found a considerable antibonding σ character of the HOMO of At_2 due to SO coupling (without the SO coupling, it is an antibonding π orbital). Thus, bonding in $(117)_2$ is predicted to have considerable π character. 117Cl is also predicted to be bound by a single π bond with a SO increased bond length [191]. The IF, AtF and 117F molecules were also considered at various levels of theory: DC and RECP plus HF/MP2/CCSD/CCSD(T) [83]. D_e(117F) was shown to be the largest among the group 17 fluorides. It was found that D_e(117F) is 0.1 eV increased by SO effects in contrast to the other group 17 fluorides. The SO effects are opposite for all the three spectroscopic constants for 113F and 117F. The RECP calculations have shown that the D_{3h} geometry is not the proper one for the $117F_3$ molecule, in difference from the sixth period compound of At, thus again indicating that the VSERP theory is not applicable to the heaviest elements.

11.7.6.2. Chemistry of Element 118

The chemistry of element 118 should be interesting due to the very large SO splitting of the 7p AO of 11.8 eV [45]. The destabilization of the four $7p_{3/2}$ electrons suggests that element 118 should be relatively reactive, in line with an increasing trend in the reactivity in group 18. It should also be the most electronegative element among the rare gases due to the relativistic stabilization of the 8s AO. (The DCB CCSD + QED calculations has given EA(118) = 0.058 eV [51].) The DC CCSD(T) α(118)

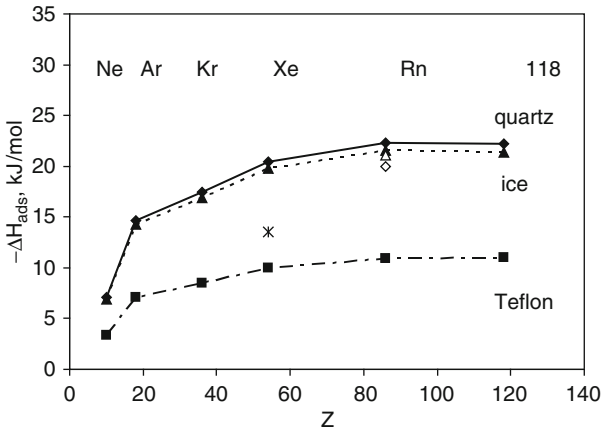

Figure 11-35. Calculated adsorption enthalpies of the noble gas atoms on quartz (rhomboids, solid line), ice (triangles, dashed line) and Teflon (squares, dashed-dotted line). Experimental data are: for Rn on quartz (an open rhomboid [192]) and ice (an open triangle [162]); for Xe on ice (a star) [193] (From [126])

= 46.3 a.u. is the largest in group 18, as also AR = 4.55 a.u., while IP = 8.92 eV is the smallest [126]. (The RECP + CCSD(T) $\alpha(118) = 52.43$ a.u. is overestimated due to the smaller basis set [95].) These extreme values reflect, in addition to the general trends in the periodic table, the relativistic expansion and destabilization of the outer valence $7p_{3/2}$ AO.

Volatility. Using calculated atomic properties and the adsorption model (Eq. (11-18)), van der Waals coefficients C_3 and ΔH_{ads} of Ne through element 118 on noble metal and inert surfaces, such as quartz, ice, Teflon and graphite, were calculated [126] (Figure 11-35).

The C_3 coefficients were shown to steadily increase in group 18, while the increase in $-\Delta H_{ads}$ from Ne to Rn does not continue to element 118: The larger AR of element 118 is responsible for its equal ΔH_{ads} with Rn. It was, therefore, predicted that experimental distinction between Rn and 118 by adsorption on these types of surfaces will not be feasible. A possible candidate for separating the two elements is charcoal; further study is needed to test this possibility.

Chemical compounds. As was mentioned above, the destabilization of the $np_{3/2}$ AOs should also result in the increasing stability of the 2+ and 4+ oxidation states in group 18. The RECP calculations for the reactions $M + F_2 \rightarrow MF_2$ and $MF_2 + F_2 \rightarrow MF_4$, where M = Xe, Rn and element 118, confirmed an increasing stability of the fluorides in the raw, as a result of the increasing polarizability of the central atom [83,89]. The SO effects were shown to stabilize $118F_4$ by a significant amount of about 2 eV, though they elongate R_e by 0.05 Å. Thus, the trends in increasing R_e and D_e are continued with element 118. Also, the following trends in the stability of the fluorides were established: $RnF_2 < HgF_2 < PbF_2$, while $112F_2 < 114F_2 < 118F_2$.

Influence of the SO interaction on the geometry of MF_4 was investigated by the RECP-SOCI [94, 194] and RECP CCSD calculations [89]. It was shown that a D_{4h} geometrical configuration for XeF_4 (calculated in agreement with experiment) and for RnF_4 (calculated) becomes slightly unstable for $118F_4$. A T_d configuration becomes more stable than the D_{4h} one in $118F_4$ by 0.25 eV [94, 194] or 0.17 eV [83, 89]. The reason for this unusual geometry was the availability of only the stereochemically active $7p_{3/2}$ electrons for bonding. This is another example of the inapplicability of the VSERP theory for the heaviest elements. An important observation was made that the fluorides of element 118 will most probably be ionic rather than covalent, as in the case of Xe. This prediction might be useful for future gas-phase chromatography experiments.

The RECP calculations [92] for 118H have shown the van der Waals bond to be stabilized by about 2.0 meV by SO effects with $\Delta R_e(\mathrm{SO}) = -0.019$ Å. Trends in the stability of hydrides was predicted as follows: RnH << HgH < PbH, 118H << 114H < 112H. The RECP calculations for a single-charge ions give $D_e(\mathrm{RnH}^+) > D_e(118\mathrm{H}^+)$ and $R_e(\mathrm{RnH}^+) < R_e(118\mathrm{H}^+)$ [95].

11.7.7. Elements with Z > 118

From element 122, a very long, unprecedented transition series that is characterized by the filling of not only 6f but also 5g AOs with partially filled $8p_{1/2}$ AO begins. These elements were called "superactinides" by Seaborg in 1968 [13]. Quite a number of theoretical calculations of the ground state electronic configurations were performed for this region (see [5] for a review and a recent work [117]). At the beginning of the superactinides, not only two but four electron shells, namely $8p_{1/2}$, $7d_{3/2}$, $6f_{5/2}$ and $5g_{7/2}$ are expected to complete simultaneously. These open shells, together with the 8s electrons, will determine the chemistry. According to the DS calculations, the g electrons appear in element 125 [5], while the relativistic DFT with QED corrections (Breit interaction) [117] found that g electrons in the atom first appear from element 126. It was also shown that the QED corrections are important for studying electronic configurations of superheavy elements. Even more accurate *ab initio* calculations are needed to accurately predict electronic states of those elements.

Due to the very strong relativistic effects, the chemistry of those elements will be much more different to anything known before. However, without relativistic effects, it would also be very different due to the very large orbital effects. Until now, no studies have been performed at the MO level for compounds of these elements, except for DF calculations (without correlation) for fluorides of element 126 [195]. Accurate predictions of properties of specific compounds will be quite a challenging task in this area. This may need inclusion of the QED effects to reach the desired accuracy.

Experimental investigations are still a matter of a far future and are dependent on discoveries of longer-lived isotopes. The evolution of the periodic table was discussed by Seaborg last in 1996 [196].

Table 11-18 Trends in volatility of the heaviest element compounds and their lighter homologs in the chemical groups

Group	Compounds	Theoretically predicted	Ref.	Experimentally observed	Ref.
4	MCl_4, MBr_4	Hf < Rf	[139]	Hf < Rf	[28]
5	ML_5 (L = Cl, Br)	Nb < Ta < Db	[197]	(DbO_3Br)	[29]
		$DbCl_5 > DbOCl_3$	[197]	$DbCl_5 > DbOCl_3$	[29]
6	MO_2Cl_2	Mo > W > Sg	[140]	Mo > W > Sg	[30]
7	MO_3Cl	Tc > Re > Bh	[143]	Tc > Re > Bh	[31]
8	MO_4	Ru < Os > Hs	[146]	Os > Hs	[26]
12	M	Hg < 112	[165, 168]	Hg < 112	[27]
14	M	Pb << 114 < 112	[168, 181]	–	–

11.7.8. Summary of Predictions of Volatility of the Heaviest Elements and Their Compounds

Predicted trends in volatility of the heaviest elements and their compounds compared to the experimental observations are summarized in Table 11-18. One can see that all the predicted trends for group 4 through 8 and 12 were confirmed by the experiments. Also, the absolute values of the adsorption enthalpies are in very good agreement with the experimental ones, as discussed above. Predictions for element 114 are still awaiting experimental verification.

11.8. AQUEOUS CHEMISTRY

11.8.1. Redox Potentials and Reduction Experiments

The stability of oxidation states of the heaviest elements is tested by reduction experiments. For that purpose, knowledge of the redox potentials E° is of crucial importance. For a reduction reaction

$$M^{z+n} + ne \leftrightarrow M^{z+}, \tag{11-19}$$

the redox potential E° is

$$E^\circ = -\Delta G^\circ / nF, \tag{11-20}$$

where F is the Faraday constant and n in the number of the transferred electrons. In reality, components of reaction (11-19) are high-coordinated hydrated, hydrolyzed and complex species, so that calculations of E° via the total energy differences may not be sufficiently accurate. Another way to obtain E° was, therefore, suggested in [198] using a linear correlation between IP and E°, since

$$\Delta G^\circ = -E^\circ nF = -(\mathrm{IP} + \Delta G^\circ{}_{\mathrm{hydr}}). \tag{11-21}$$

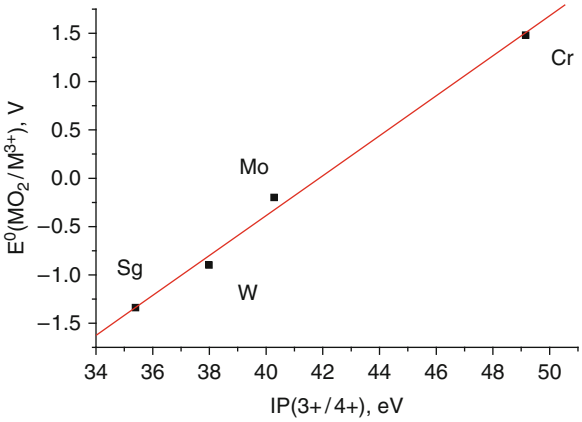

Figure 11-36. Correlation between MCDF IP(3+/4+) [66] and standard potentials $E°(MO_2/M^{3+})$ [201], where M = Cr, Mo, W, and Sg (From [200])

Here, $\Delta G°_{hydr}$ is a free energy of hydration, which is a smooth function of the atomic number and can, therefore, be evaluated. In this way, $E°$ for Rf, Db and Sg in various oxidation states were determined [198–200] using the MCDF multiple IPs [55, 65, 66] and experimental $E°$ for lighter homologs [201]. One of those correlations for the group-6 species is shown in Figure 11-36, as an example [200].

Results of those investigations have, indeed, shown that the stability of the maximum oxidation state increases in group 4 through 6, while that of lower oxidation states decreases. Along the 6d series, the stability of the maximum oxidation state decreases: $E°(Lr^{3+}/Lr^{2+}) = -2.6\,V$, $E°(Rf^{4+}/Rf^{3+}) = -1.5\,V$, $E°(Db^{5+}/Db^{4+}) = -0.93\,V$, and $E°(Sg^{6+}/Sg^{5+}) = -0.05\,V$. The redox potentials for Lr, Rf, Db and Sg and their homologs are given in [8].

A comparison of the relativistic with nonrelativistic calculations shows that the increasing stability of the maximum oxidation state is a relativistic effect due to the destabilization of the 6d AOs. The estimates of redox potentials have also demonstrated that the 3+ and 4+ states for Db and Sg, respectively, will not be stable: the ionisation process results in the $6d^2$ and not the $7s^2$ state in Db^{3+} and Sg^{4+} [200]. Since the 6d AOs are more destabilized than the 4d and 5d ones, the 3+ and 4+ states in Db and Sg, respectively, will even be less stable than those states in their lighter homologs. Based on these predictions, experiments to attempt to reduce Sg with a strongly reducing metal such as Al ($E° = -1.662\,V$) are planned.

11.8.2. Complex Formation and Extraction by Liquid Chromatography

A number of aqueous chemistry separation experiments have been conducted for Rf, Db and Sg and their homologs [202–211]. These experiments demonstrated a basic similarity in the behaviour of the heaviest elements and their lighter homologs, although they have revealed a number of controversies (see reviews

[9,34,36]). Many theoretical works based on the 4*c*-DFT calculations were devoted to predictions of the extraction behaviour of these elements [212–219]. The main features of the method used in those works are given in the following.

A model to predict hydrolysis/complex formation. For a complex formation reaction (11-1), the complex formation constant K_i is

$$\log K_i = -\Delta G^r / 2.3RT, \tag{11-22}$$

where ΔG^r is a free energy change of the reaction. Since it is almost impossible to calculate $\Delta G^r = \Delta G^f(\text{products}) - \Delta G^f(\text{reagents})$ with sufficient accuracy for large, highly coordinated aqueous species of the heavy-element complexes, the following model has been used. The formation energy ΔG^f of the $M_xO_u(OH)_v(H_2O)_w^{(z-2u-v)+}$ species can be decomposed in the following way [220]

$$\begin{aligned} &-\Delta G^f(u,v,w)/2.3RT \\ &\quad = \sum a_i + \sum a_{ij} + \log P - \log(u!v!w!2^w) + (2u+v+1)\log 55.5 \end{aligned} \tag{11-23}$$

The first term on the right hand side of Eq. (11-23), $\sum a_i$, is the non-electrostatic contribution from M, O, OH, and H_2O, related to OP of the species. For a reaction,

$$\Delta \sum a_i = \Delta E^{\text{OP}} = k\Delta\text{OP}, \tag{11-24}$$

where k is an empirical coefficient. The next term, $\sum a_{ij}$, is a sum of each pairwise electrostatic (Coulomb) interaction

$$E^C = \sum a_{ij} = -B \sum_{ij} Q_i Q_j / d_{ij}, \tag{11-25}$$

where d_{ij} is the distance between the moieties i and j; Q_i and Q_j are their effective charges and $B = 2.3RTe^2/\varepsilon$, where ε is the dielectric constant. For a reaction, ΔE^{C} is the difference in E^{C} for the species in the left hand and right hand parts. P in Eq. (11-23) is the partition function representing the contribution of structural isomers if there are any. The last two terms are statistical: one is a correction for the indistinguishable configurations of the species and the other is a conversion to the molar scale of concentration for the entropy. $\sum a_{ij}$ and $\sum a_i$ for each compound are then calculated via Mulliken numbers obtained as a result of the electronic structure calculations of complexes on interest. To predict $\log K_i$ or $\log\beta_i$ for transactinide complexes, coefficients k and B should be defined by fitting $\log K_i$ to experimental values for the lighter homologs, as it is shown in [217]. Using the suggested model in the combination with 4*c*-DFT calculations, hydrolysis and complex formation constants were predicted for a large number of aqueous compounds of Rf, Db, Sg and Hs and their group-4, 5, 6 and 8 lighter homologs [212–219].

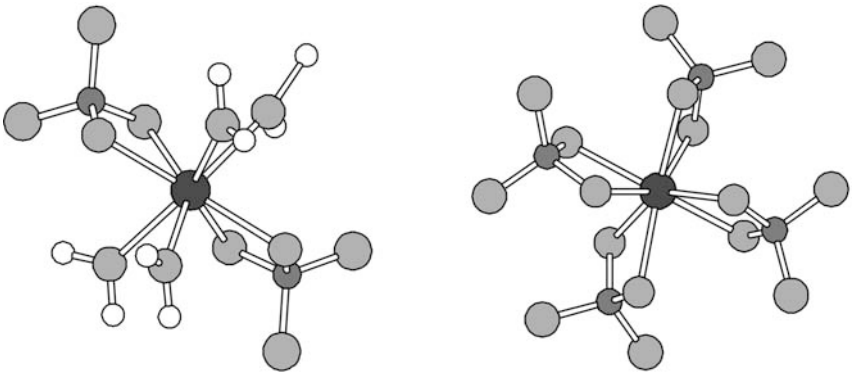

Figure 11-37. $M(SO_4)_2(H_2O)_4$ and $M(SO_4)_4{}^{4-}$ complexes of Zr, Hf and Rf (From [213])

Table 11-19 Coulomb part of the free energy change, ΔE^C (in eV) of the complex formation reactions [213]

Reaction	Zr	Hf	Rf	Trend
$M(H_2O)_8{}^{4+} \Leftrightarrow M(SO_4)_2(H_2O)_4$	−35.72	−35.84	−33.60	Hf > Zr >> Rf
$M(H_2O)_8{}^{4+} \Leftrightarrow M(SO_4)_3(H_2O)_2{}^{2-}$	−42.43	−42.43	−39.37	Zr = Hf >> Rf
$M(H_2O)_8{}^{4+} \Leftrightarrow M(SO_4)_4{}^{4-}$	−45.14	−45.02	−41.38	Zr > Hf >> Rf
$M(H_2O)_8{}^{4+} \Leftrightarrow R_4M(SO_4)_4$	−41.04	−40.78	−37.65	Zr > Hf >> Rf

As an example, a process of step-wise complexation of group-4 elements Zr, Hf, and Rf in H_2SO_4 solutions is considered here. In [213], relative values of the free energy change of the $M(SO_4)_2(H_2O)_4$, $M(SO_4)_3(H_2O)_2{}^{2-}$ and $M(SO_4)_4{}^{4-}$ (M = Zr, Hf, and Rf) formation reactions from hydrated and partially hydrolyzed cations have been calculated using the 4*c*-DFT method. (Figure 11-37 shows geometrical configurations of two of these complexes.) The obtained ΔE^C and trends for one type of complex formation reaction starting from the hydrated species $M(H_2O)_8{}^{4+}$ are given in Table 11-19.

Analogously, ΔE^C were obtained for a complex formation reaction starting from hydrolyzed complexes, i.e., $MOH(H_2O)_7{}^{3+} \Leftrightarrow M(SO_4)_n(H_2O)_{8-2n}$. The results have indicated the same trend in the complex formation, Zr > Hf >> Rf, as for the former type of reaction (Table 11-19). The obtained on their basis $\log K_d$ values for extraction of Zr, Hf and Rf by amines are shown in Figure 11-38.

The experiments on the extraction of Zr, Hf and Rf from H_2SO_4 solutions by amines confirmed the predicted trend Zr > Hf >> Rf in the complex formation and have given the K_d(Rf) values closed to the predicted ones [207].

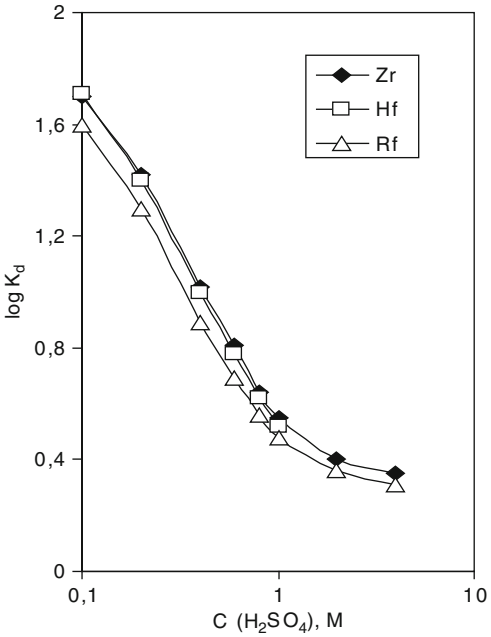

Figure 11-38. Predicted log K_d values for the extraction of Hf and Rf by amines with respect to the measured one for Zr (From [213])

11.8.3. Summary of Predictions of the Complex Formation

A summary of the predicted trends in hydrolysis, complex formation and extraction of the heaviest element complexes and their homologs as compared to the experimental results is given in Table 11-20. As one can see there, most of the predictions were confirmed by the experiments for the heaviest elements and their homologs, while some of them are still awaiting confirmation, as in the case of Sg in HF solutions.

The calculations have shown that the theory of hydrolysis [208] based on the relation between the cation size and charge does not explain all the experimental behaviour, like, e.g., the difference between Nb and Ta, or Mo and W. Only by performing relativistic calculations for real equilibria in solutions, can the complex formation or hydrolysis constants, K_d and their order in the chemical groups be correctly predicted.

Results of the calculations have also shown the predominant contribution in ΔG^r to be a change in the electrostatic metal-ligand interaction energy, ΔE^C (Eq. (11-25)). Thus, by calculating only this term trends in the complex formation can be reliably predicted.

Experimental aqueous phase studies of chemical properties of elements heavier than Sg have not yet been performed. They will depend on the development of experimental techniques which cope with production rates of less than one atom per hour and short half-lives.

Table 11-20 Trends in hydrolysis and complex formation of the heaviest element compounds and their lighter homologs in chemical groups

Group	Complexes	Theoretically predicted	Ref.	Experimentally observed	Ref.
4	Hydrolysis of M^{4+}	Zr > Hf > Rf	[212]	Zr > Hf > Rf	[202]
	$MF_x(H_2O)^{z-x}{}_{8-x}$ ($x \leq 4$)	Zr > Hf > Rf	[212]	Zr > Hf > Rf	[203, 204]
	$MF_6{}^{2-}$	Rf ≥ Zr > Hf	[212]	Rf ≥ Zr > Hf	[205]
	$MCl_6{}^{2-}$	Zr > Hf > Rf	[212]	Rf > Zr > Hf	[206]
	$M(SO_4)_4{}^{4-}$	Zr > Hf >> Rf	[213]	Zr > Hf >> Rf	[207]
5	Hydrolysis of M^{5+}	Nb > Ta > Db	[214]	Nb > Ta	[202]
	$MOCl_4{}^-$, $MCl_6{}^-$	Nb ≥ Db > Ta	[215]	Nb ≥ Db >Ta	[209]
	$MF_6{}^-$, $MBr_6{}^-$	Nb > Db > Ta	[216]	Nb > Db > Ta	[209]
6	Hydrolysis of M^{6+}	Mo > W > Sg	[217]	Mo > W > Sg	[210]
	Hydrolysis of $MO_2(OH)_2$	Mo > Sg > W	[217]	Mo > W	[210]
	$MO_2F_2(H_2O)_2$	Mo > Sg > W	[218]	Mo > W	[221]
	$MOF_5{}^-$	Mo < W < Sg	[218]	Mo < W	[221]
8	$MO_4(OH)_2{}^{2-}$	Os > Hs >> Ru	[219]	Os ≥ Hs	[211]

11.9. SUMMARY AND OUTLOOK

Many accurate calculations of atomic and molecular properties of the heaviest elements and their homologs have nowadays become available. The most accurate atomic calculations for the heaviest elements up to $Z = 122$ were performed with the use of the DC and DCB FSCC methods. Reliable electronic configurations were obtained assuring the position of the superheavy elements in the periodic table. Accurate ionization potentials, electron affinities and energies of electronic transitions are presently available and can be used to assess the similarity between the heaviest elements and their lighter homologs in the chemical groups.

The most valuable information about molecular properties of the chemically interesting compounds was obtained with the use of the 4*c*-DFT and RECP/PP CCSD(T) methods. They proved to be complimentary, both conceptually and quantitatively in studies of molecular properties, and their combination is obviously the best way to investigate properties of the heaviest elements. The calculations with the use of these methods allowed for predicting valence states, geometries, and types of stable compounds of the heaviest elements. They permitted the establishment of important trends in chemical bonding, stabilities of oxidation states, crystal-field and SO effects, complexing ability and other properties in the periodic table in going over to the heaviest elements, as well as the role and magnitude of relativistic and correlation effects.

It was shown that the heaviest elements are basically homologs of their lighter congeners in the chemical groups, though their properties may be rather different due to very large relativistic effects. This is also a reason why trends in atomic and molecular properties may change in going over to the heaviest elements. Thus, straightforward extrapolations in the chemical groups may result in erroneous predictions. Relativistic calculations also proved to be the most reliable tool

in predicting the outcome of the gas-phase and aqueous phase experiments with Rf, Db, Sg, Bh, Hs, and element 112. The synergism between theoretical and experimental research in the last decade led to a better understanding of the chemistry of these exotic species.

Although rich information has been collected, a number of open questions still remain. For elements which were chemically identified, a more detailed study, both theoretical and experimental, shall follow. New compounds of the chemically identified elements, e.g., carbonyls of Sg, or organometallic ones of Hs, should be synthesized and chemically investigated. For those elements, not yet studied, like Mt, Ds, Rg and those 114 through 118, isotopes suitable for chemical studies should be found, as well as their nuclear decay properties should be known, so that they can be positively identified. Their separation will also need new technological developments to cope with the very low production rates and short half-lives. In this area, theoretical chemistry will have a number of exciting tasks to predict the experimental behaviour in the chemical separation experiments.

For elements heavier than $Z = 118$, investigations of chemical properties is a matter of future. They will be even more exciting than those which have already been performed, since resemblance with their lighter homologues will be even less pronounced. Some further methodical developments in the relativistic quantum theory, like, e.g., inclusion of the QED effects on a SCF basis, may be needed to achieve a required accuracy of the calculations.

ACKNOWLEDGEMENTS

The author acknowledges a fruitful collaboration with J. Anton, T. Jacob, T. Bastug, A. Borschevsky, E. Eliav, U. Kaldor, and D. C. Hoffman. She appreciates many fruitful discussions with her colleagues at the GSI, Darmstadt. She thanks S. Hofmann for the chart of nuclides and Ch. E. Düllmann for the periodic table of the elements. She also acknowledges help of B. Schausten in preparing the pictures.

REFERENCES

1. Schädel, M. (ed.).: The Chemistry of the Superheavy Elements. Dordrecht, The Netherlands/Boston, MA/London (2003)
2. Proceedings of "The Robert A. Welch Foundation Conference on Chemical Research XXXIV. Fifty Years with Transuranium Elements", Houston, TX, 22–23 October 1990, pp. 255–276 (1990)
3. Greiner, W., Gupta, R.K. (eds.).: Heavy Elements and Related New Phenomena. World Scientific, Singapore (1999)
4. Wilson, S., Kaldor, U. (eds.).: Theoretical Chemistry and Physics of Heavy and Superheavy Elements, pp. 55–114. Kluwer, Dordrecht (2003)
5. Fricke, B.: Struct. Bond. **21**, 89 (1975)
6. Schwerdtfeger, P., Seth, M.: Relativistic effects on the superheavy elements. In: Encyclopedia on Calculational Chemistry, vol. 4, pp. 2480–2499. Wiley, New York (1998)
7. Pershina, V.: The chemistry of the superheavy elements and relativistic effects. In: P. Schwerdtfeger (ed.) Relativistic Electronic Structure Theory, Part II, pp. 1–80. Elsevier, Amsterdam (2002)

8. Hoffman, D.C., Lee, D.M., Pershina, V.: Transactinide elements and future elements. In: L.R. Morss, N.M. Edelstein, J. Fuger (eds.) The Chemistry of the Actinide and Transactinide Elements, 3rd edn, Ch. 14, pp. 1652–1752. Springer, Dordrecht (2006)
9. Pershina, V., Kratz, J.V.: Experimental and theoretical studies of the chemistry of the heaviest elements. In: B.A. Hess (ed.) Relativistic Effects in Heavy-Element Chemistry and Physics, pp. 219–244. Wiley, New York (1997)
10. Pershina, V.: Chem. Rev. **96**, 1977 (1996)
11. Barber, R.C., Greenwood, N.N., Hrynkiewicz, A.Z., Jeannin, Y.P., Lefort, M., Sakai, M., Ulehla, I., Wapstra, A.H., Wilkinson, D.H.: Prog. Part. Nucl. Phys. **29**, 453 (1992)
12. Flerov, G.N., Ter-Akopian, G.M.: Rep. Prog. Phys. **46**, 817 (1983)
13. Seaborg, G.T., Loveland, W.D.: The Elements Beyond Uranium. Wiley, New York (1990)
14. Münzenberg, G., Hofmann, S.: Discovery of the heaviest elements. In.: W. Greiner, R.K. Gupta (eds.) Heavy Elements and Related New Phenomena, pp. 9–42. World Scientific, Singapore (1999)
15. Hofmann, S., Münzenberg, G.: Rev. Mod. Phys. **72**, 733 (2000)
16. Morita, K., Morimoto, K., Kaji, D., Akiyama, T., Goto, S., Haba, H., Ideguchi, E., Katori, K., Koura, H., Kikunaga, H., Kudo, H., Ohnishi, T., Ozawa, A., Sato, N., Suda, T., Sieki, K., Tokanai, F., Yamaguchi, T., Yoneda, A., Yoshida, A.: J. Phys. Soc. Jpn. **76**, 045001 (2007)
17. Oganessian, Yu.: J. Phys. G: Nucl. Part. Phys. **34** R165 (2007)
18. Commission on nomenclature of inorganic chemistry. Pure & Appl. Chem. **69**, 2471; www.iupac.org (1997)
19. Möller, P., Nix, J.R.: J. Phys. G., Nucl. Part. Phys. **20**, 1681 (1994)
20. Myers, W.D., Swiatecki, W.J.: Nucl. Phys. A **601**, 141 (1996); Liran, S., Marinov, V., Zeldes, N.: Phys. Rev. C **63**, 017302–1 (2000)
21. Heenen, P.H., Nazarewicz, W.: Europhys. News, Febr. 2002, p. 5; Bender, M., Nazarewicz, W., Reinhard, P.-G.: Phys. Lett. B **515**, 42 (2001); Bender, M., Rutz, K., Reinhard, P.-G., Maruhn, J.A., Greiner, W.: Phys. Rev. C **60**, 034304 (1999)
22. Kruppa, A.T., Bender, M., Nazarewicz, W., Reinhard, P.G., Vertse, T., Cwiok, S.: Phys. Rev. C **61**, 034313–1 (2000); Cwiok, S., Dobaczewski, J., Heenen, P.H., Magierski, P., Nazarewicz, W.: Nucl. Phys. A **611**, 211 (1996)
23. Adloff, J.P., Guillaumont, R.: Fundamentals of Radiochemistry, pp. 327–52. CRC Press, Boca Raton, FL (1993)
24. Hübener, S., Zvara, I.: Radiochim. Acta **31**, 89 (1982)
25. Zvara, I., Eichler, B., Belov, V.Z., Zvarova, T.S., Korotkin, Yu.S., Shalaevsky, M.R., Shegolev, V.A., Hussonnois, M.: Sov. Radiochem. **16**, 709 (1974)
26. Düllmann, Ch.E., Brüchle, W., Dressler, R., Eberhardt, K., Eichler, B., Eichler, R., Gäggeler, H.W., Ginter, T.N., Glaus, F., Gregorich, K., Hoffman, D.C., Jäger, E., Jost, D.T., Kirbach, U.W., Lee, D.E., Nitsche, H., Patin, J.B., Pershina, V., Piguet, D., Qin, Z., Schädel, M., Schausten, B., Schimpf, E., Schött, H.J., Soverna, S., Sudowe, R., Thörle, P., Timokhin, S.N., Trautmann, N., Türler, A., Vahle, A., Wirth, G., Yakushev, A.B., Zielinski, P.M.: Nature **418**, 859 (2002)
27. Eichler, R., Aksenov, N.V., Belozerov, A.V., Bozhikov, G.A., Vhepigin, V.I., Dmitriev, S.N., Dressler, R., Gäggeler, H.W., Gorshkov, V.A., Haenssler, F., Itkis, M.G., Laube, A., Lebedev, V.Ya., Malyshev, O.N., Oganessian, Yu.Ts., Petrushkin, O.V., Piguet, D., Rasmussen, P., Shishkin, S.V., Shutov, S.V., Svirikhin, A.I., Tereshatov, E.E., Vostokin, G.K., Wegrzecki, M., Yeremin, A.V.: Nature Lett. **447**, 72 (2007)
28. Kadkhodayan, B., Türler, A., Gregorich, K.E., Baisden, P.A., Czerwinski, K.R., Eichler, B., Gäggeler, H.W., Hamilton, T.M., Jost, D.T., Kacher, C.D., Kovacs, A., Kreek, S.A., Lane, M.R., Mohar, M.F., Neu, M.P., Stoyer, N.J., Sylwester, E.R., Lee, D.M., Nurmia, M.J., Seaborg, G.T., Hoffman, D.C.: Radiochim. Acta **72**, 169 (1996)
29. Türler, A.: Radiochim. Acta **72**, 7 (1996)

30. Schädel, M., Brüchle, W., Dressler, R., Eichler, B., Gäggeler, H.W., Günther, R., Gregorich, K.E., Hoffman, D.C., Hübener, S., Jost, D.T., Kratz, J.V., Paulus, W., Schumann, D., Timokhin, S., Trautmann, N., Türler, A., Wirth, G., Yakushev, A.B.: Nature (Lett.) **388**, 55 (1997); Türler, A., Brüchle, W., Dressler, R., Eichler, B., Eichler, R., Gäggeler, H.W., Gärtner, M., Glatz, J.-P., Gregorich, K.E., Hübener, S., Jost, D.T., Lebedev, V.Ya., Pershina, V., Schädel, M., Taut, S., Timokhin, N., Trautmann, N., Vahle, A., Yakushev, A.B.: Angew. Chem. Int. Ed. Engl. **38**, 2212 (1999)
31. Eichler, R., Brüchle, W., Dressler, R., Düllman, Ch.E., Eichler, B., Gäggeler, H.W., Gregorich, K.E., Hoffman, D.C., Hübener, S., Jost, D.T., Kirbach, U.W., Laue, C.A., Lavanchy, V.M., Nitsche, H., Patin, J.B., Piguet, D., Schädel, M., Shaughnessy, D.A., Strellis, D.A., Taut, S., Tobler, L., Tsyganov, Y.S., Türler, A., Vahle, A., Wilk, P.A., Yakushev, A.B.: Nature **407**, 63 (2000)
32. Gäggeler, H.W., Türler, A.: Gas-phase chemistry. In: Ref. 1, pp. 237–290; Türler, A., Gregorich, K.E. (eds.).: Experimental techniques, ibid., pp. 117–158
33. Hoffman, D.C.: Chem. Eng. News May 24 (1994); Hoffman, D.C.: J. Chem. Ed. **76**, 331 (1999)
34. Kratz, J.V.: Liquid-phase chemistry. In: Ref. 1, pp. 159–104
35. Kratz, J.: Chemistry of transactinides. In: S. Nagy, Z. Klencsar (eds.) Handbook of Nuclear Chemistry, pp. 323–396. Kluwer, Norwell, MA (2003)
36. Schädel, M.: Angew. Chem. Int. Ed. Engl. **45**, 368 (2006)
37. Penneman, R.A., Mann, J.B., Jørgensen, C.K.: Chem. Phys. Lett. **8**, 321 (1971)
38. Jørgensen, C.K.: Angew. Chem. Int. Ed. Engl. **12**, 12 (1973)
39. Haissinski, M.: Radiochem. Radioanal. Lett. **8**, 107 (1971)
40. Seaborg, G.T., Keller, O.L.: In: J.J. Katz, G.T. Seaborg, L.R. Morss (eds.) The Chemistry of the Actinides, 2nd edn., vol. 2, p. 1629. Chapman & Hall, New York (1986)
41. Bonchev, D., Kamenska, V.: J. Phys. Chem. **85**, 1177 (1981)
42. Cotton, S.A.: Chem. Soc. Rev. 219 (1996)
43. Pershina, V.: Theoretical chemistry of the heaviest elements. In: Ref. 1, pp. 31–94
44. Pyykkö, P.: Chem. Rev. **88**, 563 (1988)
45. Desclaux, J.P.: Atom. Data Nucl. Data **12**, 311 (1973)
46. Pershina, V., Bastug, T.: Chem. Phys. **311**, 139 (2005)
47. Eliav, E., Shmulyian, S., Kaldor, U., Ishikawa, Y.: J. Chem. Phys. **109**, 3954 (1998)
48. Gaston, N., Schwerdtfeger, P., Nazarewicz, W.: Phys. Rev. A **66**, 062505 (2002)
49. Lindgren, I.: Int. J. Quantum Chem. **57**, 683 (1996)
50. Pyykkö, P., Tokman, M., Labzowsky, L.N.: Phys. Rev. A **57**, R689 (1998)
51. Goidenko, I., Labsowsky, L., Eliav, E., Kaldor, U., Pyykkö, P.: Phys. Rev. A **67**, 020102(R) (2003)
52. Schwerdfeger, P. (ed.).: Relativistic Electronic Structure Theory, Parts I and 2. Elsevier, Amsterdam (2002)
53. Kaldor, U., Eliav, E., Landau, A.: Accurate relativistic Fock-Space calculations for many-electron atoms. In: Ref. 52, vol. 2, pp. 81–119
54. Eliav, E., Kaldor, U., Ishikawa, Y.: Phys. Rev. Lett. **74**, 1079 (1995)
55. Glebov, V.A., Kasztura, L., Nefedov, V.S., Zhuikov, B.L.: Radiochim. Acta **46**, 117 (1989)
56. Johnson, E., Fricke, B., Keller, Jr. O.L., Nestor, Jr. C.W., Ticker, T.C.: J. Chem. Phys. **93**, 8041 (1990)
57. Eliav, E., Landau, A., Ishikawa, Y., Kaldor, U.: J. Phys. B**35**, 1693 (2002)
58. DIRAC Package. Dirac, a relativistic *ab initio* electronic structure program, Release DIRAC04.0 (2004)", written by Jensen, H.J.Aa., Saue, T., Visscher, L. with contributions from Bakken, V., Eliav, E., Enevoldsen, T., Fleig, T., Fossgaard, O., Helgaker, T., Laerdahl, J., Larsen, C.V., Norman, P., Olsen, J., Pernpointner, M., Pedersen, J.K., Ruud, K., Salek, P., van Stralen, J.N.P., Thyssen, J., Visser, O., Winther, T. (http://dirac.chem.sdu.dk) (2004)
59. Malli, G., Da Silva, A.B.F., Ishikawa, Y.: J. Chem. Phys. **101**, 6829 (1994)
60. Visscher, L., Aerts, P.J.C., Visser, O., Nieuwpoort, W.C.: Int. J. Quantum Chem. **25**, 131 (1991)

61. Faegri, K.: Theor. Chem. Acta **105**, 252 (2001); Faegri, K., Dyall, K.G.: Basis sets for relativistic calculations. In: Ref. 52, pp. 259–290
62. de Macedo, L.G.M., Borin, A.C., da Silva, A.B.F.: Atom. Data Nucl. Data **93**, 931 (2007)
63. Desclaux, J.P.: Comput. Phys. Commun. **9**, 31 (1975)
64. Grant, I.P.: J. Phys. B **19**, 3187 (1986)
65. Fricke, B., Johnson, E., Rivera, G.M.: Radiochim. Acta **62**, 17 (1993)
66. Johnson, E., Pershina, V., Fricke, B.: J. Phys. Chem. **103**, 8458 (1999)
67. Johnson, E., Fricke, B., Jacob, T., Dong, C.Z., Fritzsche, S., Pershina, V.: J. Phys. Chem. **116**, 1862 (2002)
68. Yu, Y.J., Li, J.G., Dong, C.Z., Ding, X.B., Fritsche, S., Fricke, B.: Eur. Phys. J. D **44**, 51 (2007)
69. Yu, Y.J., Dong, C.Z., Li, J.G., Fricke, B.: J. Chem. Phys. **128** 124316 (2008)
70. Balasubramanian, K.: Chem. Phys. Lett. **341**, 601 (2001); ibid, **351**, 161 (2002)
71. Fricke, B., Greiner, W., Waber, J.T.: Theor. Chim. Acta (Berlin) **21**, 235 (1971)
72. Visscher, L.: Post-Dirac-Fock methods. In: Ref. 52, Part 1, pp. 291–331; Saue, T.: Post Dirack-Fock-methods-properties, ibid., pp. 332–400
73. Wood, C.P., Pyper, N.C.: Chem. Phys. Lett. **84**, 614 (1981)
74. Saue, T., Faegri, K., Gropen, O.: Chem. Phys. Lett. **263**, 360 (1996)
75. Seth, M., Schwerdtfeger, P., Dolg, M., Faegri, K., Hess, B.A., Kaldor, U.: Chem. Phys. Lett. **250**, 461 (1996); Seth, M., Schwerdtfeger, P.: Chem. Phys. Lett. **318**, 314 (2000)
76. Faegri, K., Saue, T.: J. Chem. Phys. **115**, 2456 (2001)
77. Seth, M., Faegri, K., Schwerdtfeger, P.: Angew. Chem. Int. Ed. Engl. **37**, 2493 (1998); Schwerdtfeger, P., Seth, M.: J. Nucl. Radiochem. Sci. **3**, 133 (2002)
78. Seth, M., Schwerdtfeger, P., Faegri, K.: J. Chem. Phys. **111**, 6422 (1999)
79. Malli, G.L., Styszynski, J.: J. Chem. Phys. **109**, 4448 (1998); Malli, G.: J. Chem. Phys. **116**, 5476 (2002)
80. Malli, G.: J. Chem. Phys. **117**, 10441 (2002)
81. Pyykkö, P., Desclaux, J.P.: Chem. Phys. Lett. **50**, 503 (1977); Nature **226**, 336 (1977); Chem. Phys. **34**, 261 (1978)
82. Dolg, M.: Relativistic effective core potentials. In: Ref. 52, Part 1, pp. 793–862
83. Lee, Y.S.: Two-component relativistic effective core potential calculations for molecules. In: Ref. 52, Part 2, pp. 352–416
84. Seth, M.: The chemistry of superheavy elements. Thesis, University of Auckland (1998)
85. Seth, M., Dolg, M., Fulde, P., Schwerdtfeger, P.: J. Am. Chem. Soc. **17**, 6597 (1995)
86. Seth, M., Schwerdtfeger, P., Dolg, M.: J. Chem. Phys. **106**, 3623 (1997)
87. Seth, M., Cooke, F., Schwerdtfeger, P., Heully, J.L., Pelissier, M.: J. Chem. Phys. **109**, 3935 (1998)
88. Han, Y.K., Son, S.K., Choi, Y.J., Lee, Y.S.: J. Phys. Chem. A **103**, 9109 (1999)
89. Han, Y.K., Lee, Y.S.: J. Phys. Chem. A **103**, 1104 (1999)
90. Han, Y.K., Bae, C., Lee, Y.S.: J. Chem. Phys. **110**, 8986 (1999)
91. Han, Y.K., Bae, C., Son, S.K., Lee, Y.S.: J. Chem. Phys. **112**, 2684 (2000)
92. Choi, Y.J., Han, Y.K., Lee, Y.S.: J. Chem. Phys. **115**, 3448 (2001)
93. Nash, C.S., Bursten, B.E.: J. Phys. Chem. A**103**, 632 (1999)
94. Nash, C.S., Bursten, B.E.: **103**, 402 (1999); Nash, C.S., Bursten, B.E.: Angew. Chem. Int. Ed. Engl. **38**, 151 (1999)
95. Nash, C.S.: J. Phys. Chem. A **109**, 3493 (2005)
96. Nash, C.S., Crockett, W.W.: J. Phys. Chem. A **110**, 4619 (2006)
97. Balasubramanian, K.: Chem. Phys. Lett. **361**, 397 (2002)
98. Nash, C.S., Bursten, B.E., Ermler, W.C.: J. Chem. Phys. **106**, 5153 (1997)

99. Mosyagin, N.S., Petrov, A.N., Titov, A.V., Tupitsyn, I.I.: In: J.-P. Julien et al. (eds.) Recent Advances in the Theory of Chemical and Physical Systems, pp. 229–251. Springer, The Netherlands (2006)
100. Kohn, W., Becke, A.D., Parr, R.G.: J. Phys. Chem. **100**, 12974 (1996)
101. Engel, E.: Relativistic density functional theory: Foundations and basic formalism. In: Ref. 52, Part 1, pp. 523–621
102. Rosen, A., Ellis, D.E.: J. Chem. Phys. **62**, 3039 (1975); Rosen, A.: Adv. Quantum Chem. **29**, 1 (1997)
103. Bastug, T., Sepp, W.D., Kolb, D., Fricke, B., te Velde, G., Baerends, E.J.: J. Phys. B **28**, 2325 (1995)
104. Anton, J., Fricke, B., Engel, E.: Phys. Rev. A **69**, 012505 (2004)
105. Becke, A.D.: Phys. Rev. A **38**, 3098 (1988)
106. Perdew, J.P.: Phys. Rev. B **33**, 1822 (1986); ibid **34**, 7406 (1986)
107. Jacob, T., Geschke, D., Fritzsche, S., Sepp, W.D., Fricke, B., Anton, J., Varga, S.: Surf. Sci. **486**, 194 (2001)
108. van Wüllen, C.: Relativistic density functional calculations on small molecules. In: Ref. 52, Part 2, pp. 598–655
109. Liu, W., Hong, G., Dai, D., Li, L., Dolg, M.: Theor. Chem. Acc. **96**, 75 (1997)
110. Liu, W., van Wüllen, Ch.: J. Chem. Phys. **110**, 3730 (1999)
111. Liu, W., van Wüllen, W.Ch., Han, Y.K., Choi, Y.J., Lee, Y.S.: Adv. Quantum Chem. **39**, 325 (2001)
112. Mayer, M., Krüger, S., Rösch, N.: J. Chem. Phys. **115**, 4411 (2001)
113. van Lenthe, E., Ehlers, A., Baerends, E.J.: J. Chem. Phys. **110**, 8943 (1999); te Velde, G., Baerends, E.J.: J. Comput. Phys. **99**, 84 (1992)
114. Hess, B.A.: Phys. Rev. A **33**, 3742 (1986)
115. Eliav, E., Kaldor, U., Ishikawa, Y.: Phys. Rev. A **52**, 291 (1995)
116. Desclaux, J.P., Fricke, B.: J. Phys. **41**, 943 (1980)
117. Umemoto, K., Saito, S.: J. Phys. Soc. Jpn. **65**, 3175 (1996)
118. Pyper, N.C., Grant, I.P.: Proc. R. Soc. Lond., Ser A **376**, 483 (1981)
119. Eliav, E., Kaldor, U., Schwerdtfeger, P., Hess, B.A., Ishikawa, Y.: Phys. Rev. Lett. **73**, 3203 (1994)
120. Eliav, E., Kaldor, U., Ishikawa, Y.: Phys. Rev. A **52**, 2765 (1995)
121. Eliav, E., Kaldor, U., Ishikawa, Y., Seth, M., Pyykkö, P.: Phys. Rev. A **53**, 3926 (1996)
122. Landau, A., Eliav, E., Ishikawa, Y., Kaldor, U.: J. Chem. Phys. **114**, 2977 (2001)
123. Eliav, E., Kaldor, U., Ishikawa, Y.: Mol. Phys. **94**, 181 (1998)
124. Moore, C.E.: Atomic Energy Levels. Natl. Stand. Ref. Data Ser., Natl. Bur. Stand., Washington, DC (1971)
125. Eliav, E., Kaldor, U., Ishikawa, Y., Pyykkö, P.: Phys. Rev. Lett. **77**, 5350 (1996)
126. Pershina, V., Borschevsky, A., Eliav, E., Kaldor, U.: J. Chem. Phys. **129**, 144106 (1–9) (2008)
127. Lim, I., Pernpointer, M., Seth, M., Schwerdtfeger, P.: Phys. Rev. A **60**, 2822 (1999); Lim, I.S., Schwerdtfeger, P., Metz, B., Stoll, H.: J. Chem. Phys. **122**, 194103 (2005)
128. Landau, A., Eliav, E., Ishikava, Y., Kaldor, U.: J. Chem. Phys. **115**, 2389 (2001)
129. Thierfeld, C., Schwerdtfeger, P., Hessberger, F.P., Hofmann, S.: Eur. Phys. J. A **36**, 227 (2008)
130. Shannon, R.D.: Acta Crystallogr., Sect. A **32**, 751 (1976)
131. Pyykkö, P., Atsumi, M.: Chem. Eur. J. **15**, 186 (2009)
132. Pyykkö, P., Riedel, S., Patzsche, M.: Chem. Eur. J. **11**, 3511 (2005)
133. Fricke, B., Waber, J.T.: J. Chem. Phys. **56**, 3246 (1972)
134. Pershina, V., Borschevsky, A., Eliav, E., Kaldor, U.: J. Chem. Phys. **128**, 024707 (2008)
135. Pershina, V., Borschevsky, A., Eliav, E., Kaldor, U.: J. Phys. Chem. A **112**, 13712 (2008)
136. Borschevsky, A., Pershina, V., Eliav, E., Kaldor, U.: Chem. Phys. Lett. **480**, 49 (2009)

137. CRC Handbook of Chemistry and Physics, 86th edn., by D.R. Lide (ed.). CRC Press, Boca Raton, FL (2005); Goeben, D., Hohm, U.: J. Phys. Chem. **100**, 7710 (1996)
138. Pershina, V., Fricke, B.: J. Chem. Phys. **99**, 9720 (1993)
139. Pershina, V., Fricke, B.: Electronic structure and chemistry of the heaviest elements. In: Ref. 3, pp. 194–262
140. Pershina, V., Fricke, B.: J. Phys. Chem. **99**, 144 (1995); Pershina, V., Fricke, B.: ibid. **100**, 8748 (1996)
141. Nash, C.S., Bursten, B.E.: New J. Chem. **19**, 669 (1995)
142. Varga, S., Fricke, B., Hirata, M., Bastug, T., Pershina, V., Fritzsche, S.: J. Phys. Chem. **104**, 6495 (2000)
143. Pershina, V., Bastug, T.: J. Chem. Phys. **113**, 1441 (2000)
144. Pershina, V., Bastug, T., Fricke, B., Varga, S.: J. Chem. Phys. **115**, 1 (2001)
145. Pershina, V., Bastug, T., Fricke, B.: J. Chem. Phys. **122**, 124301 (2005)
146. Pershina, V., Anton, J., Jacob, T.: Phys. Rev. A **78**, 032518 (2008)
147. Burroughs, P., Evans, S., Hamnett, A., Orchard, A.F., Richardson, N.V.: J. Chem. Soc., Faraday Trans. **2** 70, 1895 (1974)
148. Krebs, B., Hasse, K.D.: Acta Crystallogr., Sect. B: Struct. Crystallogr. Cryst. Chem. **32**, 1334 (1976); Müller, A., Krebs, B.: J. Mol. Spectrosc. **24**, 180 (1967)
149. Filatov, M., Cremer, D.: J. Chem. Phys. **119**, 1412 (2003)
150. Seto, J.Y., Morbi, Z., Charron, F., Lee, S.K., Bernath, P.F., Le Roy, P.J.: J. Chem. Phys. **110**, 11756 (1999)
151. Dolg, M., Stoll, H., Seth, M., Schwerdtfeger, P.: Chem. Phys. Lett. **345**, 490 (2001)
152. Han, Y.K., Hirao, K.: Chem. Phys. Lett. **328**, 453 (2000)
153. Anton, J., Fricke, B., Schwerdtfeger, P.: Chem. Phys. **311**, 97 (2005)
154. Pitzer, K.S.: J. Chem. Phys. **63**, 1032 (1975)
155. Eichler, B.: Kernenergie **10**, 307 (1976)
156. Liu, W., Dolg, M., Schwerdtfeger, P.: unpublished
157. Pyykkö, P.: Chem. Rev. **97**, 597 (1997)
158. Zee, R.D., Blankespoor, S.C., Zweier, T.S.: J. Chem. Phys. **88**, 4650 (1988)
159. Huber, K.P., Herzberg, G.: Constants of Diatomic Molecules. Reinhold, New York (1979)
160. Schwerdtfeger, P., Li, J., Pyykkö, P.: Theor. Chim. Acta **87**, 313 (1994); Dolg, M., Flad, H.J.: J. Phys. Chem. **100**, 6147 (1996)
161. Gaston, N., Opahle, I., Gäggeler, H.W., Schwerdtfeger, P.: Angew. Chem. Int. Ed. Engl. **46**, 1663 (2007)
162. Soverna, S.: Doctoral Thesis, Universität Bern (2004); Soverna, S., Dressler, R., Düllmann, C.E., Eichler, B., Eichler, R., Gäggeler, H.W., Haenssler, F., Niklaus, J.P., Piguet, D., Qin, Z., Türler, A., Yakushev, A.: Radiochim. Acta **93**, 1 (2005)
163. Pershina, V., Bastug, T., Fricke, B., Jacob, T., Varga, S.: Chem. Phys. Lett. **365**, 176 (2002)
164. Sarpe-Tudoran, C., Pershina, V., Fricke, B., Anton, J., Sepp, W.D., Jacob, T.: Eur. Phys. J. D **24**, 65 (2003); Pershina, V., Bastug, T., Sarpe-Tudoran, C., Anton, J., Fricke, B.: Nucl. Phys. A **734**, 200 (2004)
165. Sarpe-Tudoran, C., Fricke, B., Anton, J., Pershina, V.: J. Chem. Phys. **126**, 174702 (2007)
166. Niklaus, J.P., Eichler, R., Soverna, S., Gäggeler, H.W., Tobler, L.: PSI Annual Report, p. 8. (2000)
167. Boisvert, G., Lewis, L.J., Puska, M.J., Nieminen, R.M.: Phys. Rev. B **52**, 9078 (1995)
168. Pershina, V., Anton, J., Jacob, T.: J. Chem. Phys. **131**, 084713 (2009)
169. Yakushev, A.B., Buklanov, G.V., Chelnokov, M.L., Chepigin, V.I., Dmitriev, S.N., Gorshkov, V.A., Hübener, S., Lebedev, Y.Ya., Malyshev, O.N., Popeko, A.G., Sokol, E.A., Timokhin, S.N., Türler, A., Vasko, V.M., Yeremin, A.V., Zvara, I.: Radiochim. Acta **89**, 743 (2001)

170. Eichler, R., Aksenov, N.V., Belozerov, A.V., Bozhikov, G.A., Chepigin, V.I., Dmitriev, S.N., Dressler, R., Gäggeler, H.W., Gorshkov, A.V., Itkis, M.G., Haenssler, F., Laube, A., Lebedev, V.Ya., Malyshev, O.N., Oganessian, Y.Ts., Petrushkin, O.V., Piguet, D., Popeko, A.G., Rasmussen, P., Shishkin, S.V., Serov, A.A., Shutov, A.V., Svirikhin, A.I., Tereshatov, E.E., Vostokin, G.K., Wegrzecki, M., Yeremin, A.V.: Angew. Chem. Int. Ed. Engl. **47**(17), 3262 (2008)
171. Rykova, E.A., Zeitsevskii, A., Mosyagin, N.S., Isaev, T.A., Titov, A.V.: J. Chem. Phys. **125**, 241102 (2006); Zaitsevskii, A., Rykova, E.A., Mosyagin, N.S., Titov, A.V.: Cent. Eur. J. Phys. **4,** 448 (2006)
172. Mosyagin, N.S., Isaev, T.A., Titov, A.V.: J. Chem. Phys. **124**, 224302 (2006)
173. Nakajima, T., Hirao, K.: Chem. Phys. Lett. **329**, 511 (2000)
174. Kaupp, M., von Schering, H.G.: Angew. Chem. Int. Ed. Engl. **32**, 861 (1993); Kaupp, M., Dolg, M., Stoll, H., von Schnering, H.G.: Inorg. Chem. **33**, 2122 (1994)
175. König, S., Gäggeler, H.W., Eichler, R., Haenssler, F., Soverna, S., Dressler, R., Friedrich, S., Piguet, D., Tobler, L.: PSI Annual Report (http://lch.web.psi.ch/pdf/anrep05/03.pdf) (2005)
176. Liu, W., van Wüllen, C., Wang, F., Li, L.: J. Chem. Phys. **116**, 3626 (2002)
177. Wood, C.P., Pyper, N.C.: Chem. Phys. Lett. **84**, 614 (1981)
178. Schwerdtfeger, P.: J. Phys. Chem. **100**, 2968 (1996)
179. Keller, Jr. O.L., Burmett, J.L., Carlson, T.A., Nestor, Jr. C.W.: J. Phys. Chem. **74**, 1127 (1970)
180. Thierfelder, C., Assadollahzadeh, B., Schwerdtfeger, P., Schäfer, S., Schäfer, R.: Phys. Rev. A **78**, 052506 (2008)
181. Pershina, V., Anton, J., Fricke, B.: J. Chem. Phys. **127**, 134310 (2007)
182. Pitzer, K.S., Balasubramanian, K.: J. Phys. Chem. **86**, 3068 (1982)
183. Heaven, M.C., Miller, T.A., Bondybey, V.E.: J. Phys. Chem. **87**, 2071 (1983)
184. Haenssler, F., Eichler, R., Gäggeler, H.W., Soverna, S., Dressler, R., Piguet, D., Schippering, M.: PSI Annal Report, p. 3 (2004); Eichler, R.: Private communication
185. Houdart, R., Schamps, J.: J. Phys. B **6**, 2478 (1873)
186. Rossbach, H., Eichler, B.: Akademie der Wissenschaft der DDR, Report No. ZFK-527 (1984)
187. Balasubramanian, K.: J. Chem. Phys. **117**, 7426 (2002)
188. Grant, I.P., Pyper, N.C.: Nature **265**, 715 (1977)
189. Keller, Jr. O.L., Nestor, Jr. C.W., Fricke, B.: J. Phys. Chem. **78**, 1945 (1974)
190. Visscher, L., Dyall, K.G.: J. Chem. Phys. **104**, 9040 (1996)
191. Malli, G.L.: In: Relativistic and Electron Correlation Effects in Molecules and Solids, NATO ASI Series, vol. 318. Plenum, New York (1994)
192. Eichler, B.: Private communication
193. Graham, A.P., Toennies, J.P.: J. Chem. Phys. **118**, 2879 (2003)
194. Nash, C.S., Bursten, B.E.: Angew. Chem. Int. Ed. Engl. **38**, 151 (1999)
195. Malli, G.L.: J. Chem. Phys. **124**, 071102 (2006); Malli, G.: Theor. Chem. Acc. **118**, 473 (2007)
196. Seaborg, G.T.: J. Chem. Soc., Dalton Trans. 760 (1996)
197. Pershina, V., Sepp, W.D., Bastug, T., Fricke, B., Ionova, G.V.: J. Chem. Phys. **97**, 1123 (1992)
198. Ionova, G.V., Pershina, V., Johnson, E., Fricke, B., Schädel, M.: J. Phys. Chem. **96**, 11096 (1992)
199. Pershina, V., Fricke, B.: J. Phys. Chem.**98**, 6468 (1994)
200. Pershina, V., Johnson, E., Fricke, B.: J. Phys. Chem. A **103**, 8463 (1999)
201. Bratsch, S.G.: J. Phys. Chem. Ref. Data **18**, 1 (1989)
202. Czerwinski, K.R.: Studies of fundamental properties of Rutherfordium (Element 104) using organic complexing agents. Doctoral Thesis, LBL Berkeley, CA (1992)
203. Strub, E., Kratz, J.V., Kronenberg, A., Nähler, A., Thörle, P., Zauner, S., Brüchle, W., Jäger, E., Schädel, M., Schausten, B., Schimpf, E., Zongwei, L., Kirbach, U., Schumann, D., Jost, D., Türler, A., Asai, M., Nagame, Y., Sakara, M., Tsukada, K., Gäggeler, H.W., Glanz, J.P.: Radiochim. Acta **88**, 265 (2000)

204. Ishii, A., Toyoshima, A., Tsukada, K., Asai, M., Toume, H., Nishinaka, I., Nagame, Y., Miyashita, S., Mori, T., Suganuma, H., Haba, H., Sakamaki, M., Goto, M.S., Kudo, H., Akiyama, K., Oura, Y., Nakahara, H., Tashiro, Y., Shinohara, A., Schädel, M., Brüchle, W., Pershina, V., Kratz, J.V.: Chem. Lett. **37**, 288 (2008)
205. Trubert, D., Le Naour, C., Hussonois, M., Brillard, L., Montroy Gutman, F., Le Du, J.F., Constantinescu, O., Barci, V., Weiss, B., Gasparro, J., Ardisson, G.: In: Abstracts of the 1st International Conference on Chemistry and Physics of the Transactinides, Seeheim, September 26–30 (1999)
206. Haba, H., Tsukada, K., Asai, M., Goto, S., Toyoshima, A., Nishinaka, I., Akiyama, K., Hirata, M., Ichikawa, S., Nagame, Y., Shoji, Y., Shigekawa, M., Koike, T., Iwasaki, M., Shinohara, A., Kaneko, T., Matuyama, T., Ono, S., Kudo, H., Qura, Y., Sueki, K., Nakahara, H., Sakama, M., Yokoyama, A., Kratz, J.V., Schädel, M., Brüchle, W.: J. Nucl. Radiochem. Sci. **3**, 143 (2002)
207. Omtwedt, J.P., Polyakova, D., Alstad, J., Bjornstad, T., Düllmann, C.E., Folden, C.M. III, Garcia, M.A., Gates, J., Gregorich, K.E., Hoffman, D.C., Nelson, S.L., Nitsche, H., Omtwedt, L., Pershina, V., Samadani, F., Skarnemark, G., Stavsetra, L., Sudove, R., Wilson, R.E., Zheng, L., Zielinski, P.M.: Radiochim. Acta (to be submitted)
208. Baes, Jr. C.F., Mesmer, R.E.: The Hydrolysis of Cations. Wiley, New York (1976)
209. Paulus, W., Kratz, J.V., Strub, E., Zauner, S., Brüchle, W., Pershina, V., Schädel, M., Schausten, B., Adams, J.L., Gregorich, K.E., Hoffman, D.C., Caption Lane, M.R., Laue, C., Lee, D.M., McGrath, C.A., Shaughnessy, D.K., Strellis, D.A., Sylwester, E.R.: Radiochim. Acta **84**, 69 (1999)
210. Schädel, M., Brüchle, W., Jäger, E., Schausten, B., Wirth, G., Paulus, W., Günther, R., Eberhardt, K., Kratz, J.V., Seibert, A., Strub, E., Thörle, P., Trautmann, N., Waldek, W., Zauner, S., Schumann, D., Kirbach, U., Kubica, B., Misiak, R., Nagame, Y., Gregorich, K.E.: Radiochim. Acta **83**, 163 (1998)
211. von Zweidorf, A., Angert, R., Brüchle, W., Bürger, S., Eberhartdt, K., Eichler, R., Hummrich, H., Jäger, E., Kling, H.O., Kratz, J.V., Kuczewski, B., Langrock, G., Mendel, M., Rieth, U., Schädel, M., Schausten, B., Schimpf, E., Thörle, P., Trautmann, N., Tsukada, K., Wiehl, N., Wirth, G.: Radiochim. Acta **92**, 855 (2004)
212. Pershina, V., Trubert, D., Le Naour, C., Kratz, J.V.: Radiochim. Acta**90**, 869 (2002)
213. Pershina, V., Polakova, D., Omtvedt, J.P.: Radiochim. Acta **94**, 407 (2006)
214. Pershina, V.: Radiochim. Acta **80**, 65 (1998)
215. Pershina, V.: Radiochim. Acta **80**, 75 (1998)
216. Pershina, V., Bastug, T.: Radiochim. Acta **84**, 79 (1999)
217. Pershina, V., Kratz, J.V.: Inorg. Chem.**40**, 776 (2001)
218. Pershina, V.: Radiochim. Acta **92**, 455 (2004)
219. Pershina, V.: Radiochim. Acta **93**, 373 (2005)
220. Kassiakoff, A., Harker, D.: J. Am. Chem. Soc. **60**, 2047 (1938)
221. Kronenberg, A., Mohapatra, P.K., Kratz, J.V., Pfrepper, G., Pfrepper, R.: Radiochim. Acta **92**, 395 (2004)